

Dec. 2021
vol. 28

SDGs

■ Introductory Note	2	New "Shibaura Machine"
■ Special Article	4	Slip Ahead
	7	DX by the New "Shibaura Machine"
■ Technical Paper	11	Research of Optimized Grease Film on Sliding Surfaces
	16	Development of PVD + CVD Vacuum Integrated System ; Application to Moisture-Resistant Multilayer Reflective Film for Heads-up Display Mirror
	20	Numerical Analysis on an Extrusion Process in a Twin-Screw Extruder
	24	Investigation of Pressure Propagation Characteristics in Die Casting Method
■ Technical Report	28	Development of Plasticization Device for Polyolefin-Based Resin Molding with High Color Dispersion and High Plasticization Capacity
	32	Optimization of Extrusion Process Engineering for the Invention of High-Performance Materials
	37	Development of High-Precision Machining Technology Using the BTA Deep Hole Drilling Machine DBH
	42	Ultra-Precision Machining Technology for Contributing to Higher Power Density of Fuel Cell (FC) Stacks
	47	Extended Battery Life of the Resolver Multi-Turn ABS and its Contribution to the Circular Economy
	51	Training Junior Employees using Digital Technology : Standardized Documents in Video Format
	55	Development of an AI-based Function to Monitor the State of Machining during Cutting in the Double Column Type Machining Center
■ New Product Introduction	59	Introduction of Large-Size Electric Injection Molding Machine EC1800SXIII
	62	Introduction of the Newest Die Casting Machine DC1300R-E
	64	Introduction of the High-Shear Processing Machine HSE-48
	66	Introduction of Real-time Collision Check Function to Prevent Machine Collisions and Interference
	68	Introduction of the USM-20B(H) High-Precision Grooving and Cutting Machine
	70	Introduction of the TCmini TC12 Series
■ Series	73	History of Ultra-Precision Machine Tools and Contributions of Shibaura Machine to the Development of Ultra-Precision Machining Technology
■ Patent News	93	Introduction to Patents
■ Prepared Critique	96	My Expectations for Shibaura Machine

New "Shibaura Machine"



President,
Chief Executive Officer and
Chief Operating Officer

Shigetomo SAKAMOTO

Our company became independent from the Toshiba Group of our parent company, Toshiba Corporation, in March 2017, changing our name from Toshiba Machine to Shibaura Machine on April 1, 2020 to mark a fresh start. As Shibaura Machine, we have established a medium-term "Management Reform Plan" and a more forward-looking "Long-term Vision 2030", aiming at further growth, as we also address structural reforms on a larger scale.

The business environment around us is dramatically changing, and technological innovation is advancing at a breathtaking pace. Now more than ever, we need to be committed to the ongoing creation of technologies to accommodate megatrends, such as climate change and resource scarcity, changes in population structures, and technological advancements, which global manufacturers like Shibaura Machine are now facing. To achieve this, we endeavor to further develop the technologies which have been in our hands since the very beginning, while actively incorporating new technologies to supplement them. We have a history of changing with the demands of the times during these periods of transition.

Our company started operation as Shibaura Machine Tool Co. in December 1938 with capital investment of 10 million yen by Shibaura Engineering Works Co. (predecessor of Toshiba Corporation) in order to meet wartime demands stemming from the Second Sino-Japanese War which occurred during the early Showa period. Our origins lie in the successive introduction of various types of large machine tools, an area which other manufacturers were hesitant to enter. At the time the company was founded, our factory was located in the Tsurumi Plant of Shibaura Engineering Works Co., where the persons involved were passionate in their determination to establish the first factory specializing in large machine tools in Japan, flying to the U.S. and Germany to acquire technology and

introduce machinery and equipment.

The factory was later designated a munitions plant. Although the company experienced hardship over its long history, we managed to find a way to survive with a wide range of machinery and equipment through all-out efforts to provide technical education and training for employees, laying the foundation for us to rebuild after the war.

Thereafter, our company has continued to develop machinery and equipment to meet the demands of the times and has provided a wide range of high-performance manufacturing equipment which supported rapid economic growth in post-war Japan, such as printing machines, roll grinders, master gear hobbing machines (designated as a Mechanical Engineering Heritage), and our core products today which include injection molding machines, die casting machines, and extrusion machines.

However, the world's goals have dramatically changed, shifting from an economy-oriented era of mass production and mass consumption to an age focusing on a balance between the economy, environment, and society, with an aim to achieve sustainability, the SDGs, and the creation of a decarbonized society.

Our company is strengthening our efforts to contribute to the world's goals by solving these issues in our society through our business activities.

Specifically, we will create and provide society with products, systems, and processes with the added value of "product + service" in areas such as energy saving, energy creation, energy storage, safety, productivity, and LCA, to help solve social issues, while increasing our own value at the same time, thereby making a lasting contribution to society.

This technical report highlights some of the results of the

technological developments we are working on. I hope this will provide an opportunity for readers to understand Shibaura Machine’s commitment to becoming integral to society, the environment, and our stakeholders, and our aim to work together to create value which will contribute to society. If so, this technology report is one worth publishing. We hope you enjoy reading it.

Slip Ahead



Chairman

Yukio IIMURA

When creating a new product, the development and design team generally follows a process which starts off with planning, moves on to determining specifications, developing conceptual and detailed designs, and creating drawings, and concludes by verifying the product's performance. Evaluating strength is a critical factor within this process.

I worked in the engineering field of injection molding machines for a number of years after joining the company, taking great care when handling fatigue fractures because a clamping force of 30 to 3500 tf is applied every cycle.

At that time, both small and large injection molding machines used hydraulic clamping and had large internal-pressure containers. For small machines, an operating condition of two million cycles per year is common, which means ten to the seventh power of cycles will be reached in about five years. If the stress concentration area is inside the internal-pressure container and the maximum stress value exceeds the fatigue limit, this creates a situation very much like a ticking time bomb as fatigue fracture may occur within five years after the machine is shipped. The size of the customer's mold, which is the starting point of stress generation, is not constant, so stress generation exceeding the elastic limit is completely out of the question.

Although stress around the periphery of the internal-pressure container was measured with more than 200 strain gauges at the development stage, it was extremely difficult to take actual stress measurements on the inner side of the container, so designs were based on actual results and empirical values accumulated over a long period of time multiplied with a large safety factor.

To solve this problem, Shibaura Machine introduced structural analysis to some injection molding machines in the early 1980s to

deal with a series of strength evaluation issues. When this was first introduced, we drew two-dimensional maps with a drafter, generated meshes, and then requested the Information Department to keypunch the massive amount of point group coordinate results for calculation on a large computer at night when the processing load was low. About one month passed between the start of drawing to output to obtain the results for one model. I remember the constraint conditions were limited, and there were discrepancies between simulations and actual measurement values.

The first time I heard of the finite element method was about 44 years ago when I was a student and my professor had me work on a research project analyzing the dangerous cross-section of gears using the three-node triangular element method. I remember pulling my hair out because the simulation results of my self-made program were the polar opposite of the measurement results obtained by the strain gauge. That nightmare-the discrepancy between simulation and actual measurement values-had been reproduced in our company.

Later, Shibaura Machine was able to create point groups and element data using 3D modeling and mesh generation functions, and gradually developed an interactive analysis environment using a dedicated computer. The use of triaxial strain gauges, which can calculate the maximum stress value without considering the stress direction, has improved the accuracy of measurement values.

The introduction of 3D CAD since 1997 had a tremendous effect on the development of electric injection molding machines, which the Injection Molding Machine Division worked on as a last-ditch effort, while other companies were miles ahead in the transition from hydraulic to electric injection molding machines. The 3D CAD system made it possible to seamlessly apply structural analysis to

models drawn in 3D CAD, which significantly reduced development man-hours. The analysis of a stationary platen using conventional software required at least 80 man-hours, but with the new software, analysis could be completed in 8 hours, a reduction of analysis man-hours to 1/10. Converting this reduction in analysis time alone into a launch schedule translates into a savings of two months for one model and 14 months for a series of seven model changes.

The advantage of the new software is, while conventional software required the designer to subdivide the mesh and make corrections for suspected areas where stress was concentrated, the new software automatically adjusts the shape function up to the ninth-order function while monitoring the convergence of the calculation without changing the mesh, thereby increasing the calculation accuracy.

The new software lowered the required level for analytical skills, resulting in a considerable increase in the limited number of analysts. Indeed, the constant process of comparing calculation results with actual measurements using hundreds of triaxial strain gauges and then reviewing the differences by optimizing the constraint and boundary conditions is looped. As for materials, when casting materials are manufactured from end materials of automobile sheet metal, it is necessary to extract samples from large casting materials and measure their substantive strength, and then review allowable stress standards for spheroidal graphite cast iron parts. In Digital Twin manufacturing, where manufacturing is carried out with the constant feedback of data and actual measurements, it is possible to systematically accumulate know-how on the types of dynamic loads and responses to singular points. If this loop can be maintained even if analysis software changes, quality can be guaranteed.

In the development of electric injection molding machines at that time, motion analysis and interference analysis using mechanism analysis with 3D CAD were effective tools for developers who used the toggle mechanism for the first time in a clamping unit. I remember how impressed I was when the developer created a linkage structure using 3D CAD and showed me an image where a link worked using the motion function. This was 24 years ago.

Shibaura Machine excels in the development of specialized and large machines which other companies are reluctant to deal with. Our mission is to contribute to key industries, and this is imprinted in our very DNA.

An iconic example of this which comes to mind is the “master gear

hobbing machine”. The idea of this machine had been gestating since before World War II, and in October 1953, after the unsettling days during and after the war, we completed our first machine, Japan’s first large precision hobbing machine, the HRS-500. This ultra-high precision machine eventually outclassed its competitors in Japan and abroad, and played a principal role behind the scenes in Japan’s continued dominance in the world of shipbuilding. In April 1964, the machine was awarded the Okochi Memorial Technology Prize, and most recently, in 2009, the master worm wheel, which is the heart of the hobbing machine, was designated as a Mechanical Engineering Heritage.

The second wheel built into the first machine had a cumulative pitch error of 49 μm to a diameter of 3400 mm (the table diameter was 5000 mm). Subsequent improvements in manufacturing and corrections to the wheel resulted in a cumulative pitch error of 4 μm in the seventh and final wheel (1970), an unprecedented degree of accuracy. This error factor is so accurate that a bullet fired from the Numazu factory at a clock with a diameter of 60 cm at Tokyo Station would land inside the dial. The advancement of measurement technology through strong industry-academia collaboration and the development of cutting oils have contributed significantly to the achievement of this accuracy.

The historical story of our company and employees burning with a sense of mission never fails to warm my heart. However, 17 long years passed between that first machine and the achievement of that performance in the final model.

Today, half a century since that time, we must achieve a cumulative pitch error of 4 μm since the very first machine by adopting the passion of our predecessors and using the latest technology, and thereby inspire and earn the trust of our customers.

The key to achieving this is manufacturing by DX (digital transformation) and Digital Twin. This idea is based on the concept of creating 3D CAD drawings and performing structural, mechanical, thermal, vibration, and fluid analysis. In addition to this, if we are able to correlate an actual design with its digitally represented model twin and perform simulations in a virtual space, then we can analyze what will happen in the actual design and product.

In this context, the most important thing from the viewpoint of our company’s know-how is the use of IoT to collect customer and laboratory data and feed this back into the virtual space to improve the accuracy of the simulation. This is a method called model-based engineering or model-based design, which involves thorough front-

loading. This method enables us to create an environment for agile development.

Designers may be vaguely or clearly aware of insecure and vital points during the product development stage, but if they pin their hopes on a miracle with little evidence, they will not only burn their fingers but also lose the trust of their customers.

Why not we start with a thorough simulation of vital and insecure points? I think such a simulation will help us build a trusting relationship with our customers where we can engage in data-based, guarantee-based conversations or even delve into proposed processing methods.

Companies must be able to respond quickly and easily to issues which are in line with the trends of the times, such as dramatically improving production efficiency with built-in systems and improving LCA (life cycle assessments), including decarbonization.

DX by the New "Shibaura Machine"



Director and Executive
Operating Officer

Akiyoshi KOBAYASHI



Research & Development Center,
DX Promotion Project

Hiroyuki MAEHARA

1 Introduction

The Ministry of Economy, Trade and Industry (METI) studied the actions which Japanese companies should take and the measures which the government should take in order to accelerate the digital transformation (DX) of Japanese companies, and published an interim report on December 28, 2020 as "DX Report 2"⁽¹⁾. In September 2018, METI published "DX Report: Overcoming of '2025 Digital Cliff' Involving IT Systems and Full-fledged Development of Efforts in Digital Transformation"⁽²⁾ and has been developing measures to promote DX. Nearly three years have passed since then, and the uncertainty surrounding the corporate environment has steadily increased due to circumstances such as the COVID-19 pandemic, among others.⁽³⁾ The "DX Report" released in 2018 states it is understood DX is essential to promote the creation of new business models which use digital technology to enhance future growth and competitiveness. However, the following three issues were pointed out as obstacles to its realization.

- 1) Existing systems are built for each business division, so they are not able to utilize data across the entire company.
- 2) Existing systems are built with excessive add-ons and customizations onto standard systems. As a result, existing systems are complicated and black-boxed.
- 3) There is strong resistance by people in the field against the revision of existing systems or review of operations for data utilization.

The report further points out, if we cannot overcome these challenges, we will not only be unable to achieve DX, but also will face the possibility of significant economic losses in 2025 and beyond, which is described as the "digital cliff of 2025". The report

indicates the following two points are required to achieve DX.

- 1) Eliminate the black box status of existing systems to make full use of data.
- 2) Introduce digital technology and promote the creation of new businesses and global expansion with digital native human resources playing a leading role.

The report shows a strong sense of crisis that Japan will become a loser in the competition in the digital world if it lags in its efforts to utilize data while European and U.S. platformers are expediting the ability of businesses to make full use of digital data.

When people talk about DX in the manufacturing industry the focus is on improving the efficiency and productivity of production sites through technologies such as IoT and AI. However, the heart of DX is not there. It is said DX is a shift in business model from "manufacturing, providing 'products', and getting paid by customers" to "providing 'services' and creating value together with customers to increase the value of their experience."⁽⁴⁾

In the midst of such movements, in April 2020, we changed our corporate name from Toshiba Machine to Shibaura Machine and set forth a new long-term vision. We below describe the DX to which we are aiming.

2 Shibaura Machine's Approaches to DX

2.1 Long-Term Vision and the Mission of the R&D Center

On February 4, 2020, we announced our "Long-Term Vision 2030 (Our Ideals)", which is to "achieve both resolving of social issues and enhancing corporate value by responding to the megatrends facing the global manufacturing industry with outstanding technological

innovations". In the future, we will respond to megatrends (climate change and resource scarcity, changes in population structure, and advancements in technology, among other things) through technological innovations (monetization of processes and knowledge, breakaway from in-company management, and enhancing M&A) in the form of added value of "product + service".

One of the management reform plans to achieve this goal is the establishment of the R&D Center, which will serve as the core for technological development, and will lead the company's technological development in terms of both software and hardware with the three missions shown in Fig. 1.



Fig. 1 Missions of the R&D Center

2.2 | About SHIBAURA DX

One of the missions of the R&D Center is to "promote digitization/development standardization" to realize SHIBAURA DX, our DX strategy for manufacturing.

In DX, digitized data is of utmost importance. By acquiring data on all kinds of things, sharing and analyzing the accumulated data, and utilizing the simulation results, it is possible to reproduce what exists in the real world (which is "real") in the digital space (which is "virtual") (Digital Twin). With digital data, it is even possible to realize a virtual space where the skills of master craftsmen are reproduced (digital triplet). This is the goal of SHIBAURA DX: to enable simulation not only in design, but also in all scenes of manufacturing and maintenance, thereby creating products which have never existed before and producing new value for customers.



Fig. 2 SHIBAURA DX for manufacturing

2.3 | R&D Center's Goal : "DX for Technology"

"Shibaura Machine must become a manufacturer which flexibly and quickly responds to the need for Engineer-to-Order (ETO) manufacturing with connected machines". In order to make ETO-based machines a pillar of profit, the R&D Center aims to build "ultimate manufacturing of products at high productivity with ETO", and then further aims to transform the company into a corporate group which can respond to megatrends in the global manufacturing industry by achieving "high completion degree of a product at the design stage", "highly efficient production", and "quick delivery of high value-added ETO-based machines". To achieve this goal, the company is working on two reforms: "DX for enhancement of commodity power" and "DX for improvement of productivity", as shown in Fig. 3.



Fig. 3 Transformation brought about by SHIBAURA DX

2.3.1 Transformation 1 : DX for Enhancement of Commodity Power

The point of Transformation 1 is the digitization of the development and design process.

By using digital data of 3D models which can be analyzed throughout the entire process, information from inside and outside the company can be linked, machine performance, costs, and delivery dates can be grasped in a timely manner without the need to create drawings, and planning, manufacturing, sales, and service can be addressed, even for requests for ETO-based machines. Similar work can be completed in a shorter time, allowing more focus on

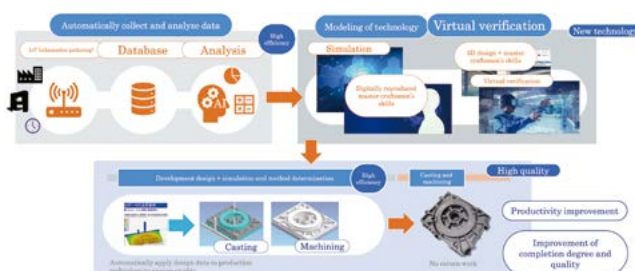


Fig. 4 Manufacturing realized with digital information

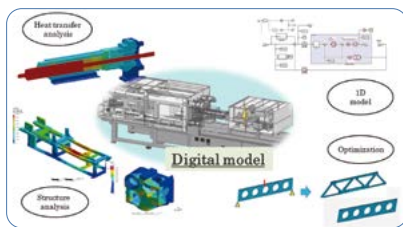
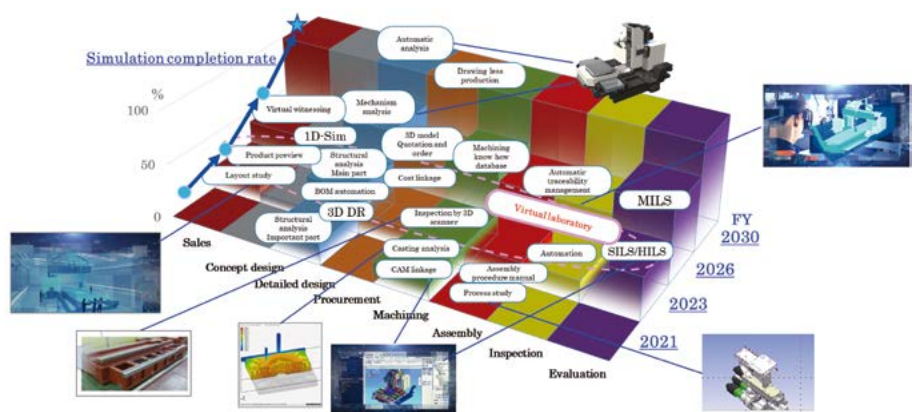


Fig. 5 Overall image of MBD (above figure) and outline of approaches (right figure)



creating new value for customers.

Model based development (MBD) is the technique for achieving this goal. This technique is used for modeling with 3D digital data, automation of boundary conditions through thorough simulation, FEM analysis of the entire machine, and coupled analysis of strength, mechanism, and heat transfer, among other things, with the aim of eliminating prototypes.(Fig. 5)

2.3.2 Transformation 2 : DX for Improvement of Productivity

The point of Transformation 2 is digitization of business processes.

In order to make digital data usable throughout the entire process, it is essential to digitize information and comprehensively manage data (base) in a highly productive manufacturing infrastructure. In this case, data is connected like a thread, and the data created in the upstream process is utilized in the downstream process (digital thread).

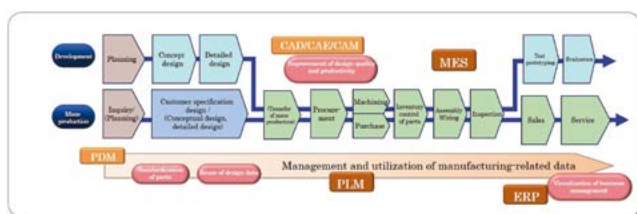


Fig. 6 Digital thread

2.3.3 SHIBAURA Virtual Lab

We are planning to establish the SHIBAURA Virtual Lab with a showroom in the Sagami Plant as a base for “providing services”. To realize SHIBAURA DX, the Lab will play a role as a base for research and development equipped with the most advanced environment, as a creative office for remote work, industry-academia collaboration, and IoT/AI utilization, and as a value co-creation base for creating new values with our customers.

3 Sustainable Future and SHIBAURA DX

3.1 How Does DX Relate to the SDGs?

Even more than “DX”, the “SDGs” are increasing their presence as keywords in business.

While tackling the SDGs leads to a sustainable society and thereby contributes to the public good, at the same time it has the added benefit of reducing costs due to increased efficiency and sustaining business with profits in compensation for providing value to customers. The realization of DX can be a means to that end. Therefore, the relationship between DX and the SDGs is of great importance, not only introducing the latest technologies when promoting DX, but also in examining how and what we want to transform.

It can be said DX has a significant role to play in achieving the SDGs by designating goals for the realization of a sustainable society.

3.2 Contribution to Decarbonization and Resolution of SDG Issues

As global sustainability is now being actively considered, and as the world has begun feeling the length of a time axis extending beyond one's own life into the future, customer value standards are also changing. The significance of company efforts to realize sustainability is dramatically increasing.

Fig. 7 shows the direction of Shibaura Machine's efforts toward sustainability, and Fig. 8 shows the overall image of the efforts.

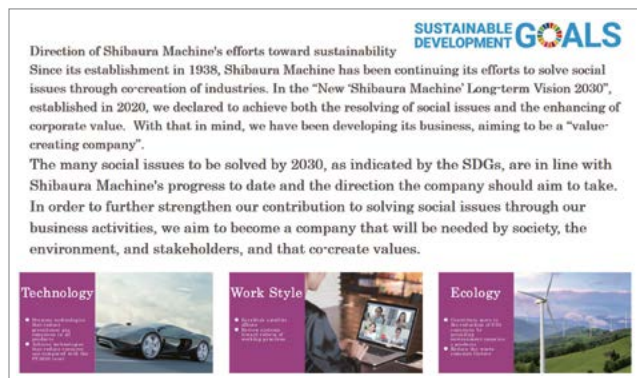


Fig. 7 Shibaura Machine's efforts toward sustainability



Fig. 8 Overall image of the efforts to achieve SDGs

We will make efforts on development to solve social issues, starting with the SDGs, and aiming at future-oriented manufacturing.(Fig. 9)

4 Conclusion

In the above we have introduced an overview of Shibaura

Machine's approach to DX and how it clearly is related to our contribution to the SDGs. This technical report gives you some of our specific initiatives. We hope this will help readers understand the new Shibaura Machine, lead to creation of customer value, and help us receive advice from the customer's perspective.

DX will transform a company's products, services, and business models through the use of digital technology and data. Meanwhile, DX holds the promise of changing the market structure itself and solving social issues. The transformation into a sustainable society can use DX to create a so-called ecosystem which goes beyond the company's borders to reform the value chain. While realizing DX, Shibaura Machine will continue to contribute to the solution of social issues.

References

- 1) <https://www.meti.go.jp/press/2020/12/20201228004/20201228004.html>
- 2) https://www.meti.go.jp/shingikai/mono_info_service/digital_transformation/20180907_report.html
- 3) Isao FUKUMOTO, "Explaining the DX Report 2. Two years since the 'Digital Cliff of 2025'. What is the current situation of domestic companies? and what will become of them?", installment dated January 19, 2021 in the series "Essay on Business Practices for the 4th Industrial Revolution" in "Business + IT", SB Creative.
- 4) Source: Isao FUKUMOTO, Keiichiro NABENO, Tomoki KOSAKA, "Digital First Society", Nikkan Kogyo Shimbun, 2019.

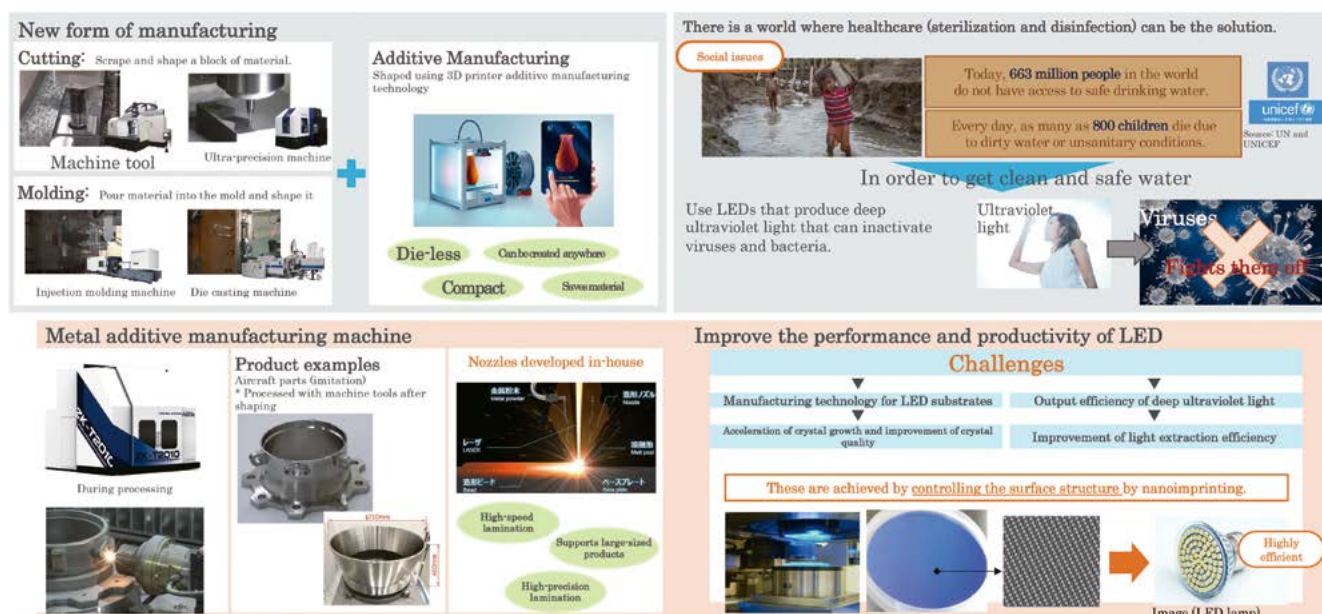


Fig. 9 Aiming at future-oriented manufacturing

Research of Optimized Grease Film on Sliding Surfaces

In this research, we confirmed it is possible to estimate the lubrication film thickness on a sliding surface based on the dimensionless central film thickness formula in EHL theory and by additionally applying the grease film thickness and the correction formula for temperature dependence of oil viscosity. Based on the above, we identified the conditions for achieving stable lubrication film with appropriate surface roughness under a specific range of material, contact pressure, and sliding speed. This confirmed the possibility metallic material, such as spheroidal graphite cast iron, which we did not use for the sliding surface, can be used.



Research & Development Center
Research & Development Department

Hiroyuki ONUMA

1 Introduction

Shibaura Machine manufactures industrial machinery having sliding surfaces which allow rotation, direct advance, etc. to achieve functions. Those sliding surfaces are often made of copper alloy which can resist damage and they are lubricated with oil or grease. In addition, most of Shibaura Machine products are large machines, and their principal structural parts are frequently made of spheroidal graphite cast iron, which has strength and toughness and can be produced in-house.

Responding to a recent trend, Shibaura Machine is striving to take measures to reduce environmental loads with the aim of achieving the SDGs and considers it a mission to provide environment-conscious products through corporate activities. As part of this effort, it is important to take measures to reduce the use of lubricants and adopt materials with low environmental loads. When considering the environmental load unit of copper alloy and cast iron, the CO₂ emission intensity of copper alloy based on physical quantity is 4.49 tons, and the CO₂ emission intensity of cast iron is 3.49 tons which is lower than that of the copper alloy. Since cast iron is produced in-house, CO₂ emissions which occur during the transportation of parts can be reduced.

Conventionally, contact pressure and PV value loads are mainly evaluated at the design phase of the sliding surface. However, by evaluating sliding properties according to the lubrication state of the sliding surface, it may be possible to reduce the use of lubricants and adopt cast iron. In this research, we estimate the thickness of lubrication film on the sliding surface based on the ElastoHydro-dynamic Lubrication theory (hereafter, referred to as “EHL theory”) and by performing experiments, and we confirmed the optimization

of lubricants and the possibility of selecting different materials.

2 EHL Theory

2.1 Oil Lubrication

The EHL theory was established based on a great deal of research and is described in various types of literature, and therefore, detailed explanation of the EHL theory is omitted. In brief, EHL theory is used for calculating the thickness of oil film accompanied by elastic deformation of the contact surface based on the Reynolds fluid-film lubrication theory which considers viscosity of lubricants, and EHL theory is suitable for studying the lubrication state in cases when loads are concentrated in a small area of contact.

In the wear test, a point contact occurs on the sliding surface when viewed from a micro perspective. As a basic formula, the formula (1) for obtaining the dimensionless center film thickness resulting from the point contact, which is referred to as “Hamrock-Dowson formula”, is used.

$$H_c = 2.69G^{0.53}U^{0.67}W^{-0.067}[1 - 0.61\exp(-0.73k)] \quad (1)$$

where G denotes a material factor, U denotes a speed factor, W denotes a load factor, and k denotes an ellipticity of contact ellipse. G , U , and W are expressed as shown below.

$$G = \alpha E'$$

$$U = \eta_0 u / E' R$$

$$W = w / E' R$$

α : Pressure viscosity coefficient

E' : Equivalent elastic coefficient

η_0 : Normal-pressure base oil viscosity

u : Flow rate of lubricant

R : Axial equivalent curvature radius

w : Normal direction load

This applies to cases where lubricants are oil. As for grease, explanation will be given in the next section.

2.2 | Grease Lubrication

Concerning the thickness of grease lubrication film, a regression formula (2) based on the measured value has been established.¹⁾

$$H_g / H_{oil} = (1 + m^n M')^{0.67} \quad (2)$$

H_g : Dimensionless grease film thickness

H_{oil} : Dimensionless base oil film thickness obtained by the formula (1)

wherein,

$$M' = k_2 / k_1 (u / h_{oil})^{n-1}$$

$$m = (1 + M'/n) / (1 + M')$$

The following are physical properties of grease:

k_1 : Viscosity of base oil

k_2 : Plastic viscosity

n : Exponent

h_{oil} : Center film thickness

Using these properties, the thickness of lubrication film on the sliding surface is obtained.

3 Experiment

3.1 | Experimental Equipment

3.1.1 | Film Thickness Measurement Test

To measure the thickness of grease film, we used an EHL oil film thickness measuring instrument which is based on optical interferometry (Fig. 1). In this method, a steel ball is pressed onto the surface of the glass disk coated with grease and rotated, and then the thickness of generated lubrication film is measured. In addition, by changing the rotation speed, the thickness of lubrication film at each speed was measured.

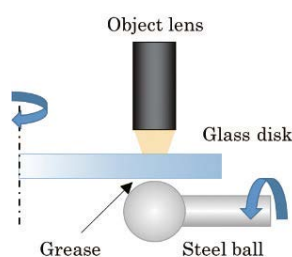


Fig. 1 EHL oil film thickness measuring instrument

3.1.2 | Wear Test

To confirm the galling properties of metallic material, we used a pin-on disk scuffing tester. Fig. 2 shows a schematic diagram. This machine is designed such that a pin test piece is pressed onto a disk test piece by a pneumatic cylinder and the disk test piece is rotated. Using this machine, the amount of wear and friction force during operation were measured as the scuffing properties of the material by means of a displacement gauge and a load cell provided on the handgrip portion of the pin test piece. Temperature of the pin test piece was also measured by a thermocouple.

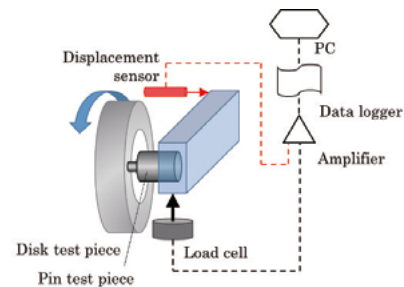


Fig. 2 Schematic diagram of the pin-on disk scuffing tester

3.2 | Measurement of Film Thickness

3.2.1 | Conditions for Film Thickness Measurement

To measure the film thickness, we used a chrome-coated siliconized glass disk and a steel bearing ball. In addition, the maximum surface pressure was set to 0.55 GPa, and rolling speed was changed within the range between 0.002 m/s and 1.0 m/s. We used grease containing lithium-based or urea-based thickening agents to measure the thickness of lubrication film.

3.2.2 | Measurement Results

Fig. 3 shows the relationship between the ratio of the measured film thickness to the theoretical film thickness, obtained by formulas (1) and (2), and the rolling speed. It also shows the image of changes in theoretical film thickness according to the rolling speed.

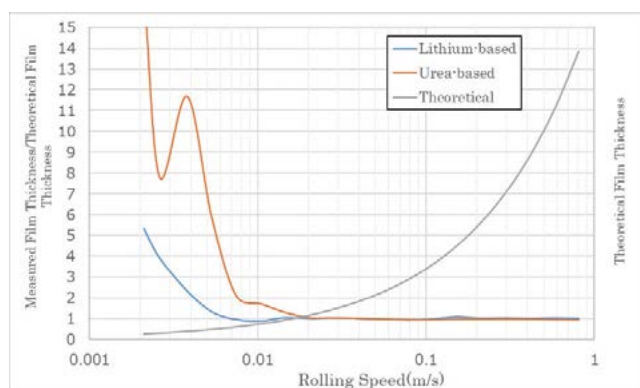


Fig. 3 Results of film thickness measurement

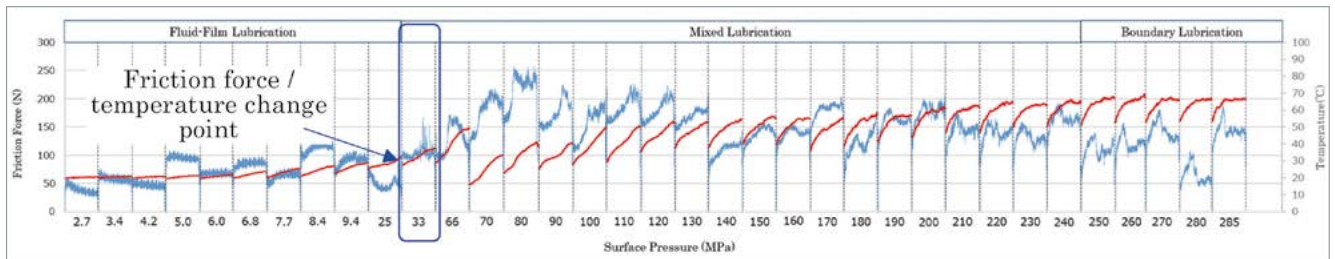


Fig. 4 Measurement results of wear test (copper alloy)

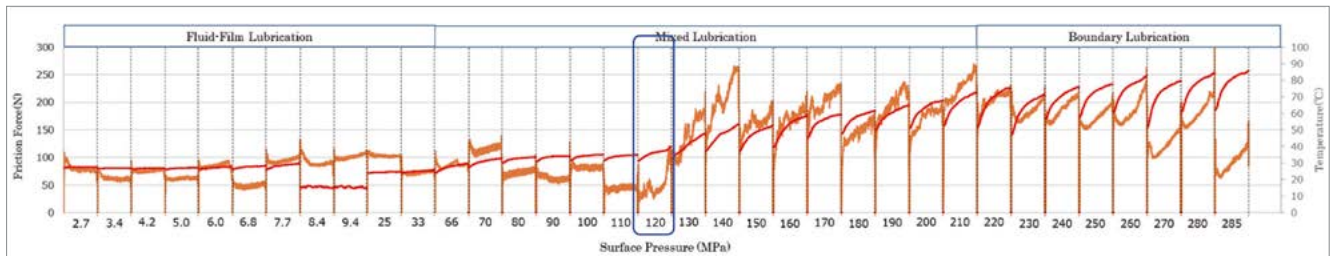


Fig. 5 Measurement results of wear test (spheroidal graphite cast iron)

According to Fig. 3, the ratio of the measured EHL film thickness to the theoretical film thickness is around 1 at the rolling speed of 0.02 m/s or higher. This indicates the measured film thickness is almost the same as the theoretical film thickness. However, at rolling speeds of 0.01 m/s or lower, the ratio of the measured film thickness to the theoretical film thickness is more than 1. This indicates the actual film thickness tends to become thicker than the theoretical film thickness. It is considered necessary to review the theoretical film thickness at a low-speed range.

3.3 | Wear test

3.3.1 | Conditions for wear test

Thermally-refined chrome molybdenum steel disk test pieces, spheroidal graphite cast iron pin test pieces, and copper alloy pin test pieces were used for the test.

Rotation speed of the disk test piece was set to 180 min^{-1} , and surface pressure was changed step by step within a range between 2.7 MPa and 280 MPa by changing the pressing force by means of a pneumatic cylinder.

As a lubricant, lithium-based grease was applied to the disk test piece. In addition, to uniformize the lubrication state under each surface pressure condition, grease was applied to the disk test piece every time the surface pressure condition was changed.

This research was not conducted to observe the degree of progress of wear occurring between metals. However, it is important to prevent the occurrence of wear and adhesion, so we measured the friction force and temperature. (Fig. 2)

3.3.2 | Measurement Results

Fig. 4 and Fig. 5 show the measurement results when copper alloy and spheroidal graphite cast iron were used. The friction force and temperature of both materials are stable at low surface pressure. However, the friction force of copper alloy became significantly disordered in the latter part of the surface pressure of 25 MPa, and that of spheroidal graphite cast iron became disordered at the surface pressure of 120 MPa. Accordingly, temperature also increased. Fig. 6 shows the results of observing the spheroidal graphite cast iron test piece at that time by means of a SEM. According to the SEM images, the spheroidal graphite exposed on the surface of the pin test piece is missing, and scratch-like streaks can also be seen. This indicates abrasive wear resulting from contact is occurring.

According to the measurement data, disorder of the friction force and the increase of temperature in copper alloy occurred at lower surface pressure when compared with spheroidal graphite cast iron. During testing, as the surface pressure increased, metal contact noise, vibration, etc. were greater in spheroidal graphite cast iron.

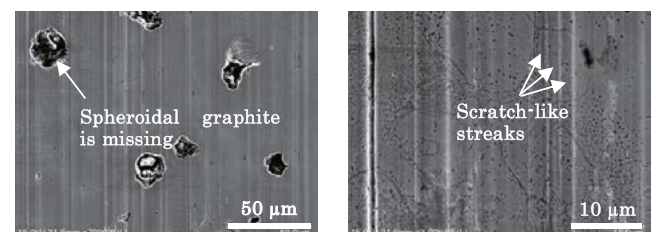


Fig. 6 Observation of the surface of the pin test piece

4 Consideration

4.1 Grease Film Thickness

A gap between the theoretical film thickness and the measured EHL film thickness at rolling speeds of 0.01 m/s or lower results from the composite effects of viscosity change and the deposition of the grease thickening agent.

In the above-mentioned Hamrock-Dowson viscosity formula (1) and the regression formula for grease (2), viscosity is regarded as being constant. This means the base oil of grease is considered as a Newtonian fluid. It is well-known the viscosity of grease is close to the viscosity of base oil at high shear rates, and grease is considered to be a non-Newtonian fluid whose viscosity changes as the shear rate increases.

Change of viscosity of non-Newtonian fluid can be obtained by the Carreau-Yasuda viscosity formula (3).

$$\eta_{\infty} = (\eta_0 - \eta_{\infty}) \left[1 + (\lambda \dot{\gamma})^{\alpha} \right]^{\frac{n-1}{\alpha}} \quad (3)$$

η_0 : Zero shear viscosity

η_{∞} : Infinite shear viscosity

$\dot{\gamma}$: Shear rate

α : Pressure viscosity coefficient

λ : Time constant

Formula (3) is applied to the theoretical film thickness included in the results of film thickness measurement mentioned above. (Fig. 7)

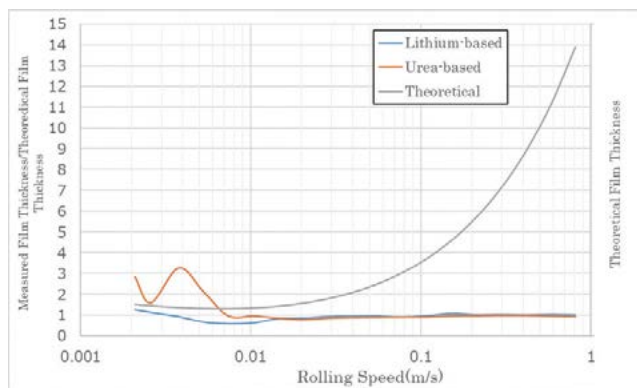


Fig. 7 Results of film thickness measurement (correction of non-Newtonian fluid)

When urea-based grease was used, the ratio of the EHL film thickness to the theoretical film thickness in the low-speed range is close to but more than 1. This results from the deposition of the grease thickening agent on the contact surface. This indicates urea-based grease forms thick film in the low-speed range where the EHL film becomes thin.

4.2 Wear Test

Based on the results of the wear test, we confirm the lubrication state using the film parameter under each condition as an index. Generally, the film parameter is expressed by the ratio of the theoretical film thickness to the standard deviation of composite roughness of root-mean-square roughness of each surface (4).

$$\Lambda = h_{\min} / \sqrt{\sigma_1^2 + \sigma_2^2} \quad (4)$$

Because composite roughness is a standard deviation, the height of roughness protrusion is 3 (3 sigma) or less, and two planes are completely separated by the lubrication film when $\Lambda > 3$. This state is referred to as "fluid-film lubrication". When $\Lambda < 1$, two metal planes interfere with each other almost 100% and this state is referred to as "boundary lubrication". In addition, in-between the lubrication state is referred to as "mixed lubrication".

The lubrication state estimated from the film parameter is described in the test results shown in Fig. 4 and Fig. 5. Herein, in the calculation of the theoretical film thickness, the Wasler-ASTM formula was used to correct the temperature dependence of viscosity. According to Fig. 4 and Fig. 5, in the area of fluid-film lubrication, the friction force of both copper alloy and spheroidal graphite cast iron shows stable behavior, and in the area of mixed lubrication where both surfaces start to come in contact with each other, the friction force becomes disordered and temperature increases. This indicates it is important to check the film parameter at the design phase and determine necessary surface roughness.

When compared with spheroidal graphite cast iron, the friction force of copper alloy fluctuated at lower surface pressure. Because contact noise and vibration did not change even when surface pressure increased, scuffing may not easily occur even though wear progresses.

5 Conclusion

We obtained the following findings from this research:

- We have confirmed it is possible to estimate the lubrication state by focusing the thickness of grease lubrication film based on the EHL theory and by use of the correction formula for temperature dependence of viscosity.
- It has been clarified the evaluation using the film parameter at the design phase is effective. Also, the design criteria for determining surface roughness has been clarified.

- c) Urea-based grease is effective depending on the sliding speed from the aspect of forming appropriate film thickness.
- d) We have confirmed the possibility spheroidal graphite cast iron, etc. can be applied to the sliding surface of industrial machinery. The remaining issue is to confirm a material use limit for each surface roughness from the aspect of the PV value of the sliding surface.

References

- 1) Tsuyoshi Kochi, Ryosuke Ichimura, Michitaka Yoshihara, Daming Dong, and Yoshitsugu Kimura, "Film Thickness and Traction in Soft EHL with Grease", Tribologist, 61, 12 (2016), 874.

Development of PVD + CVD Vacuum Integrated System ; Application to Moisture-Resistant Multilayer Reflective Film for Heads-up Display Mirror



Research & Development Center
Research & Development Department

Kazuhiro FUKADA



Research & Development Center
Research & Development Department

Satoshi FUKUYAMA



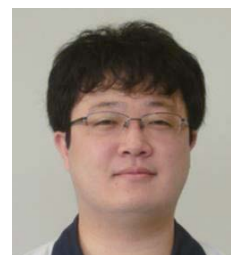
Research & Development Center
Research & Development Department

Takeshi NAMBA



Research & Development Center
Research & Development Department

Yoshiaki KURIHARA



Research & Development Center
Research & Development Department

Rintaro SUEKI

We developed a head-up display (HUD) mirror film deposition system and utilized CAE gas-fluid analysis to optimize process conditions. The plasma generator has an advantage in film formation on a resin molded product because the workpiece is not easily damaged and a thicker SiO₂ film can be formed with a short tact due to the high plasma density. Due to these advantages, the plasma generator can be applied not only to HUD mirror film formation, but also to AR coating and hard coating, among other things.

1 Introduction

Finished molded products are manufactured by injection molding machines by applying decoration and adding functionality by means of various types of surface treatment. Recently, not only metal film decoration applications but also techniques which provide functional film properties have become indispensable in various fields including optical, medical, biotechnology, electronics, and automobile industries.

Shibaura Machine has recently developed a vacuum deposition system as a turnkey system which can be functionally interconnected with a molding machine. Generally, the vacuum deposition system requires long tact time and sometimes causes the deterioration of quality resulting from the stock of molded products. Herein, we will report about the development of the vacuum integrated deposition system which can form high-quality film in the medium vacuum area with very short tact time which cannot be achieved by conventional vacuum deposition systems. We will also report about the application of this new system to form optical film.

2 Deposition System

The newly developed vacuum integrated deposition system is so designed so the plasma treatment zone for performing surface

modification and polymerization and the sputtering zone for forming metal film are integrated in one treatment room. In the conventional vacuum deposition system, the treatment room is evacuated for a long period of time to generate a high vacuum condition before the process starts. However, to link the tact time with the injection molding machine, our newly developed deposition system has achieved a process which can satisfy required performance in the medium vacuum area which is generated in a significantly reduced exhaust time. Features of this deposition system are below described.

- ① This is a vacuum integrated deposition system with a processing chamber consisting of two zones to enable the plasma treatment and the sputtering process.
- ② When compared with conventional vacuum deposition systems, it is possible to achieve significantly higher productivity.
- ③ It is possible to form film on resin because thermal load is small.
- ④ It is possible to achieve high-quality plasma polymerization and highly efficient plasma modification by use of newly-structured plasma electrodes.
- ⑤ It is possible to perform high-quality vacuum deposition without being affected by gas generated from resin immediately after the resin molding process.

2.1 Basic Principles

Basic principles of plasma treatment and sputtering technique will

be herein described. As shown in Fig. 1, by applying high-frequency voltage to gas present between electrodes, electrons collide with gas molecules, thereby generating plasma.

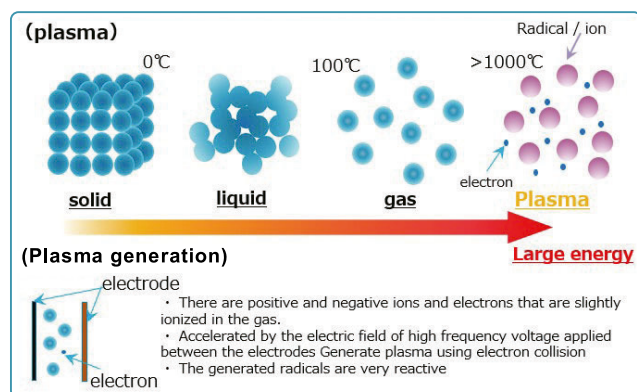


Fig. 1 Plasma

Generated plasma has significantly high energy which enables high-quality polymerization and surface modification.

As shown in Fig. 2, sputtering is a dry plating technique wherein target metal for forming thin film is placed in a vacuum chamber, the target metal is bombarded with a rare gas element (argon etc.) ionized by high voltage, causing metal atoms to be removed from the target metal surface and reach the substrate, thereby forming film.

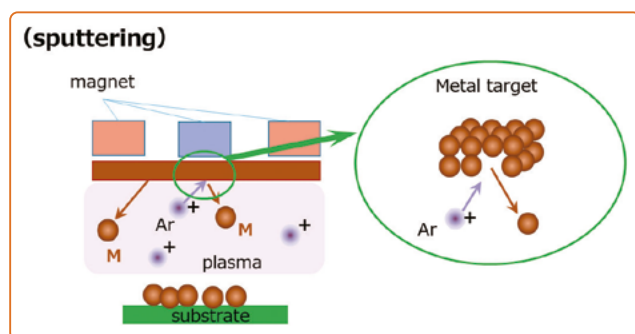


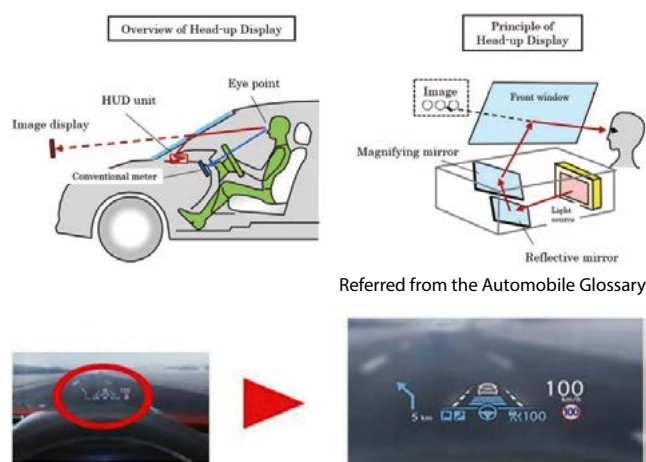
Fig. 2 Sputtering

3 Application of the New System to Optical Parts for Automobiles

As a turnkey system made by Shibaura Machine, we focused mirror (optical film) for the heads-up display (HUD) (Fig. 3) and studied the enhanced reflective film formed by the vacuum deposition system on the surface of high-quality molded products manufactured by the injection molding machine.

3.1 Background of Development

In many countries, there have been moves to mandate the installation of a HUD in new cars, which will likely result in future market growth.



Referred from Panasonic website

Fig. 3 Head-up display

Technically, the HUD is required to display more information at high luminance without strain, and it is necessary to increase the size of two reflection mirrors loaded on the HUD and achieve high reflectance and low strain.

The reflection mirror of the HUD is metal reflective film created by forming metal film on PC (polycarbonate) of the substrate. Higher reflectance can be achieved by use of enhanced reflective film in which layers of film having different refractive indexes are laminated (Fig. 4).

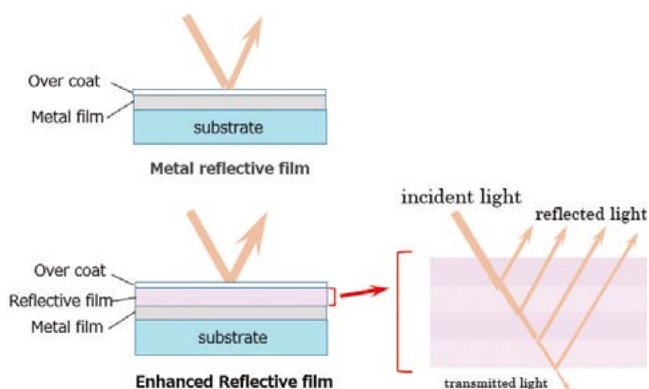


Fig. 4 Enhanced reflective film

To achieve high productivity, the vacuum deposition system developed for the HUD is a carousel type system consisting of two-target magnetron sputtering equipment loaded with metal targets, i.e. aluminum (Al) and niobium oxide (Nb_2O_5), and plasma electrodes which can form SiO_x overcoat by plasma-enhanced chemical vapor deposition (P-CVD) using HMDSO as raw material. It is possible to produce high-quality mirrors with high reflectance and less strain by means of vacuum integrated treatment of the enhanced reflective film formed by the lamination of Al, Nb_2O_5 , and SiO_x film generated by sputtering and SiO_x overcoat.

Considering the solution to the above-mentioned issues and the future scalability, Shibaura Machine developed a vacuum deposition system having features as below described.

- Vacuum integrated system which combines magnetron sputtering (2 targets) and CVD processes;
- Adoption of high-density plasma electrode CVD to form film with a low refractive index;
- Reversal mechanism type two-carousel system to perform automated operation between the injection molding machine and the deposition system;
- Maximum dimensions of target workpiece: L400 mm × W200 mm × D125 mm (18 combiner-type workpieces can be loaded).

The HUD mirror requires the formation of film with reflectance of at least 90% in the visible-light area. Generally, such film is formed by combining three types of optical thin film, which are metal film, film with a low refractive index, and film with a high refractive index, formed on a polycarbonate molded product. Shibaura Machine adopted Al (DC sputtering), SiO₂ (CVD) and Nb₂O₅ (DC sputtering) for the film, respectively. The reason for this is if three types of film are formed by a sputtering technique, an RF method needs to be performed for SiO₂ and Nb₂O₅, and accordingly, each of the three

【Appearance of prototype machine for head-up display mirror】



【Refractive coating flow】

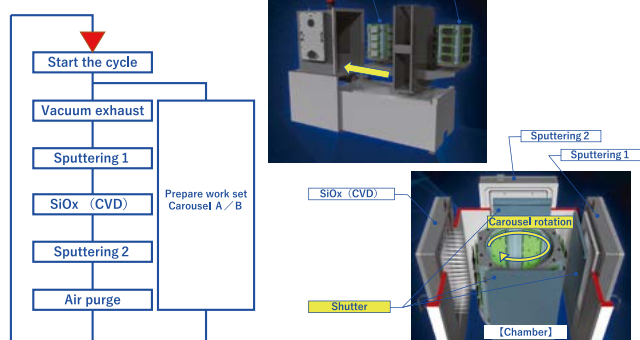


Fig. 5 Vacuum deposition system for HUD

types of targets requires an individual power source; however, in the Shibaura Machine process, the CVD technique is adopted to form the SiO₂ film, and as for the Nb₂O₅ film, oxygen-deficient Nb₂O₅ to which a DC power supply can be applied is used as target material. As a result, the number of power sources can be reduced, which reduces cost.

This system is capable of using more than three kinds of material to form film, and also forming film other than SiO₂ film by the new plasma generator CVD system, and further performing chemical decoration using O₂ gas, N₂ gas, H₂ gas, etc. It is also possible to increase adhesion of the HUD mirror thin film by performing chemical decoration on the surface of the injection molding material.

3.3 Design and Improvement using CAE

At the design phase of the vacuum deposition system we performed fluid analysis of the plasma condition which could greatly affect CVD, including; diffusion, heat, and mass partial ratio, and analysis of the magnetic field of the magnet for the sputtering process so as to achieve an efficient system most suitable for the processes. Herein, the gas-fluid analysis will be described in detail.

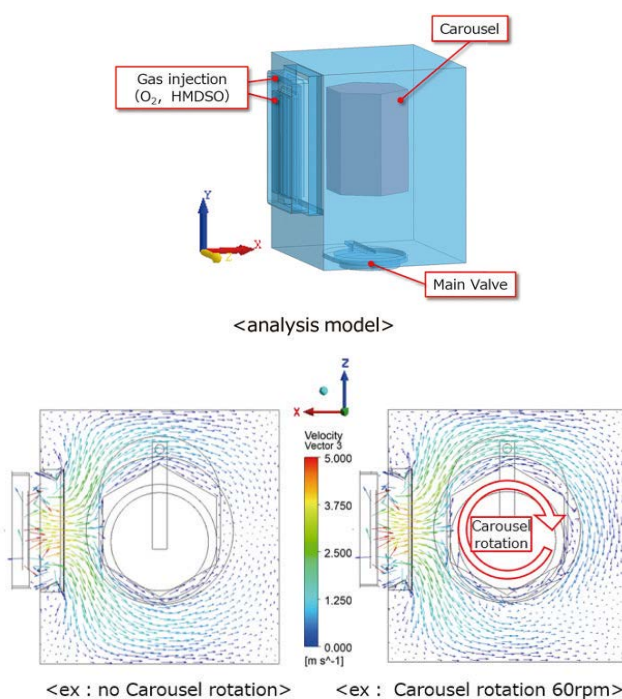


Fig. 6 Analysis of gas flow in the chamber

Fig. 6 shows the results of analysis of feed gas flow under process pressure (medium vacuum) conditions both in the case where the carousel rotates and where the carousel does not rotate. Fig. 6 indicates material gas is efficiently fed to the products placed in the carousel by rotating the carousel.

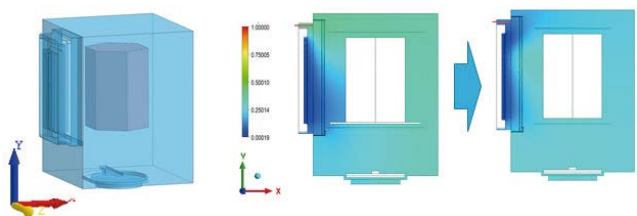


Fig. 7 Analysis of CVD feed material in the chamber

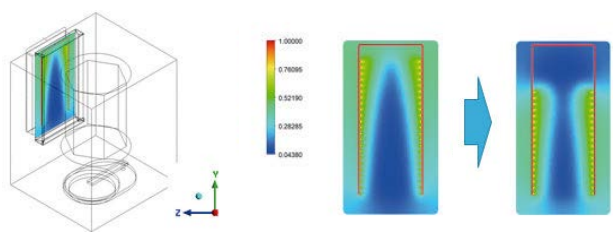


Fig. 8 Analysis of CVD feed material in the raw material feed unit

In the CVD, SiOx film is formed by means of the reaction of oxygen radicals generated by using raw material and plasma. To form desired SiOx film, it is necessary to uniformize the mass ratio of oxygen radicals which react with the material. Fig. 7 and Fig. 8 show the results of calculating the mass partial ratio in the chamber and in the raw material feed unit. At the initial development phase, large reflectance distribution in the vertical direction according to location was confirmed on the samples placed in the carousel. As shown in Fig. 9, results of analysis of the mass partial ratio in the chamber supported the distribution of mass partial ratio of actual samples. Thus, by optimizing the raw material feed unit which affects the distribution in the chamber based on the analysis results, the distribution has been successfully improved.

3.4 Results (Performance Evaluation and Trial Production Results)

The HUD mirror film was formed on a polycarbonate substrate under the SiO₂ film formation conditions optimized based on the above results, and the reflectance was measured. Fig. 10 shows the results.

In Fig. 10, the horizontal axis indicates wave-length and the vertical axis indicates reflectance. The black line indicates sample film formed on the upper stage, the blue line indicates sample film formed on the middle stage, and the red line indicates sample film formed on the lower stage.

As shown in the drawing, the general reflectance standard of the HUD mirror (reflectance of 90% between the wave length of 450 nm and 650 nm) has been achieved in the sample film formed on the upper, middle, and lower stages of the carousel. When 30 batches of

film were formed using the same recipe, all the batches satisfied the reflectance standard. In addition, in the constant-temperature high-humidity test, reflectance of the HUD mirror thin film is within the standard, which indicates the mass production criteria can be satisfied.

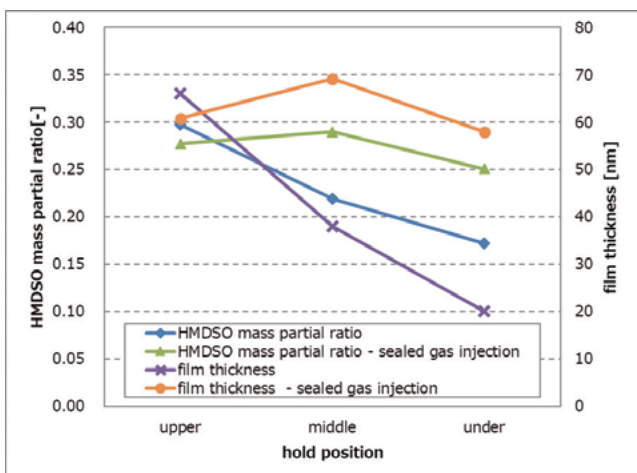


Fig. 9 Comparison between the SiO₂ film thickness and the mass partial ratio of precursor gas

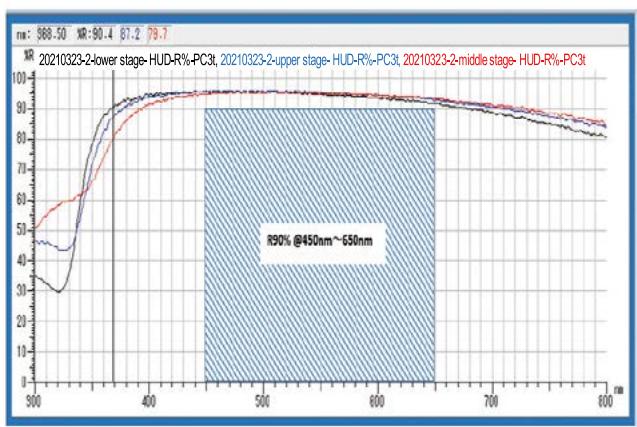


Fig. 10 Reflectance of HUD mirror

4 Conclusion

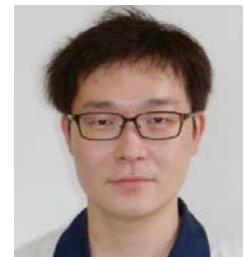
Unlike general plasma generators, the plasma generator adopted for this system does not easily cause damage to the workpiece and it is therefore advantageous in forming film on resin which tends to deteriorate. Since plasma density is high, it is possible to form thick SiO₂ film with short tact time. With these advantages, the plasma generator can be applied not only to the formation of HUD mirror film, but also to AR coating, hard coating, water-shedding coating, among other things.

References

- | | |
|--------------------|---------------------------------|
| Patent number | Patent registration No. 6625728 |
| Title of invention | Plasma generator |

Numerical Analysis on an Extrusion Process in a Twin-Screw Extruder

Twin-screw extruders are very versatile continuous polymer processing machines which contribute to both energy and environmental conservation and make it possible to manufacture many kinds of plastics. This article reports the study on numerical analysis to grasp phenomena and increase efficiency in an extrusion process. This article is a summary of the doctoral dissertation the author wrote when completing the doctoral course at Kanazawa University.



Metal & Plastics Industrial Machine Company
Extrusion Machine Engineering Department

Masatoshi OHARA

1 Introduction

In recent years, plastics are attracting both producer and consumer attention in the fields of energy and environment. The Co-Rotating, Fully Intermeshing Twin-Screw Extruder TEM Series, which Shibaura Machine manufactures and sells (hereafter called the Twin-Screw Extruder), is mainly used to process or manufacture plastics. The Twin-Screw Extruder is an extrusion molding machine equipped with screws featuring especially high kneading performance and versatility. The Twin-Screw Extruder is configurable in an almost infinite combination of screws and barrels particularly because these key components are modularized. Fig. 1 shows typical screw elements.

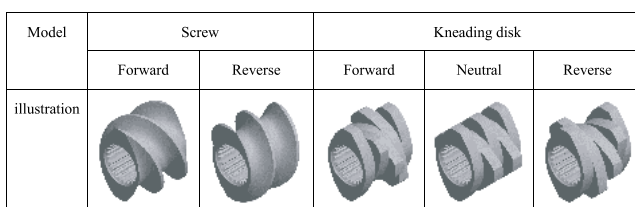


Fig. 1 Screw elements

These characteristics allow the Twin-Screw Extruder to be adaptable to a wide variety of materials, but to achieve superior kneading performance, it is necessary to design and select the most suitable configuration for materials and specifications. In such a configuration design process, a trial-and-error approach is conventionally taken so the mix of raw materials, screw configurations, and operating conditions are adjusted to achieve the desired product quality. However, from the perspective of the fields of energy and environment, demand for product development has been increasing in recent years. Therefore, it is desirable to establish a configuration design process of the Twin-Screw Extruder based on theoretical

analysis for the purpose of improving product quality, reducing waste of raw materials, and shortening development lead time.

In this study, 2.5D FEM, which has been developed in the injection molding CAE field, was applied to the Twin-Screw Extruder to propose a practical solution to the simulation of a flow of resin, and then comparison and verification were made through experiments in cooperation with HASL Co., Ltd.

2 Theory

The Twin-Screw Extruder is conventionally analyzed only by means of 1D FAN and 3D numerical analysis. 1D FAN is a method of quickly calculating a leveled fill ratio and pressure distribution in the axis direction of the screw across the extruder by factoring screw shapes. Also, 3D numerical analysis is a process of performing physical calculation in detail by three-dimensionally discretizing fluid resin into grids or particles. In this study, the Hele-Shaw flow model is applied. The Hele-Shaw flow model is a two-dimensional flow of incompressible resin in a thin layer, and predominantly affected by viscosity. This article will propose an approach of efficiently calculating the fluidity of resin not only in the axis direction but also the circumference direction of the screw across the extruder. Fig. 2 illustrates the overview of the configuration of

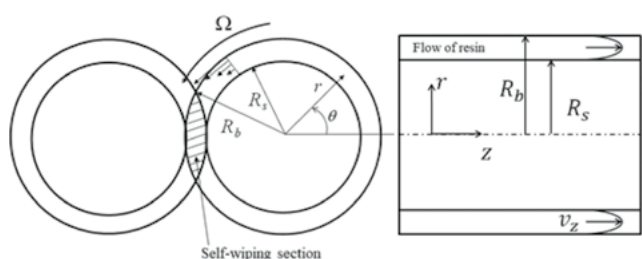


Fig. 2 Hele-Shaw flow model in the Twin-Screw Extruder

the Twin-Screw Extruder considered in the analysis.

In Fig. 2, r represents the direction of the radius of the screw, z the axis direction, θ the rotational direction, R_s the radius of the screw, and R_b the radius of the barrel. The equation below is true on the screw surface.

$$v_\theta = 0, v_z = 0 \text{ at } r = R_s$$

In the equation, v_θ and v_z represent the flow velocity in the θ direction and the z direction respectively. In addition, assuming the relative velocity of the barrel with respect to the rotating screw is Ω , the following equation is true on barrel surface R_b .

$$v_\theta = R_b \Omega, v_z = 0 \text{ at } r = R_b$$

Applying the Hele-Shaw flow model results in $v_r = 0$. Also, v_θ and v_z are functions of only r . Since the flow velocity in the direction of the normal is ignored, the number of variables necessary for calculation is reduced, and consequently, a time for calculation is shortened.

2.5D FEM discretizes two adjacent cylindrical columns into finite elements along the outsides of the screws as shown in Fig. 3. Where the elements of the two cylindrical columns overlap, the flow of resin between them can be calculated.

This has made it possible to analyze the fluidity of resin not only in the axis direction but also in the circumference direction of the screw across the screw element.

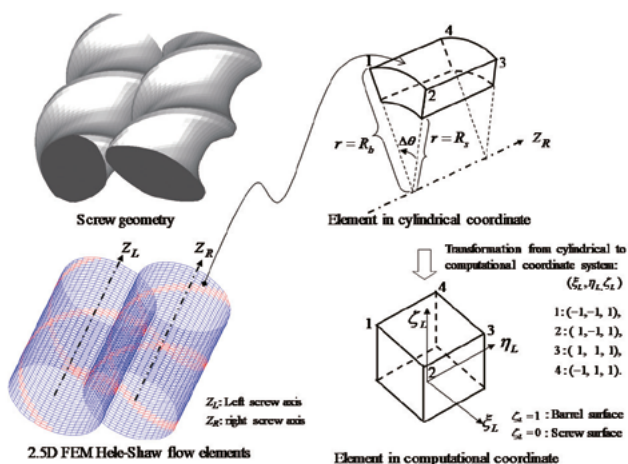


Fig. 3 2.5D FEM Hele-Shaw flow model element for the Twin-Screw Extruder

3 Experiment and Verification

3.1. Experiment and Verification Based on Resin Pressure Distribution

In the experiment, the results obtained through the analytical approach proposed herein were validated through the measurement

of resin pressure distribution. The flow channel at the exit of the Twin-Screw Extruder was narrowed to make resin reside. Then pressure caused by the flow of resin was measured using a pressure gauge.

In the experiment, homo polypropylene (F-704NP, MFR 7.0g/10min, prime polymer) was used. Also, a rheometer (MCR 302, Anton Paar) was set up to measure the viscoelasticity of the material used in the analysis. The fitting of the obtained complex viscosity data was performed using the Cross Model, constitutive equation of viscosity. In addition, TEM-26SX (L/D=64) was used in the experiment. Fig. 4 illustrates the screw configuration and the positions of pressure gauges used in the experiment. (See 1, 2, 3, and H in the figure below.)

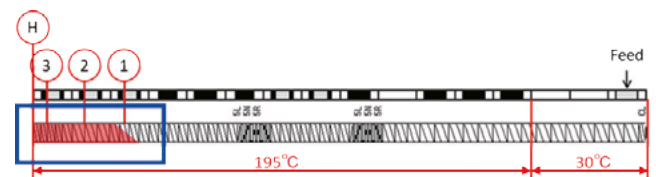


Fig. 4 Device configuration

Fig. 5 shows the results obtained when pressure at the exit was increased up to 5.5MPa with a throughput of 10kg/h and a screw speed of 70min⁻¹. The solid line represents analytical values, and each dot an experimental value. An experimental value is an average over time while an analytical value is a mean value of pressure distribution in the circumference direction of the screw. As a result of the experiment, it was revealed the analytical values were in good agreement with the experimental values.

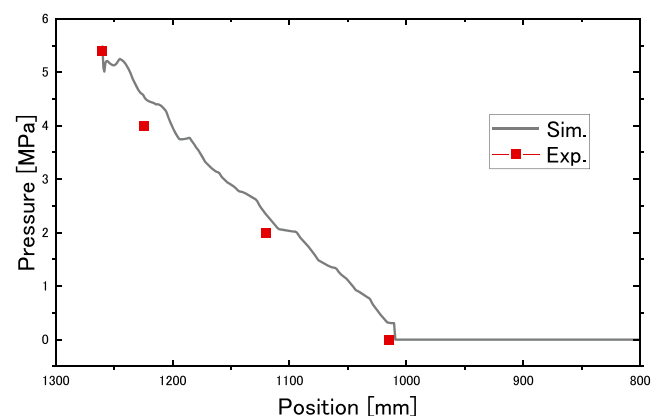


Fig. 5 Comparison of the experimental values and the analytical values

3.2. Application of the Laser Light-Section Method for Fill Ratio Measurement

Next, the results obtained through the analytical approach proposed herein were validated in another experiment in which a fill ratio was measured. Note a fill ratio is one of the status indicators of the fluidity of resin in the Twin-Screw Extruder. It indicates how

much resin resides relative to the feed volume of the screw. The laser light-section method was applied to measure a fill ratio. The laser light-section method is a method of measuring the profile of an object by applying a laser beam as a line around it. In the experiment, a line laser was used to apply a laser beam onto the open port of the Twin Screw Extruder, and then the cross-sectional profiles of the screw and the resin were recorded using a high-speed camera. After that, the amount of resin resided relative to the conveyable volume of the screw was measured through the image analysis on the recorded data. Fig. 6 illustrates the profile of the twin screws and the system layout.

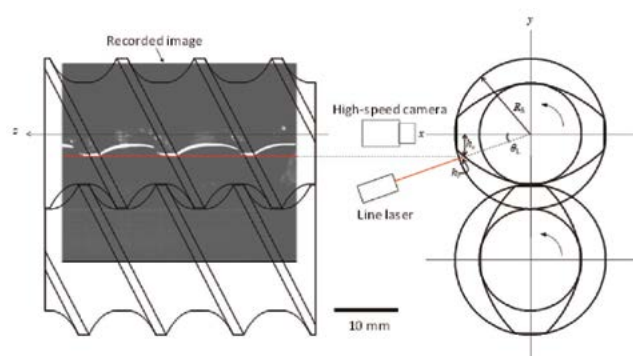


Fig. 6 System overview

The experimental material used was homo polypropylene (F-704NP), which was the same as the measurement of resin pressure distribution. Also, TEM-26SX (L/D = 40) was used. Fig. 7 shows the screw configuration and the point of measurement of a fill ratio.

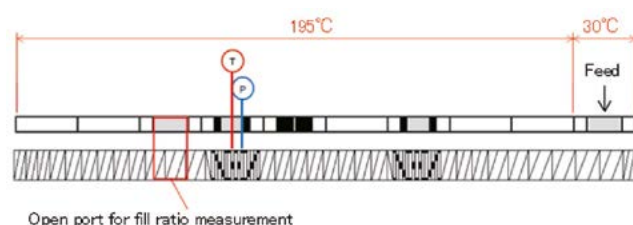


Fig. 7 Device configuration

Table 1 shows the operating conditions in the experiment. Screw speed was changed from 37 to 88 min^{-1} , and throughput from 1.0 to 3.0 kg/h. It is investigated the independence on a screw speed at a throughput of 1.0 kg/h, and on a throughput at a screw speed of 88 min^{-1} for fill ratio. This article will just present the results of the independence on a throughput for fill ratio.

The shape of the laser beam applied onto the screw and the surface of the resin was captured from a video file using MATLAB® Image Processing Toolbox® (MathWorks®) and Signal Processing Toolbox® (MathWorks®). The volume of resin was calculated by taking the line

Table 1 Operating conditions

Screw speed [min^{-1}]	Feed rate [kg/h]
37	1.0
49	1.0
58	1.0
69	1.0
88	1.0
88	1.5
88	2.0
88	2.5
88	3.0

shape on the screw surface from the one captured through image processing. Fig. 8 is a graph representing how the screw is filled with resin based on the captured line shape. The black line represents the cross-sectional profile of the screw, and the red line that of resin. This figure shows resin resides in the area between the black line and the red line on the right side. Next, Fig. 9 shows the graphs to compare the experimental values with the analytical values based on the results.

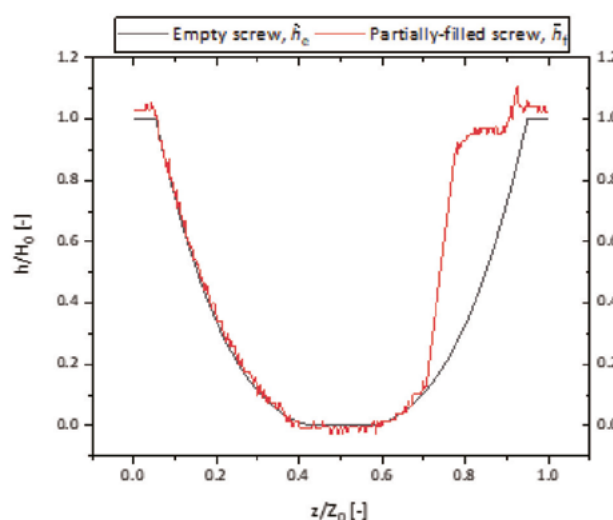


Fig. 8 Profiles of the resin and the screw surface (88 min^{-1} , 1 kg/h)

The analytical approach proposed herein made it possible to output a detailed profile of resin on the flow channel of the screw. Then, the amount of resin filling the screw can be identified as shown by the red lines in Fig. 9. The results of the experiment are almost identical to those of analysis. This means as throughput increases at the same screw speed, the fill ratio similarly increases.

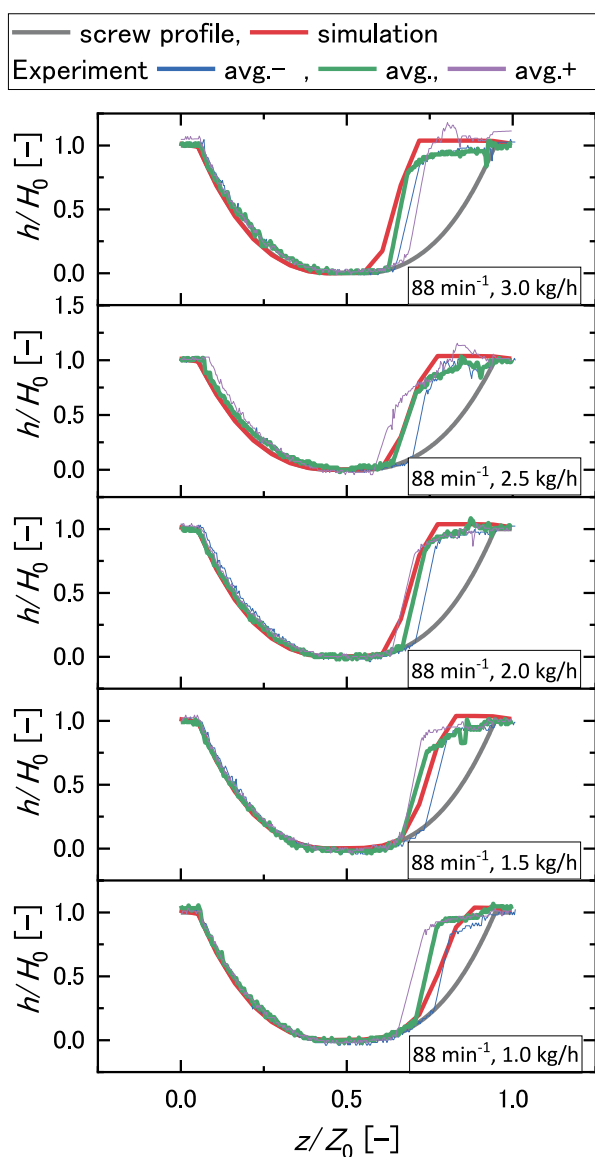


Fig. 9 Comparison of the experimental values and the analytical values (Fill ratio in the profile of the screw)

4 Conclusion

The laser light-section method, in which a laser beam is applied as a line for image processing, was introduced to measure the profile of resin in the Twin-Screw Extruder online. It was found through the experiment as throughput increased, fill ratio also increased.

The resin pressure distribution and the fill ratio derived from 2.5D FEM numerical analysis based on the Hele-Shaw flow model were almost identical to the data obtained through the experiment. The analytical approach proposed herein has enabled us to accurately determine the flow of resin in the Twin-Screw Extruder and predict the physical properties of a product based on distribution of residence time, thermal history, strain history, and others.

5 Summary

This study has revealed the Hele-Shaw flow model-based 2.5D FEM analysis enables us to analyze the state of the flow of the resin in detail in the axis direction and the circumference direction of the screw inside the Twin-Screw Extruder by solving the equation of the viscous fluid between the two adjacent cylindrical columns. In addition, this result has proved it is possible to design a device configuration from the perspective of a molding process in response to increasing demand for more advanced product development using the Twin-Screw Extruder. Additional experiments and verification were conducted on devolatilization and fiber length attrition, which actually take place in product development, and demonstrated the analytical values were in good agreement with the experimental values, though the details are omitted due to the page restriction.

Acknowledgements

I would like to express sincere gratitude to Professor Kentaro TAKI, Kanazawa University, College of Science and Engineering, School of Mechanical Engineering for his kind help and advice.

In addition, I wish to extend special thanks to Mr. Shinichiro TANIFUJI and Mr. Daisuke YORIFUJI, HASL Co., Ltd. for offering the analytical software, improving its performance, and giving me kind advice and opinions.

Reference

Masatoshi OHARA, Study on an Effect of a Fill Ratio in a Twin-Screw Extruder on Devolatilization and a Rupture of Glass Fibers Based on a Newly Developed Numerical Analysis Method, Doctoral Dissertation at Kanazawa University, 2021

Investigation of Pressure Propagation Characteristics in Die Casting Method

It is generally ideal that casting pressure, which is one of the injection settings of the die casting machine, is started in the shortest time after molten metal is filled in a product cavity. However, to effectively transmit casting pressure to the product cavity, it is affected not only by the injection settings but also by the molten metal and the mold temperature. Moreover, it was not enough to confirm the effectiveness of the casting pressure based on these factors in actual casting. In this study, we attempted to clarify how casting pressure, together with other factors, affects product quality.



Research & Development Center
Research & Development Department

Hiroki AMEZAWA

1 Introduction

In the automobile industry, efforts to reduce CO₂ emissions on a life cycle basis, including not only when driving a car but also from production to disposal, are accelerating in order to curb global warming. Therefore, production machines also need more technology which contributes to CO₂ reduction.

Considering the technology in die casting machines, the development of energy-saving technology by downsizing the machine is notable. For downsizing the machine, it is necessary to have a low-pressure technology which enables casting with the minimum casting pressure to achieve the required product quality. However, since the setting standard of casting pressure is not clear, it is often judged from the experience of die casting and product quality, which makes it difficult to easily reduce casting pressure. Therefore, to develop technology for lowering the pressure, it is first necessary to clarify how the casting pressure propagates to the product. In this study, we report the role of casting pressure on product quality and the relationship between casting pressure and other factors for the purpose of clarifying the propagation of casting pressure.

2 About the Role of Casting Pressure and Product Quality

In die casting, gas porosity formed by gas entrained during filling of molten metal, and shrinkage porosity formed by volume shrinkage due to a decrease in temperature of the molten metal, are generated inside products. Generally, casting pressure improves internal quality of products by shrinking porosity.

On the other hand, product quality depends not only on casting pressure but also on various factors such as intensify time, high-

speed range, and molten metal temperature, so it is not sufficient to quantitatively judge how much casting pressure alone affects product quality. Therefore, we investigated how casting pressure affects product quality by orthogonal array experiments based on quality engineering.

3 Methods

3.1 | Orthogonal Array Experiment Conditions

Based on quality engineering, we selected factors which may affect product quality and evaluated the effects of each factor and interaction. We conducted experiments under 8 factors and 2 levels according to the orthogonal array in Table 1. The factors to be taken up in the interaction of casting pressure were high-speed injection speed, intensify time, molten metal temperature, temperature of mold temperature controller, vacuum setting, and pouring time.

Table 1 Orthogonal array

Factor symbol	A	B	C	D	E	F	G	H
Factor	Casting Pressure	High-speed injection speed	High-speed range	intensify time	Molten temperature	Temperature of mold temperature controller	Vacuum setting	Pouring time
Level								
1	60MPa	2.0m/s	90mm	20msec	+50°C	50°C	✓	5.1sec
2	80MPa	3.0m/s	110mm	70msec	+100°C	180°C	—	1.4sec
Condition 1	60MPa	2.0m/s	110mm	70msec	680°C	180°C	✓	5.1sec
Condition 2	80MPa	2.0m/s	110mm	70msec	680°C	180°C	✓	1.4sec
Condition 3	60MPa	2.0m/s	90mm	20msec	680°C	180°C	—	1.4sec
Condition 4	80MPa	2.0m/s	90mm	20msec	680°C	180°C	—	5.1sec
Condition 5	60MPa	3.0m/s	110mm	20msec	680°C	50°C	✓	1.4sec
Condition 6	80MPa	3.0m/s	90mm	70msec	680°C	50°C	—	1.4sec
Condition 7	60MPa	3.0m/s	90mm	70msec	680°C	50°C	—	5.1sec
Condition 8	80MPa	3.0m/s	110mm	20msec	680°C	50°C	✓	5.1sec
Condition 9	80MPa	2.0m/s	90mm	20msec	630°C	50°C	✓	1.4sec
Condition 10	80MPa	2.0m/s	110mm	70msec	630°C	50°C	—	5.1sec
Condition 11	60MPa	2.0m/s	90mm	20msec	630°C	50°C	✓	5.1sec
Condition 12	60MPa	2.0m/s	110mm	70msec	630°C	50°C	—	1.4sec
Condition 13	60MPa	3.0m/s	90mm	70msec	630°C	180°C	✓	1.4sec
Condition 14	80MPa	3.0m/s	90mm	70msec	630°C	180°C	✓	5.1sec
Condition 15	60MPa	3.0m/s	110mm	20msec	630°C	180°C	—	5.1sec
Condition 16	80MPa	3.0m/s	110mm	20msec	630°C	180°C	—	1.4sec

Fig. 1 shows the half-pipe shaped test piece and various sensors / quality evaluation measurement points. Other conditions are shown in Table 2. Table 3 shows the specifications of the die casting machine

(DC350R-EH) used. ADC12 was used for the experiments.

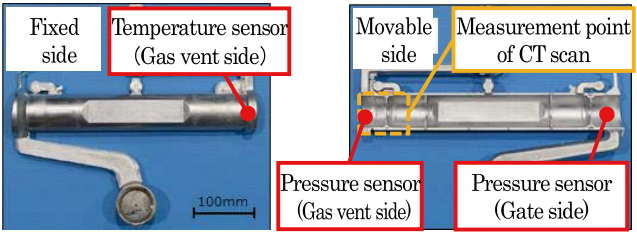


Fig. 1 Test piece shape and various measurement points

Table 2 Mold conditions

Wall thickness	2 mm
Shot weight	975 g
Part weight	390 g
Product weight	200 g
Gate area	1.76 cm ²
Diameter of chip	Φ60 mm

Table 3 Specifications of the machine

Injection force	344 kN
Maximum injection	11 m/s
Die-locking power	3500 kN
Type of die closing	Electric toggle

In order to effectively transmit the casting pressure produced by the injection piston of the machine to the product cavity filled with the molten metal, it is important to pressurize the molten metal before it solidifies. Therefore, an optical fiber type radiation thermometer temperature sensor was installed in the product cavity to directly measure the temperature of the molten metal. Since it is necessary to measure the temperature of the molten metal in the product cavity in a non-contact manner, we created the pin shown in Fig. 2 with glass placed at the tip of the pin to protect the sensor from the molten metal. In addition, pressure sensors were installed to measure the change in pressure due to the temperature change in the solidification process.

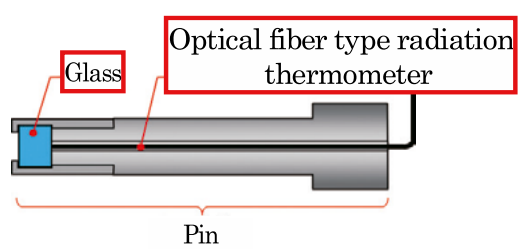


Fig. 2 Temperature sensor

On the other hand, the measurement data of the injection position, the injection speed, and the mechanical pressure were measured at the same time so the molten metal temperature and the pressure inside the mold could be compared with the injection state. Fig. 3 shows an example of the measurement waveform and the measurement definition. However, the pressure inside the mold in 3.2 experimental results deals only with the gas vent side facing the measurement point of the molten metal temperature.

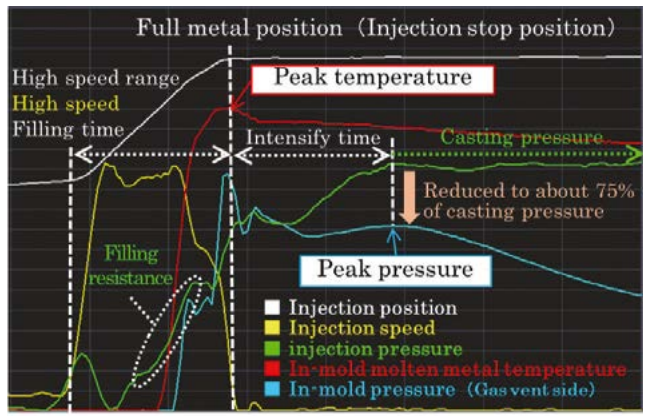


Fig. 3 Measurement waveform example and measurement definition

From the measurement waveform, the start of rising pressure in the mold results from resistance when the molten metal fills the product cavity and the molten metal passes to the gas vent side, which almost coincides with the detection timing of the molten metal temperature. In addition, the peak pressure transmitted to the product cavity is about 75% lower than the casting pressure. This results from molten metal solidification progressing due to temperature decrease with pressure propagation deterioration.

Five samples were taken under each condition, and the quality evaluation was based on the ratio of porosity at the CT scan measurement points in Fig. 1. From these results, the influence of each factor on product quality was evaluated.

3.2 | Experimental Results

Fig. 4 shows the ratio of porosity by the CT scanner under each condition. In general, gas vent with a vacuum device is effective in reducing the gas porosity, and the results of this experiment show the porosity ratio has decreased by 60% on average. On the other hand, conditions 3, 10 and 12 are not good because there is no vacuum. Therefore, it was determined the porosity ratio is greatly affected by the amount of gas. However, since the porosity ratio is lower even under conditions 15 and 16 without vacuum than under condition 2 with the vacuum, it is apparent the results are not always

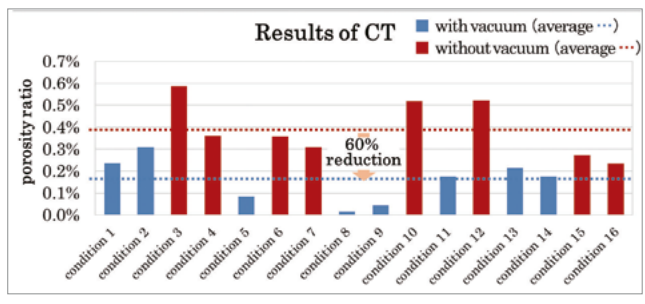


Fig. 4 Porosity ratio

good if a vacuum device is used.

Fig. 5 shows the results of classifying the effects of peak pressure in the mold on the porosity ratio by vacuum setting. With vacuum, the porosity ratio tends to decrease as the peak pressure in the mold increases, but there is no correlation without vacuum. In this experiment, it is apparent the porosity ratio was more influenced by the gas than the peak pressure in the mold.

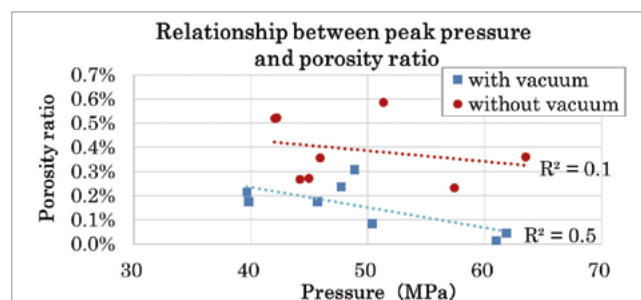


Fig. 5 Effect of peak pressure on porosity ratio

Next, in order to confirm which factors other than vacuum affects the porosity ratio, the graph of factorial effects of Fig. 6 is shown. The casting pressure is not recognized as the main effect, but high-speed, intensify time, vacuum setting, and pouring time are recognized. In particular, the effect of high-speed / vacuum setting is great. The factors which increase the interaction with casting pressure are intensify time, temperature of mold temperature controller, and pouring time. From these results, it is apparent casting pressure alone does not significantly affect the porosity ratio, but interaction with the other above factors are affective.

From here, the evaluation was performed only with vacuum to reduce the influence of gas. From the graph of factorial effects, the factor which increased the main effect / interaction is the intensify

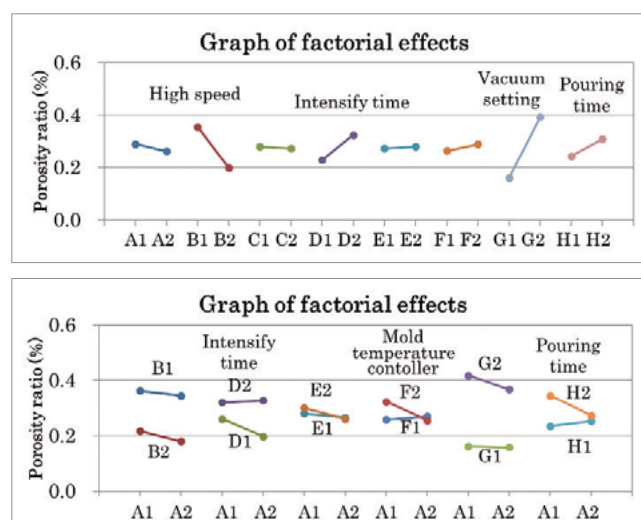


Fig. 6 Graph of factorial effects

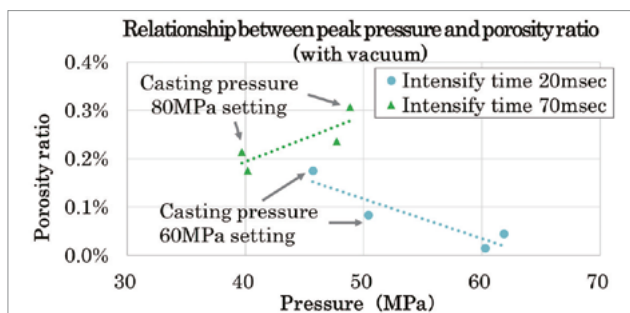


Fig. 7 Effect of intensify time on porosity ratio

time. Fig. 7 shows the effect of the intensify time on the porosity ratio. When the intensify time is short, the peak pressure can be increased even if the casting pressure is low, and the porosity ratio is reduced. Therefore, it is clear casting with a reduced casting pressure is possible by shortening the intensify time.

In addition to the intensify time, high speed is the main effect in the graph of factorial effects, so time is an important factor for increasing the peak pressure. Fig. 8 shows the effect of pressure transmission efficiency on elapsed time (filling time + intensify time). The pressure transmission efficiency indicates the ratio of the peak pressure to the casting pressure. From Fig. 8, the pressure transmission efficiency increases as the time becomes shorter. This is because the shorter the elapsed time, the higher the molten metal temperature is maintained and the higher the peak pressure, as shown in Fig. 9.

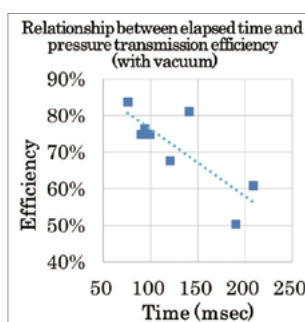


Fig. 8 Effect of pressure transfer efficiency on elapsed time

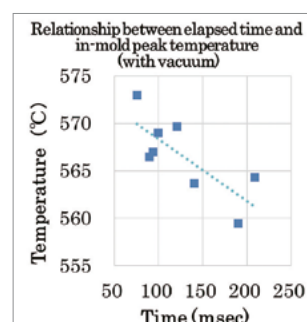


Fig. 9 Effect of in-mold peak temperature on elapsed time

Fig. 10 shows the relationship between peak temperature and pressure transfer efficiency. Fig. 10 shows efficiency increases as the peak temperature rises. From the above, it was found it is important to keep the molten metal temperature high by shortening the elapsed time to increase the pressure transmission efficiency, which is the actual efficiency of the casting pressure.

However, in Fig. 10, condition 13 has a faster injection speed than condition 1, that is, the pressure transfer efficiency is about 10% lower despite the shorter time. Since the vacuum, intensify time,

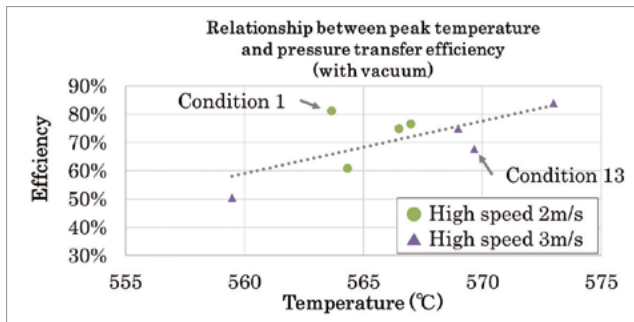


Fig. 10 Relationship between peak temperature and pressure transfer efficiency

and casting pressure settings are the same, other factors must have an effect.

4 Discussion

Fig. 11 shows the representative injection waveforms of conditions 1 and 13. Condition 13 has a higher peak temperature than condition 1 due to its high speed, but the peak pressure (gas vent side) is lower than condition 1. On the other hand, under condition 13, the pressure inside the mold (gate side) reacts at the same time as the filling resistance suddenly rises, and the pressure inside the mold drops earlier than under condition 1.

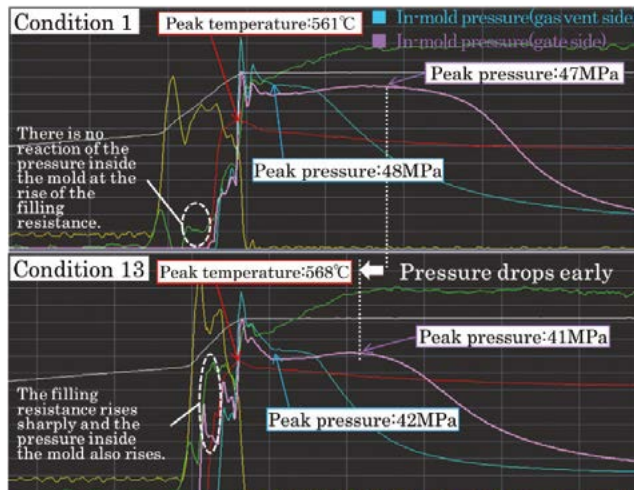


Fig. 11 Representative injection waveform of conditions 1 and 13

In general, the narrower the gate, the higher the filling resistance. Therefore, in condition 13 in which the high-speed range is short, the molten metal was filled to the vicinity of the product gate at a low speed, so the molten metal was easily solidified. As a result, the gate portion solidified and closed at an early stage in the pressure increasing process, the pressure was not effectively transmitted to the gas vent side, and the peak pressure (gas venting side) did not rise. Fig. 12 shows the effect of different high-speed range on

pressure transmission efficiency. If the high-speed range is short, the pressure transmission efficiency tends to decrease. This is because the pressure transmission efficiency on the gate side was reduced as shown in Fig. 13, and the gate was blocked early if the high-speed range was short.

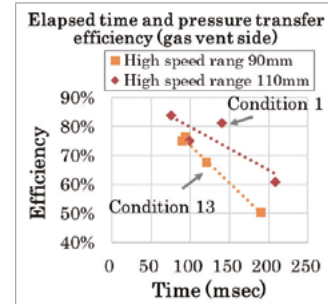


Fig. 12 Effects of high-speed range on pressure transmission efficiency 1

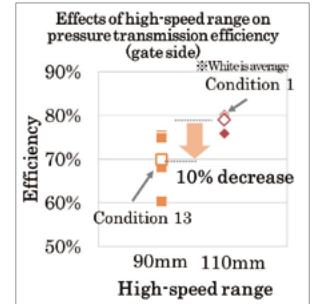


Fig. 13 Effects of high-speed range on pressure transmission efficiency 2

In this study, we did not consider condition 1 in Fig. 10, which has a low peak temperature but a high pressure transfer efficiency. In the next survey, we would like to install a temperature sensor on the gate side and measure at the same time on both the gate / gas vent side to acquire data which will lead to further consideration and advance elucidation of pressure propagation.

5 Conclusions

- 1) The casting pressure has a small effect on the internal quality of the product and is affected by the interaction between the intensify time, the molten metal temperature, and the pouring time.
- 2) The peak pressure in the mold, which is the effective value of the casting pressure, is increased by shortening the intensify time, and the internal quality of the product is improved.
- 3) The pressure transmission efficiency, which is the actual efficiency of casting pressure, increases as the peak temperature rises, but this is not always the case due to the influence of other factors.

Reference

- 1) Satoru AIDA, et al. : Papers of Japan Die Casting Conference (2018) JD18-3

Development of Plasticization Device for Polyolefin-Based Resin Molding with High Color Dispersion and High Plasticization Capacity

Molded parts using a polyolefin-based resin are often used in vehicle parts, and in future, the volume used is expected to increase due to an expansion in their scope of applications. On the other hand, as the number of molded parts using this resin in any particular vehicle is large, compared to molded parts using other resins, the cost demand is stringent, and thus both a reduction in production cost and a guarantee of exterior quality, strength and other physical properties is required. As a result, a plasticization device which permits stable plasticization of the resin even at a high screw rotating speed during high-cycle molding is required in injection molding machines. This paper reports on a plasticization device for polyolefin-based resins which was developed to meet this requirement.



Metal & Plastics Industrial Machine Company
Metal & Plastics Industrial Machine Technology
Department

Takahiro WATANABE

1 Introduction

Molded parts using a polyolefin-based resin are mainly used for exterior and interior fittings in vehicle parts, and these are produced to meet weight reduction and diverse design needs. On the other hand, regarding our initiatives to reduce costs, material costs are reduced by changing the coloring method for molded parts from colored pellets that emphasize quality over cost to adding a masterbatch to natural pellets, and we were able to shorten the charging time required for plasticization of the resin and achieve high-cycle molding to increase the production quantity per unit time. However, shortening charging time is achieved at the expense of the color dispersion condition of molded parts using a master batch. As a result, plasticization defects of the resin easily occur due to an insufficient amount of heat received etc., which often leads to color unevenness and other molding defects. In order to achieve both an improvement in the production quantity per unit time through high-cycle molding and molded parts with no color unevenness by improving the color dispersion of the master batch with a high dilution factor, we have been working on the development of a plasticization device for polyolefin-based resin molding.

2 Issues and Features of Plasticization Device

The key quality issue in molding parts using a master batch is to ensure the resin is melted, dispersed, and distributed uniformly even at the highest screw rotating speed, and this is an important factor in eliminating color unevenness in molded parts. To resolve this issue, we developed an ESB screw which can achieve both higher plasticization capacity and more even melting than our

standard screw (hereinafter standard screw), and a color dispersion element which can minimize the drop in plasticization capacity while raising the color dispersion of the master batch.

(1) ESB screw for high plasticization capacity and uniform melting

An ESB screw has an extended effective screw length compared to a standard screw (Fig. 1). The extended length is used to expand the area of the compression zone, and by providing a long sub-flight design over the metering zone from the middle of the compression zone, a sufficient quantity of heat was imparted in this area, ensuring uniform melting of polyolefin-based resins having a large melting latent heat. Based on this, charging at a screw rotating speed higher than a standard screw becomes possible, thereby achieving a high plasticization capacity.

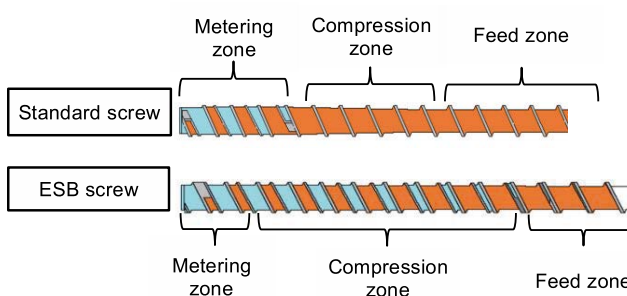


Fig. 1 Standard screw and ESB screw

A comparison of the plasticization capacity of polypropylene based on a standard screw and an ESB screw of diameter of $\Phi 60$ mm and $\Phi 115$ mm is shown in Fig. 2. Compared to a standard screw, an ESB screw with a diameter of $\Phi 60$ mm has an increased plasticization capacity of 114% and one with a diameter of $\Phi 115$ mm has an increased plasticization capacity of 67%.

Test conditions

- Resin : Japan Polypropylene Corporation
Polypropylene JP5GA

- Screw rotating speed:

Φ 60 mm	Standard screw	220 min ⁻¹
	ESB screw	320 min ⁻¹
Φ 115 mm	Standard screw	110 min ⁻¹
	ESB screw	138 min ⁻¹

- Soak ratio^{Note)} 1:2

- Back pressure: 3 MPa

- Charging stroke: 2.5D

Note) Soak ratio is the ratio of the charging time per cycle and non-charging time

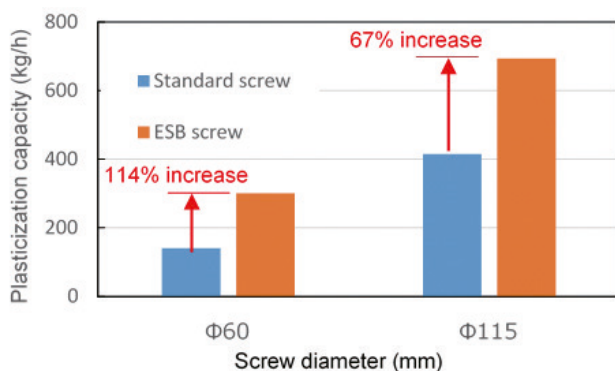


Fig. 2 Plasticization capacity of polypropylene by screw

In order to verify the uniform melting of each screw, we measured the range of fluctuation in the resin pressure of polypropylene during purging in a standard screw and an ESB screw of diameter Φ115 mm. (Fig. 3, Fig. 4)

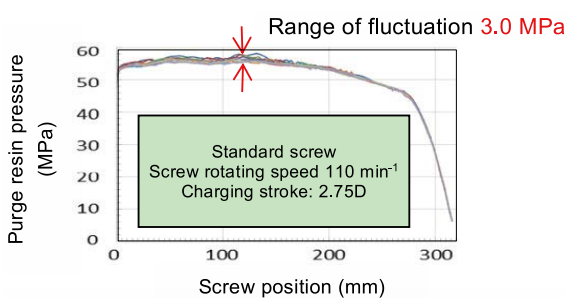


Fig. 3 Resin pressure when purging of a Φ115mm standard screw

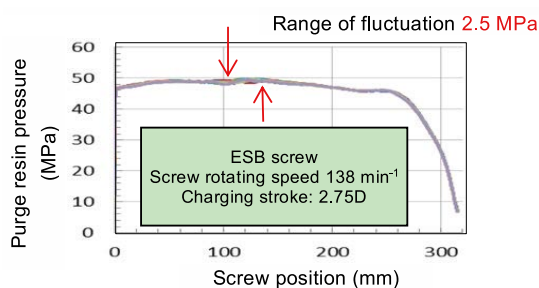


Fig. 4 Resin pressure when purging of a Φ115mm ESB screw

As fluctuations in the resin pressure occur due to changes in the resin viscosity and contamination by unmelted resin during charging, the results show the smaller the range of fluctuations, the more uniform the charged resin is in a melted state.

In a standard screw, the range of fluctuation in the resin pressure at a plasticization capacity of 415 kg/h reaches 3.0 MPa at maximum. However, in an ESB screw, the same range of fluctuation at a plasticization capacity of 693 kg/h is 2.5 MPa at maximum. Therefore, we confirmed the melting condition is more uniform while achieving a plasticization capacity which is 1.6 times higher or more compared to a standard screw.

(2) Cross ring effect as a color dispersion element

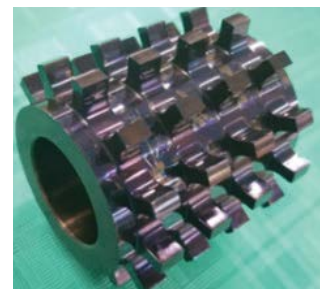
In colored molding by master batch, when molding a master batch at a high dilution factor in order to reduce material costs, non-uniform dispersion of the master batch tends to easily appear as color unevenness on the molded part surface. This defect tends to easily occur at a low back pressure and high screw rotating speed to shorten the charging time.

To improve color dispersion, we can either attach a uni-melt ring like that shown in Fig. 5 to the screw tip as in the past, or use a special nozzle known as a mixing nozzle which is equipped with a dispersion function inside the nozzle. However, as the uni-melt ring constricts the flow path of the melted resin just before the screw tip, this results in a drop in plasticization capacity and increases charging time, thereby increasing the molding cycle. Although a mixing nozzle is able to maintain the plasticization capacity, the amount of resin which needs to be discarded when changing resin or color is more than that of an open nozzle, increasing the working time required to change color, causing a pressure loss in the nozzle part, and decreasing the pressure which can be used in filling the mold, which all leads to a drop in productivity.

To resolve this issue, we reviewed the design of the uni-melt ring



Uni-melt ring



Newly developed cross ring

Fig. 5 Color dispersion element

and developed a cross ring to achieve a color dispersion on par with a mixing nozzle while minimizing the drop in the plasticization capacity (Fig. 5).

In order to compare the effect a difference in back pressure has on color dispersion at the following specifications, data obtained under the following test conditions is shown in Fig. 6.

- Specification 1 : ESB screw
- Specification 2 : ESB screw + uni-melt ring
- Specification 3 : ESB screw + cross ring

Test conditions

- Screw diameter: $\Phi 60$ mm
- Molded part: Document case
- Molded part weight: 450 g
- Resin: Japan Polypropylene Corporation
Polypropylene JP5GA
Master batch: 1wt% (beige)
- Molding cycle: 60 s
- Screw rotating speed: 320 min⁻¹
- Back pressure: 3 MPa, 7 MPa, 10 MPa, 15 MPa

	Back pressure [MPa]			
	3	7	10	15
Specifi- cation 1				
Specifi- cation 2				
Specifi- cation 3				

Fig. 6 Comparison of color dispersion

Fig. 6 shows the status of color dispersion in the molded part for each specification, indicating color dispersion is better when the color unevenness is smaller. Although color dispersion improves the higher the back pressure is at all specifications, poor color dispersion was observed even at a back pressure of 15 MPa in the ESB screw (Specification 1). On the other hand, the color dispersion is about the same at a back pressure of 10 MPa or higher for both the ESB screw + uni-melt ring (Specification 2) and ESB screw + cross ring (Specification 3). (inside red box of Fig. 6)

Next, based on the data obtained with Fig. 6, a numerical rating (vertical axis) of color dispersion and plasticization capacity (horizontal axis) are shown in Fig. 7 for each back pressure setting. The figure for a standard screw (Specification 4) is also indicated for reference purposes.

Test condition

- Screw diameter: $\Phi 60$ mm
- Screw rotating speed : ESB screw 320 min⁻¹
Standard screw 220 min⁻¹

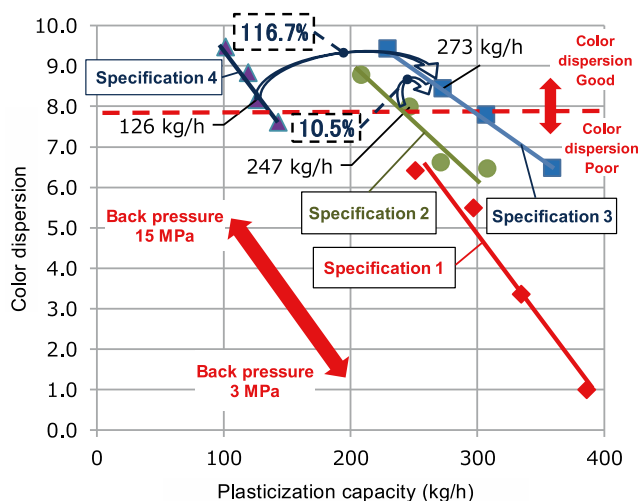


Fig. 7 Comparison of color dispersion and plasticization capacity

The color dispersion rating in Fig. 7 is a score according to a color dispersion evaluation method which we developed, with a score of 8.0 or higher indicating good color dispersion. The ESB screw (Specification 1) has a high plasticization capacity compared to other specifications at all back pressures, but the color dispersion is poor even at a back pressure of 15 MPa. At a back pressure of 10 MPa, the ESB screw + uni-melt ring (Specification 2) and ESB screw + cross ring (Specification 3) have good color dispersion, and a plasticization capacity of 247 kg/h and 273 kg/h respectively, while that of the cross ring (Specification 3) is 10.5% higher than the uni-melt ring (Specification 2). Although the standard screw (Specification 4) has good color dispersion at a back pressure of 7 MPa, the plasticization capacity is 126 kg/h, so compared to the standard screw, the ESB screw + cross ring (Specification 3) has a plasticization capacity which is 116.7% higher.

Based on this result, a case in which the plasticization capacity for each specification was replaced by the charging time is shown in Fig. 8.

Test condition

- Screw diameter: $\Phi 60$ mm
- Screw rotating speed :
ESB screw 320 min⁻¹
Standard screw 215 min⁻¹
- Shot mass 450 g

•Molding cycle 60 s

•Back pressure ESB screw 10 MPa
 Standard screw 7 MPa

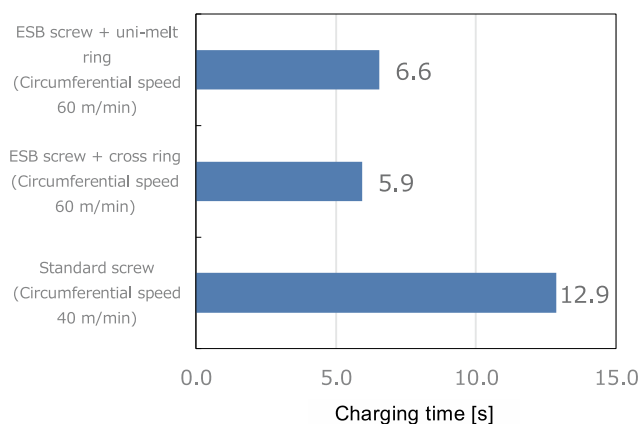


Fig. 8 Charging time comparison

When an ESB screw + cross ring (Specification 3) is fitted, the charging time becomes 5.9 s, shortening by 7.0 s compared to the 12.9 s for the standard screw. By shortening the charging time, it is also possible to shorten the cycle time when cooling time is less than 12.9 s. In addition to increasing the production quantity per unit time by adopting a high-cycle, generally it is also possible to

achieve molding with good color dispersion and reduced material costs even when the content ratio of the master batch is diluted from 2 to 3wt% to 1wt% with an open nozzle specification.

3 Summary

In this paper, we reported on the development of a plasticization device with a high plasticization capacity and high color dispersion for molding polyolefin-based resins which can help contribute to an improvement in productivity in the molding site. Besides being used in the master batch for coloring purposes, a dispersion element is also an important technique used in the molding of master batch addition for quality improvement, physical strengthening and other purposes. In addition to creating benefits by reducing the amount of waste caused by quality defects, reducing material costs, improving productivity and so on, it also contributes to a reduction in the environmental load which has also been cited as a SDGs.

Going forward, we will continue to contribute to society through the development of technology to resolve issues for a variety of resins and molded parts.

Column

Upon Receipt of a Request



Research & Development Center
Research & Development Department

Miyu OGAWA

When I was a university student, one day I went to a machine tool room in the university with a drawing to ask for the manufacture of a part to be used in an experiment. The machine tool room was dedicated to production of equipment and parts for use in experiments. When I stepped into the room, I found many machine tools, along with the smell and clank of metal, with which workers were devotedly working. When I asked one of the workers to make the part I needed, upon showing him the drawing he advised me my drawing was not adequate. Since the information on the drawing created by me, who belonged not to the Mechanical Engineering Department but to the Information Department, was insufficient,

the worker kindly asked me questions in detail, including the meaning of the dimensions on the drawing, the level of precision required, the environment in which the part was to be used, and whether another material could be used since the designated material was difficult to process. I was not able to provide adequate information then because I did not yet understand what information was needed to produce the part I desired. I also realized it is essential for the person receiving a request to carefully listen to the requester to obtain all necessary information to fully understand what was really required. So, when we make a request, we should carefully consider what information is needed from the standpoint of the person receiving the request. On the other hand, when we receive a request, I hope we can try to correctly understand the content of the request and respond in an appropriate way.

Optimization of Extrusion Process Engineering for the Invention of High-Performance Materials

Plastics, featuring high moldability, high functionality, and light weight, are finding wider application while the circumstances surrounding the plastics industry are becoming more challenging, with focus on environmental loads typified by microplastics in the ocean and efforts by society to reduce the usage of plastics. In connection with SDGs, this article is titled Optimization of Extrusion Process Engineering for the Invention of High-Performance Materials. It reports the manufacturing of plastics and our optimization of process engineering for the effective utilization of biomass-derived materials from the perspective of reducing environmental loads.



Metal & Plastics Industrial Machine Company
Extrusion Machine Engineering Department

Shozo SUZUKI



Metal & Plastics Industrial Machine Company
Extrusion Machine Engineering Department

Hiroshi MOMOCHI

1 Introduction

Plastic pollution has been receiving global attention and there are a rapidly increasing number of initiatives to reduce the usage of plastics, including material bans and charging for plastic shopping bags and straws. Considering such circumstances, we expect society to quickly evolve toward low-carbon and sound material-recycling in the near future, further reducing environmental loads.

Looking around the world, individual nations are working toward achieving SDGs (Sustainable Development Goals), which were adopted at the UN Summit in 2015. Consistent with this trend, the plastics industry is also pushing forward with the effective use of natural resources, anti-pollution measures, 3R (Reduce, Reuse and Recycle) based on resource recycling, development of alternative materials, and automation and labor saving in manufacturing plants.

On the other hand, plastics have excellent material properties allowing them to be flexibly used according to the application purposes of products. Therefore, plastics are expected to play roles in reducing CO₂ emissions through weight saving and lowering environmental loads.

In addition, as measures against climate change and global warming, the shift to electric vehicles (EVs) or hybrid electric vehicles (HEVs) continues to make low-carbon society a reality. EVs and HEVs are equipped with lithium-ion batteries (LIB) as power sources, in which battery separator films are made from plastics.

Furthermore, bioplastics are gaining the spotlight as materials which will likely contribute not only to reduction in the consumption of exhausted resources such as oil, but also the prevention of global warming. For this reason, endeavors are being made to; invent

materials containing bioplastics or bioplastic compounds, identify extensive applications, and promote mass production.

As described above, extrusion process engineering is involved in the manufacture of plastics and alternative materials and has a direct effect on reduction of environment loads in many aspects. The following sections will introduce specific examples of the efforts for process improvement utilizing our lineup of extruders and the optimization of extrusion process engineering for the invention of high-performance materials.

2 Ultra-Deep Channel Type Twin Screw Extruder (TEM-DS/DSS)

Shibaura Machine's product lineup offers several models of twin screw extruders (TEM Series) with different screw profiles and torques according to application purposes.

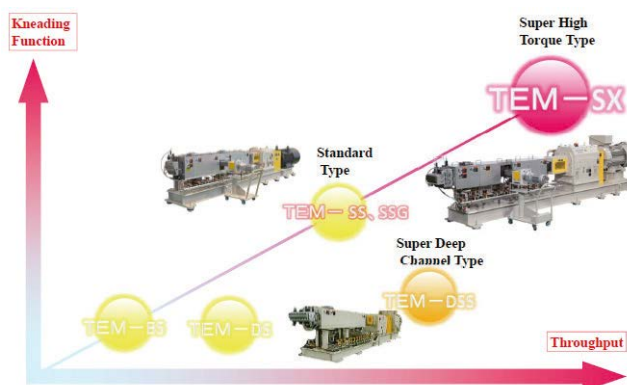


Fig. 1 Lineup of twin screw extruders (TEM)

Among the models, the Ultra-Deep Channel Type "TEM-DS/DSS Series" has high torque and a D/d of 1.8. This makes it possible to keep a minimum flight top necessary to provide effective shear

performance, and consequently the space volume has increased by 1.4 times compared to the conventional Deep Channel Type. The Ultra-Deep Channel Type has the following advantages.

- Low-shear forces and mild kneading

Fig. 2 shows a comparison between the Ultra-Deep Channel Type and the Deep Channel Type in a profile. In addition, Fig. 3 shows the simulated resin temperature distribution of each profile. As shown in Fig. 3, temperature locally rises near the flight top (yellow) in the Deep Channel Type while such temperature rise is suppressed in the Ultra-Deep Channel Type.

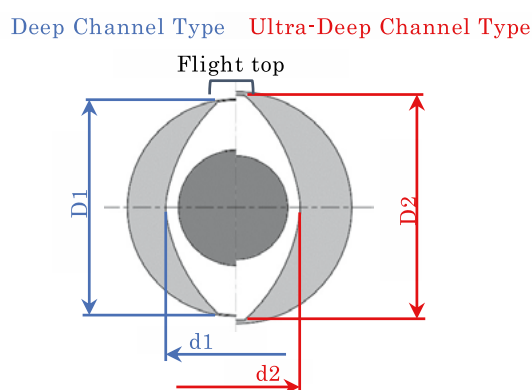


Fig. 2 Cross-sectional profiles

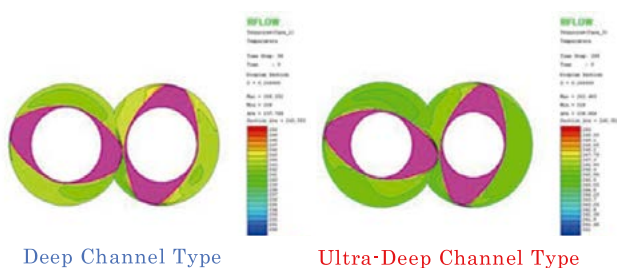


Fig. 3 Difference in a resin temperature distribution between the profiles

- Discharge increase from high feed acceptance performance

When the conventional Deep Channel Type is used to process raw materials with a low bulk specific gravity such as fluff, pulverized materials, and powders, a suitable bore diameter must be selected based on a feed limit in the same process. On the other hand, if the Ultra-Deep Channel Type, with a large space volume, is used, a model with a smaller bore diameter can be selected due to its high feed acceptance performance of raw materials. This will lead to reduction in energy consumption and an increase in both operability and productivity.

- High distribution and compounding performance, prolonged residence time, and devolatilization performance

Compared to the Deep Channel Type with constant screw center distances, the Ultra-Deep Channel Type can offer a large space volume, thereby lowering fill ratio with the same throughput. This means an increase in space with low fill ratio or free surface area of ingredients. Therefore, the Ultra-Deep Channel Type is superior to the Deep Channel Type in both the thorough and continuous movement of ingredients with even kneading, and the surface renewal effect per unit area under the same operating condition.

In addition, when a comparison is made in the process parameters under the same conditions, ingredients reside in the machine longer (See Fig. 4). Therefore, the Ultra-Deep Channel Type is more effective than the Deep Channel Type in reactive processing, which involves a melting and kneading process through a chemical reaction. For this reason, there are an increasing number of cases where conventional batch production is replaced with continuous production using the Ultra-Deep Channel Type twin screw extruder.

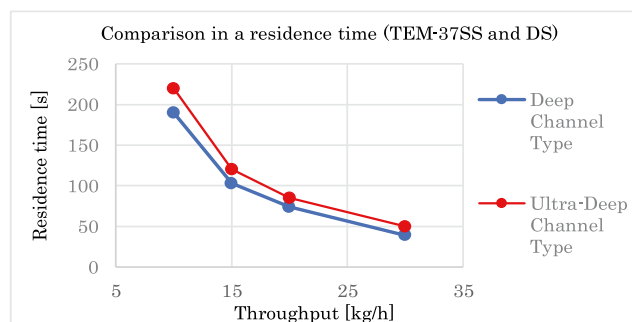


Fig. 4 Comparison in a residence time (Raw material : PP + talc 30%)

Combined with its superior surface renewal effect, the Ultra-Deep Channel Type provides a larger exposure area than the Deep Channel Type, which is important in a devolatilization process. This gives the Ultra-Deep Channel Type superb capability to remove or separate volatile components, and eventually it will contribute to the invention of low VOC materials. Moreover, the Ultra-Deep

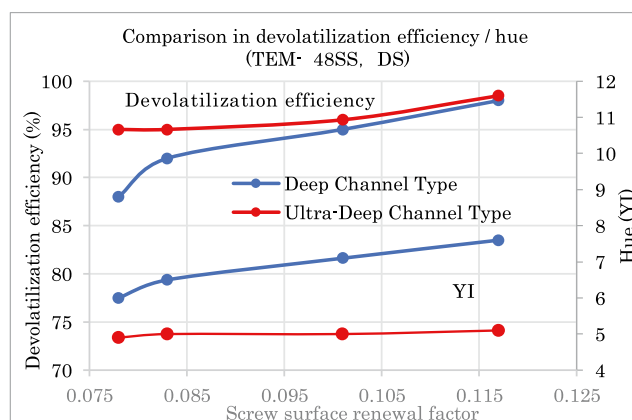


Fig. 5 Comparison in devolatilization efficiency and hue (YI)

Channel Type can suppress local temperature rise near the flight top. Therefore, it offers an advantage in both devolatilization and hue (YI). Fig. 5 shows the results of comparison and verification.

3 Recycling

The large space volume in the Ultra-Deep Channel Type can also be effectively used for the purpose of recycling pulverized PET bottles and films. In particular, the most likely case is where wastage due to trim loss or stamping in the secondary processing, or pulverized defective moldings, are directly returned to the production line for recycling without being pelletized in the process of manufacturing plastic sheets or films.

Furthermore, the effective use of the twin screw extruder in combination with vacuum equipment can prevent molecular mass reduction or polymer degradation due to hydrolysis without pre-drying raw materials. As a result of this advantage, along with low-temperature extrusion performance, the Ultra-Deep Channel Type is rapidly finding application in sheet or film manufacturing. In fact, there is a case where materials with a pulverized raw materials content of at least 70% by weight is used in actual sheet manufacturing. A-PET sheets, which are materials for food trays, food containers and covers, are typical application examples.

Some of the sheets introduced above are commercialized as recycled trays. They consist of multiple layers. A recycled material is used to form an intermediate layer, and virgin resin forms the surface layer in contact with food.

In this process, hydrolysis develops so quickly at high temperature in PET resin it is important to efficiently melt resin and quickly dewater it without exerting excessive shear energy in order to maintain quality. But these challenges can be solved by optimizing the screw configuration of the twin screw extruder.

4 Finely Porous Film

Finely porous films have countless fine pores in the $0.01\mu\text{m}$ to $50\mu\text{m}$ size range. They are high-performance materials which can control the passage of fluids or particles by the hole diameters and structures. Finely porous films are conventionally used as breathable films, which are raw materials for disposable diapers, feminine hygiene products, and protective clothes. They are also alternatives to paper because of their good light transmittance and texture and

used as films for illuminated signboards or synthetic paper. Recently, there is growing demand for finely porous films because they find their ways into battery separator films in lithium-ion batteries (LIB).

EVs are expected to rapidly become widespread in the future, but their driving range cannot be improved without increasing the capacity of batteries. Also, battery separator films need to be made thinner, and productivity, film strength, and physical properties should be further improved. Therefore, endeavors are being made to further upgrade the characteristics of raw materials and the plasticizing process.

In addition, because of rapidly growing demand for batteries and price competition, the need for more battery separator film manufacturing equipment, as well as increased extrusion speed and width, are growing to address increased production efficiency. It is vital to establish production engineering to meet such market needs.

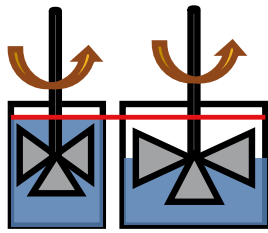
5 Application of the Ultra-Deep Channel Type to Battery Separator Manufacturing

Extension and phase separation is an important process in battery separator film manufacturing. Besides this, an extrusion process where raw materials are kneaded also significantly influences film quality.

It is very beneficial to use the Ultra-Deep Channel Type in the extrusion of wet battery separator films, where base resin and incompatible plasticizer (fluid paraffin) are compounded in large quantity. In particular, it will greatly help to minimize damage to the base resin, achieve high dispersion in phase separation, and eventually strengthen thinned films.

The large space volume in the Ultra-Deep Channel Type increases the space not filled with resin and enhances ease of kneading as shown in Fig. 6. This makes it possible to produce the effect of distribution and evenly kneaded resin.

In addition, as mentioned above, the Ultra-Deep Channel Type makes it possible to suppress local temperature rise caused by shear. Therefore, it can maintain higher viscosity and more effective kneading at a lower shear speed compared to the Deep Channel Type. As a result, it becomes possible to homogenize the raw materials of a super-high molecular battery separator, whose average number of molecules exceeds 1 million. Fig. 7 shows the results of comparison in film strength between an ultra-high molecular mass compound and an existing product.



Deep Channel Type Ultra-Deep Channel Type

Fig. 6 Difference in kneading between Deep Channel Type and Ultra-Deep Channel Type

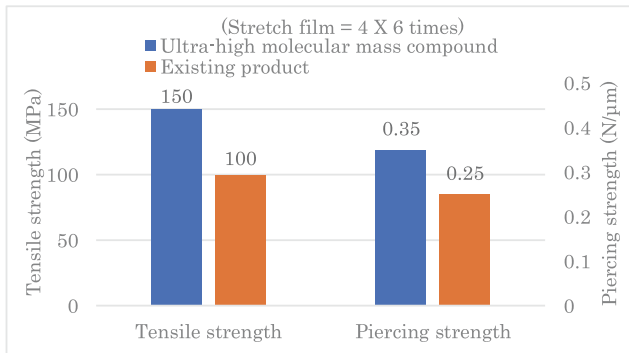


Fig.7 Comparison in film strength between an ultra-high molecular mass compound and an existing product

6 Bioplastics

Bioplastic is a generic name of biomass plastics which are made from recyclable organic materials such as plants, and biodegradable plastics which are naturally decomposed by microorganisms. Biodegradable plastics are expected to gain popularity but are less productive and cost-effective in production compared to common petroleum-derived general-purpose plastics.

In addition, biodegradable plastics are inferior in moldability and thermal stability. Therefore, they are easily colored due to excessive heat or shear. Fig. 8 shows the relationship between barrel temperatures and hues when extruding glucose biodegradable plastics.

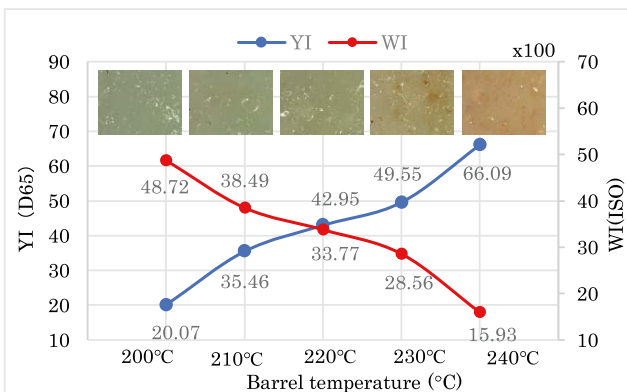


Fig. 8 Relationship between mold temperatures and hues

Low-temperature extrusion is a key to improving hue, so it is necessary to come up with an ingenious way of effectively kneading at lower shear speed. (The next section will describe the example application.)

7 Example Application of the Ultra-Deep Channel Type

Shibaura Machine owns the core technology of extrusion dewatering which was developed in the manufacture of ABS resin and the dewatering and drying of synthetic rubber. This technology can also be applied to the extrusion of bioplastics, which have hydrophilicity. (See Fig. 9 for Shibaura Machine's approach to dewatering.)

This section introduces the case where we succeeded in mass production while maintaining the hue of biodegradable plastics with water content of approximately 20%.

When a standard approach with a Deep Channel Type profile was used for extrusion, vent-up or cut strand frequently arose from an excessive amount of remaining moisture. When the approach of compression dewatering was adopted, dewatering performance was improved, but hue was considerably worsened due to excessive shear after compression. Then the approach of vaporization was adopted, where water was successfully removed in stages utilizing latent heat of vaporization of moisture content. Finally, good results were obtained.

These results were applied to the Ultra-Deep Channel Type. Due to the suppression of local temperature rise, hue was significantly improved, but it did not lead to increased throughput due to insufficient dewatering. One reason the expected result could not be obtained was the application of the Deep Channel Type device

Water content	Approach to dewatering	Device configuration
0 to 5%	Standard	
5 to 20%	Vaporization	
20% or higher	Compression	

Fig.9 Extrusion dewatering with a twin screw extruder

configuration. Based on these findings, the screw configuration was optimized, and a thorough search was made for the best operating conditions. Finally, throughput was successfully improved by 1.4 times compared to the Deep Channel Type.

8 Conclusion

As the industrial structure changes and the economy matures, the need for the type of extruders produced by Shibaura Machine is becoming more diverse. It is therefore important to develop a process of inventing high-performance materials with the purpose of not only increasing capacity and high quality, but also environmental conservation and the achievement of low-carbon society. We consider it our responsibility as a manufacturer to continuously strive to contribute to the development of a sustainable society through our business activities.

Development of High-Precision Machining Technology Using the BTA Deep Hole Drilling Machine DBH

BTA is an abbreviation acronym for Boring & Trepanning Association, and it refers to deep hole cutting, which is one of the most important processes in metalworking. BTA processing has the advantage of being able to drill clean and accurate deep holes (deep hole drilling) at high speed. Since most hole machining is done at the beginning of the machining process and the hole machined at that time is used as the reference in the subsequent processes, lesser accuracy has been required for the bend (out of position) and roundness of the machined hole. However, in recent years, to integrate processes and improve machining efficiency, the standard in the final process has been set as the outer dimension standard, and hole machining accuracy to that standard is often required. This paper presents an overview of BTA deep hole drilling and the technology used to achieve high-precision deep hole drilling aimed at process integration.



Machine Tools Company,
Machine Tools Engineering
Department

Kazuhiro SEKI



Machine Tools Company,
Machine Tools Manufacturing
Department

Ken ITO

1 Introduction

The global market for deep hole drilling machines is expected to grow at an annual average growth rate of 5.8% from 2020 to 2027, expanding to 126% over 2019 in 2027. Also, the global market for deep hole drilling tools is expected to grow at an annual average growth rate of 4.75% from 2020, with the growth drivers including: the automotive industry, which is increasingly focusing on electric vehicle parts; industrial machinery, where high-precision operations will increasingly be required even for large-sized machines in response to growing demand for automation; infrastructure; energy industries; aerospace; and defense¹⁾⁻²⁾. If deep holes can be machined more cleanly and accurately, it will help to integrate processes, improve machining efficiency, and reduce frictional resistance in the driving parts of automobiles, construction machinery, and industrial machinery, thereby contributing to improved fuel efficiency and reduced energy consumption. In the case of power generation-related components, improved deep hole drilling results in reduced losses, leading to more efficient power generation, which is closely related to efforts to achieve the SDGs. In the following, we will introduce the details and results of our efforts to improve the accuracy of deep hole drilling using our product, the BTA deep hole drilling machine DBH-1015C.

2 Outline of BTA Deep Hole Drilling Machine

2.1 What is BTA Processing?

Deep hole drilling is a process in which the depth of the hole is generally 100 to 200 times the hole diameter. The BTA method, because of its superior structure in terms of chip evacuation, rigidity, and productivity, has the advantage of high-speed and clean drilling, which is why the BTA method is the first choice for deep hole drilling. In the BTA method, cutting oil is pumped from the tank to the oil pressure head (pressure head) in contact with the workpiece, passes through the ring-shaped space between the drilled hole and the boring bar, reaches the cutting edge, and returns to the oil tank with the chips through the boring bar (Fig. 1).

Therefore, the chips do not contact the inner surface of the drilled hole, so they do not damage the inner surface of the hole, resulting in a very clean machined surface.

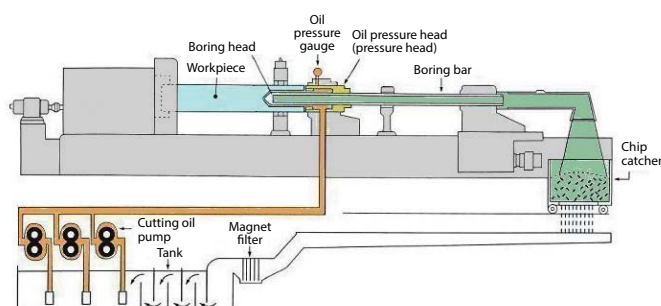


Fig. 1 Schematic diagram of a BTA deep hole drilling machine³⁾

2.2 | Types of BTA Processing

There are three types of BTA processing methods: solid boring, trepanning, and counter boring. Each of them has its own purpose and characteristics (Fig. 2).




Solid boring	Trepanning	Counter boring
		
The most common method for drilling deep holes in solid state material	A method of drilling that leaves a core in the center of the hole, allowing large diameter holes to be drilled even with low horsepower.	A method of widening the hole, used when dimensional accuracy of inside diameter is required, or when the hole is being prepared for honing.

Fig. 2 Types of BTA processing³⁾

2.3 | Types of BTA processing machines

BTA processing often uses structural steel, stainless steel, pre-hardened steel, bearing steel (bare steel), tool steel (such as carbon, alloy, and high-speed tool steel), corrosion and heat resistant alloys, titanium, aluminum, copper, resin, among others, as work materials. In BTA processing, it is possible to process not only round bars but also square bars and block shapes. However, since the specifications of the machine and the machining method differ depending on the shape of the work material, general specifications are shown in Fig. 3.

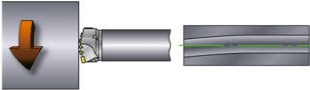
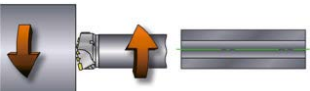
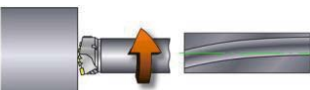
Workpiece: rotation+Tool: fixed	
Used for center hole drilling of round bars or square bars (chuck jaw forming required). * The DBH applies to this type. (Fig. 4)	Hole bending: Small
Workpiece: rotation+Tool: rotation	
Used for center hole drilling of round bars or square bars (chuck jaw forming required). It is generally called a "relative rotation type" and features a smaller hole bending than other machining centers.	Hole bending: Minimum
Workpiece: fixed+Tool: rotation	
Can be used for any material shape; can be used even for multi-hole drilling. It has a moving axis on either the workpiece side or the tool side. The hole bending is large.	Hole bending: Large

Fig. 3 Types of BTA processing machines (Refer to the website of KAWAHARA.)⁴⁾



Fig. 4 BTA deep hole drilling machine DBH-1015C

2.4 | Main Specifications of the DBH-1015C

Table 1 Specifications

1	Maximum length of workpiece	1500	mm
2	Minimum length of workpiece	220	mm
3	Diameter of the workpiece steady support	φ30 to φ200	mm
4	Maximum mass of the workpiece steady support	500	kg
5	Gripping range of workpiece	φ30 to φ200	mm
6	Drilling diameter	Solid boring	φ12.0 to φ65
		Trepanning	φ50 to φ100
		Counter boring	φ16 to φ100
7	Maximum drilling length	1500	mm
8	Pressure head clamp diameter	180	mm
9	Pressure head clamp length	285	mm
10	Usable range of pressure head	U2 to U5	
11	Maximum diameter of the bar steady support	94	mm
12	Travel distance of boring table	2980	mm
13	Spindle speed	100 to 1400	min ⁻¹
14	Cutting feed rate of boring table	1 to 1260	mm/min
15	Rapid traverse speed of boring table	4000	mm/min
16	Output of electric motor for spindle drive	45/37	kW
17	Output of electric motor for cutting oil pump	For high pressure (7.0 MPa)	7.5
		For medium pressure (4.0 MPa)	11
		For low pressure (1.5 MPa)	11
18	Output of electric motor for boring table feed	1.4	kW
19	Machine mass	9400	kg

3

High-Precision Deep Hole Drilling Test

3.1 | Target Machining Accuracy

Table 2 Target machining accuracy

Material	Surface roughness	Drilling [mm]	Machining accuracy [mm]		
		Diameter × Length	Coaxiality	Roundness	Diameter variation
SCM440 normalizing material	Rz12.5	φ40.0×700	◎0.05	○0.02	φ0.03

Based on the recent market requirements, we conducted various verifications with the goal of achieving the machining accuracy shown in Table 2 for five consecutive holes by solid boring. As mentioned above, deep hole drilling is generally the first process, and the required accuracy is often only surface roughness and straightness. This is because the deep hole is used as the standard for the next and subsequent processes. For this reason, to emphasize high-efficiency machining with high feed rate, the standard for deep hole drilling accuracy is generally considered to be a diameter tolerance of IT10 and a coaxiality of 1mm/1000mm.

3.2 | Results of Normal Processing Test

In order to check the current machining accuracy, we conducted a machining test under the cutting conditions shown in Table 3. The machining results are shown in Table 4. (Tool used: Throw-away type with rear guide)

Table 3 Cutting conditions

Peripheral speed	Feed rate	Cutting oil amount
73 m/min	0.04 mm/rev	55 L/min

Table 4 Results of normal processing test

	Machining accuracy [mm]		
	Coaxiality	Roundness	Diameter variation
1	$\phi 0.070$	0.014	$\phi 0.008$
2	$\phi 0.095$	0.015	$\phi 0.005$
3	$\phi 0.020$	0.018	$\phi 0.007$

The results show one out of three consecutive machinings are within the target accuracy. However, it is clearly difficult to continuously meet the target accuracy with the current machining method.

3.3 | Verification of Machine-Related Factors

Based on the results shown in Section 3.2, we investigated the factors which affect the coaxiality of deep hole drilling.

- ① Poor alignment of spindle table etc. (static accuracy)
- ② Insufficient rigidity of the machine body (static and dynamic)
- ③ Poor centering of workpiece
- ④ Uneven hardness of the workpiece (metallurgical structure, uneven wall thickness in the lower hole)
- ⑤ Cutting speed and feed rate
- ⑥ Supply flow rate, pressure, and temperature of the cutting fluid
- ⑦ Shape and material of the tool (tip/guide pad)

We conducted verification through machining for each item, but improvements and changes in items ① through ⑥ did not achieve the target accuracy. The verification results for each item are as follows.

- ① In the case of the workpiece rotation type, the centering effect where the drilling tool moves closer to the workpiece rotation axis will be produced, so the effect of the alignment of the boring table or bar support is small. However, the alignment of the spindle (workpiece) and guide bushing affects the diameter tolerance.
- ② The DBH-1015C has sufficient capacity in terms of both static and

dynamic rigidity.

- ③ As in ① above, the effect on coaxiality is small, but attention should be paid to the effect on diameter tolerance.
- ④ We compared the hardness between the workpiece and SCM440 raw material, but no significant difference was found. However, the coaxiality tends to be better when the hardness is higher and the microstructure is less uneven.
- ⑤ The faster the feed rate, the worse the coaxiality tends to be.
- ⑥ No effect of the flow rate, pressure, and temperature of the cutting fluid on coaxiality was observed. It should be noted as the cutting fluid flow rate was increased, deterioration of surface accuracy was observed due to micro-vibration of the tool within the workpiece.

3.4 | Verification of Tools

As stated in Section 3.3, we could not find any item which had a significant relationship to machining accuracy, so we verified the tool-related factors. For tools, we verified the shape and the dimensional adjustment of the guide pad (Fig. 5).

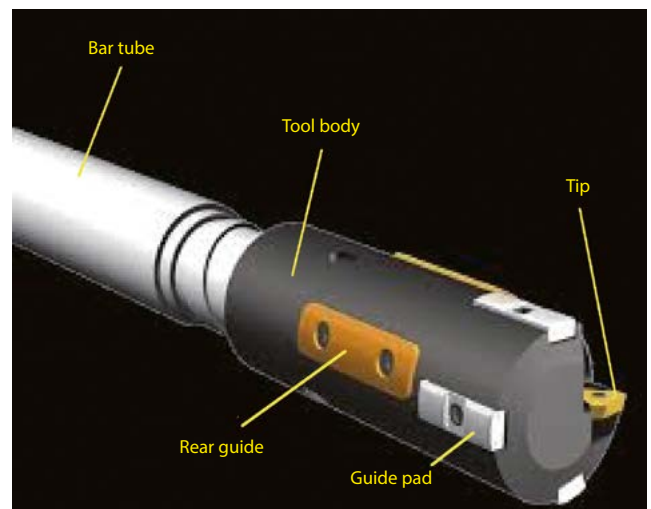


Fig. 5 Name of each part of the tool

3.4.1 | Verification with Different Tool Structures

Three types of tools were used to verify the change in machining accuracy under the same machining conditions as those in Table 3.

- ① Throw-away type tool with rear guide
- ② Throw-away type tool without rear guide
- ③ Brazing tool without rear guide

* ① and ② are tools of the same manufacturer.

The results of machining with each tool are shown in Table 5.

Table 5 Tool verification results

Tool	Machining accuracy [mm]	
	Coaxiality	Diameter variation
①	$\phi 0.205$	$\phi 0.015$
②	$\phi 0.580$	$\phi 0.010$
③	$\phi 0.350$	$\phi 0.042$

It was confirmed the machining accuracy varied depending on the tool, even under the same cutting condition. As shown in Fig. 6, when the machining results of ① and ② were compared, there was a difference in straightness (hole bending) depending on the presence or absence of the rear guide, indicating the rear guide has an effect on straightness.

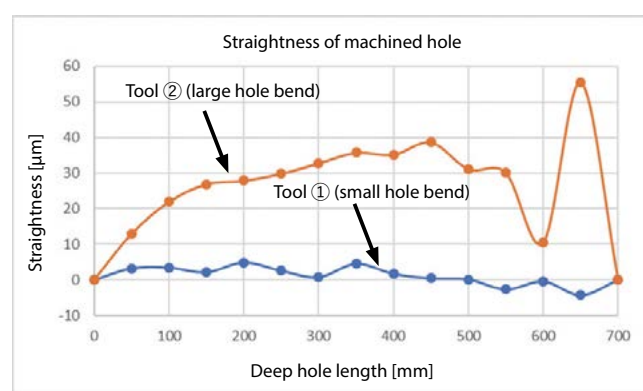


Fig. 6 Difference in straightness depending on the presence or absence of a rear guide

3.4.2 | Tool Adjustment

In general, the recommended tolerances for the inner diameter of the guide bush are G6 tolerance for the machined hole diameter and h8 tolerance for the tool diameter. Based on this, we adjusted the clearance of the tool diameter and the rear guide diameter to the guide bush inner diameter within the tolerance range and verified the effect on the coaxiality. The conditions used for verification were as follows.

- ① Near the lower limit of the clearance tolerance range (small clearance)
- ② Near the middle of the clearance tolerance range
- ③ Near the upper limit of the clearance tolerance range (large clearance)

The machining results are shown in Table 6

Table 6 Tool adjustment verification results

	Machining accuracy [mm]	
	Coaxiality	Diameter variation
①	$\phi 0.015$	$\phi 0.020$
②	$\phi 0.038$	$\phi 0.012$
③	$\phi 0.155$	$\phi 0.017$

It was confirmed the larger the clearance amount between the tool diameter and the rear guide diameter relative to the guide bush inner diameter, the worse the coaxiality tended to be. It was also confirmed an excessively small clearance amount, like the condition ①, would lead to poor roundness.

4 Continuous Processing

Based on the verification results, we optimally adjusted the clearance amount of the tool diameter and the rear guide diameter to the guide bush inner diameter of the tool with rear guide, and then conducted a continuous machining test. We used the same machining conditions as those in Table 3. By appropriately managing the clearance amount, the target accuracy was successively achieved. The machining results are shown in Table 7.

Table 7 Continuous machining results

	Machining accuracy [mm]		
	Coaxiality	Roundness	Diameter variation
1	$\phi 0.028$	0.006	$\phi 0.009$
2	$\phi 0.012$	0.005	$\phi 0.007$
3	$\phi 0.016$	0.006	$\phi 0.006$
4	$\phi 0.020$	0.006	$\phi 0.006$
5	$\phi 0.043$	0.004	$\phi 0.007$

5 Consideration

From the above verification and results, it was confirmed in deep hole drilling the dimensional control of tool diameter, guide bush inner diameter, and rear guide outer diameter affects the coaxiality and roundness of deep holes (red text in Fig. 7).

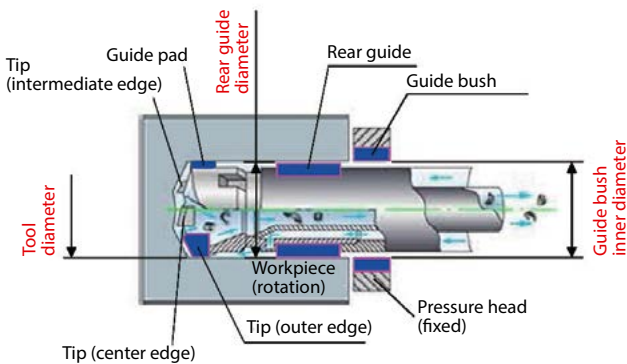


Fig. 7 Details of machining section

In general, the management of tools and the operation of guide bushings are under the control of the customer, and the machining accuracy is also under the control of the customer. In the future, we will be able to offer our know-how to customers who wish to use BTA deep hole drilling machines for high-precision machining to improve their productivity, using this verification as an example. Moreover, to such customers, we would like to make a proposal not only for machining tools but also for methods of utilizing deep hole drilling tools and optimal tools, through partnerships with tool manufacturers. If these proposals lead to the formalization of machining conditions and the improvement of the quality and performance of deep hole drilling tools and their long life, we can expect the optimization of the production process through the improvement of machining quality and the reduction of industrial waste such as defective products and consumables, which will have the effect of reducing the environmental load.

6 Conclusion

In this report, we have examined the machining accuracy of deep hole drilling, which has not been required so far. We will continue to examine different materials, different types of tools, and different machining methods such as counter boring and trepanning.

References

- 1) Reportocean.com, "Deep Hole Drilling Machine Market Research Report"
- 2) ANCA, "NewsLetter", January 2020.
- 3) Excerpted from the website of Japan BTA Co., Ltd. <http://www.fukaanaake.com/btaex.html> (Ref. on 2021-11-18)
- 4) Excerpted from the website of KAWAHARA https://www.kawahara-machine.com/product/bta_index.html (Ref. on 2021-11-18)

Ultra-Precision Machining Technology for Contributing to Higher Power Density of Fuel Cell (FC) Stacks

With the challenge of decarbonizing mobility being set forth as a green growth strategy in conjunction with attaining carbon neutrality by 2050, there are particularly high expectations for fuel cell vehicles. Fuel cell stacks, which act as the power supply unit, are being rapidly developed with higher power densities for practical use, and one reason for these dramatic technological innovations is the high precision of the flow channels of the thin metal sheets called bipolar plates (separators), of which several hundred are mounted in the power supply unit. This paper will present an application example where ultra-precision machining technology was developed for enabling ultra-precision machining of this micro-bipolar plate shape.



Machine Tools Company
Machine Tools Engineering
Department

Kunitaka KURIYAMA

1 Introduction

At the end of 2020, the Japanese government declared its policy goal of achieving a carbon-neutral, decarbonized society by 2050, in which the amount of carbon dioxide and other greenhouse gases emitted and absorbed will be net zero. According to 2018 results, about 20% of the country's 1.1 billion tons of carbon dioxide emissions came from automobiles,¹⁾ and so major changes are needed to adapt to a decarbonized society in the future. In response, recent years have seen the rapid development of technologies in fields such as electric vehicles (EVs) and fuel cell vehicles (FCVs). FCVs are fueled by hydrogen and emit only water, and since they are not fueled by fossil fuels and hydrogen can be generated indefinitely, there are high expectations for them as the ultimate in clean mobility for solving many environmental problems.²⁾

The fuel cell used in FCVs is actually a small generator which generates electricity through an electrochemical reaction between hydrogen and the oxygen in the air. A fuel cell consists of a membrane electrode assembly (MEA) with electrocatalysts coated on both sides of a polymer electrolyte membrane sandwiched between thin plates called bipolar plates, which are composed of separate air and hydrogen flow channels. Fig. 1 shows an overview of the set of structures called a cell. Hundreds of these cells are stacked on top of each other to form the actual fuel cell stack unit.³⁾

The initial fuel cell stack developed in 2008 had a maximum output/volume of 1.4 kW/L (maximum output 90 kW/volume 64 L (108 kg)), but the latest model has a maximum output/volume of 3.1 kW/L (maximum output 114 kW/volume 37 L (56 kg)), which is a 2.2-fold increase in volumetric output density and demonstrates the rapid pace of miniaturization and performance improvements.⁴⁾

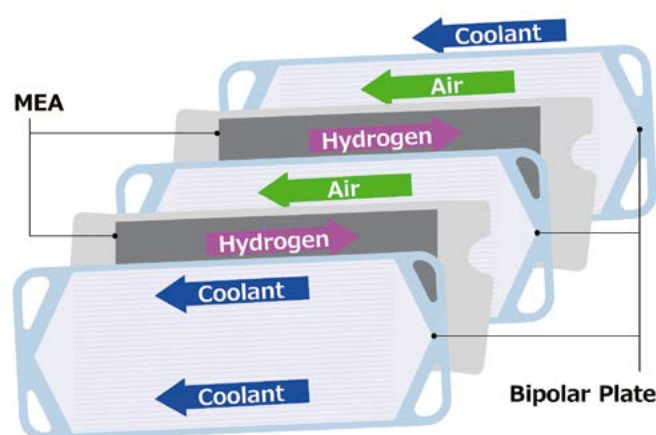


Fig. 1 Unit cell structure of a fuel cell stack³⁾

Higher performance of elements, such as the MEA and bipolar plate, is a factor in the improved output density, but the bipolar plate must have three main features: (1) Complete separation of hydrogen and air flowing on the front and back surfaces, (2) Fine and complex channel shapes to increase the contact area with hydrogen and air, and (3) Thin cells to increase the overall unit density. However, in the conventional press, the thickness of the plate is not uniform due to insufficient machining accuracy of the mold, resulting in extremely thin parts. This can lead to holes in the plate and the mixing of hydrogen and air. Therefore, the bipolar plate requires a high-precision mold which can press the fine channel shape and plate thickness uniformly. This paper presents examples of using an ultra-precision channel machining and compensation method which was developed to improve the performance of fuel cell stacks.

This paper examines the use of ultra-precision machining center UVM to achieve high precision in fuel cell bipolar plates. The UVM series is an ultra-precision machining center which incorporates the nanometer-order elemental technology⁶⁾ developed for the ULG series, which is used in the field of optical lenses, into the realm of general-purpose machining. Fig. 2 shows the four models in the UVM series lineup. The UVM-450C series standard model has a table size of 450 mm x 450 mm. To handle large workpieces, the UVM-700C's table work surface size has been increased to 700 mm x 700 mm, and the maximum loading weight has been increased to 400 kg. The UVM-450D is equipped with a thermostatic system for strengthening the structure against environmental fluctuations and an enhanced internal structure for vibration control and high-precision positioning. The UVM-700E (5AD) is a 5-axis model which provides a high degree of freedom for large workpieces such as automobile headlights. All UVM series models are equipped with Shibaura Machine's aerostatic bearing spindle featuring a maximum speed of 60,000 min⁻¹, and linear motor control with a minimum setting unit of 10 nm is used for all linear axes.

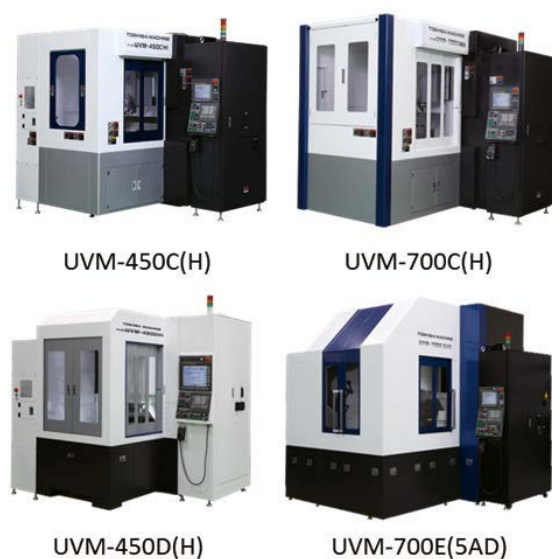


Fig. 2 UVM series lineup

3.1 | Aerostatic Bearing Spindle

Shibaura Machine has been developing aerostatic bearing spindles for their high-precision machine tools since the 1970's. However, general machining centers use ball bearing spindles, and

even most machining centers which claim to be high-precision use ball bearings. While it is true that for high-precision applications, the bearings are designed to be ultra-lightly pressurized, the rolling elements of the bearing are in constant contact with the inner and outer rings, and so vibration, heat generation and wear are inevitable when the bearing rotates. Compared to aerostatic bearings, ball bearing spindles have the following undesirable characteristics: (1) Inferior rotational accuracy, (2) Heat generation during high-speed rotation, and (3) Inevitable deterioration over time.

The aerostatic bearings used in the UVM series have a structure where compressed air is supplied between the rotating shaft and housing to lift the spindle out of the bearing and hold it in place by aerostatic pressure. The air layer smooths out the accuracy error components, making it possible to rotate smoothly, exceeding the machining accuracy of each component adversely affecting the rotational accuracy, such as the roundness and roughness of the rotating shaft and bearings, and reducing the effect of vibrations. Fig. 3 shows a comparison of the actual rotational accuracy measured by a displacement sensor. The ball bearing spindle in the figure on the left shows abnormal vibration errors due to the rolling elements' turning motion as they rotate, while the aerostatic bearing in the figure on the right shows no abnormal vibration errors and rotates with a smooth path.

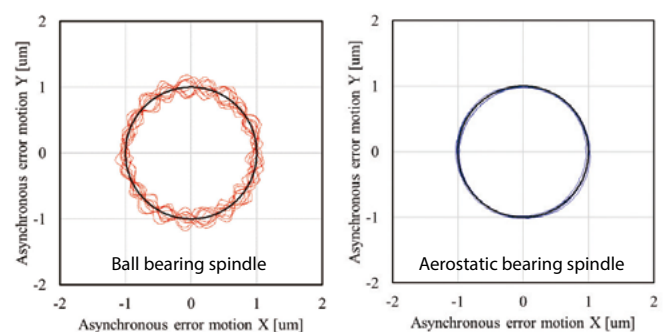


Fig. 3 Comparison of rotational accuracy

3.2 | Linear Motor Drive Control

All linear axis drives of the UVM series are equipped with cored linear motors. The high-rigidity guiding mechanism has a structure which minimizes the degradation of motion accuracy due to magnetic attractive force, which is a concern with cored linear motors, and has the advantage of allowing the setting of high position loop gain and a control resolution of 0.5nm scale feedback. As a result, the performance of the feed system has been improved to a level where steps of 10 nm can be accurately controlled.

Fig. 4 shows the response waveform for a 10nm step feed measured at the same actual machining point as the tool tip. The waveform shows positioning error at the cutting edge was reduced, and accurate and smooth reversing motion characteristics were obtained with high response, which improves the machined surface quality and minimizes manual finishing such as polishing and deburring in mold fabrication.⁷⁾

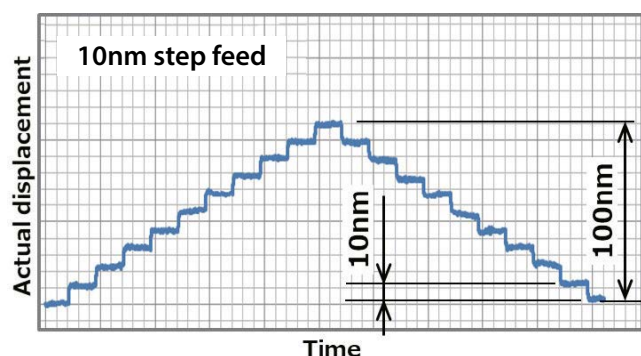


Fig. 4 10nm step response at machining point

4 Machining Technology

Two main evaluation criteria are used for accuracy in ultra-precision machining. These are form accuracy, which indicates the correctness of the form, and surface quality (roughness), which indicates the specularity of the surface. In the field of ultra-precision milling, in addition to high-precision positioning of the machine itself, high form accuracy has been achieved by calculating the correct tool path using 3D CAD/CAM with high calculation accuracy, and high surface quality has been achieved by using a high-speed rotating spindle to minimize chip formation and to reduce workpiece deformation. However, current machining technology is not adequate for bipolar plate molds requiring high form accuracy, and so we developed a machining technology which corrects the accuracy error component of ball end mills to achieve even higher accuracy.

4.1 High-Precision Tool Shape Detector FormEye

Tool measuring devices are installed in conventional machining centers to measure the position and diameter of rotating tools for machining. The UVM series also uses a line sensor type tool measuring instrument, which has the capability to measure the contour of the tool itself. However, in the conventional methods for measuring the tool contour, there is a large interior error on the measuring instrument side when the line sensor is switched between horizontal and vertical, resulting in a large step near the 45° angle of

the tool, which is a major barrier to achieving high-precision correction machining. Since the sensor structure makes this error unavoidable, we studied replacement of the sensor with a method capable of measuring the tool contour more accurately and found the imaging method to be the most suitable. However, the imaging method tends to result in more expensive units and longer measurement times. There are two reasons why imaging-type measurement takes a long time: (1) Image processing of the entire screen takes time, and (2) Because the phase of the high-speed rotating tool cannot be known when shooting, shooting must be performed repeatedly until the photo with a required phase is taken. For (2), because the aerostatic bearing is manufactured in-house, a rotation sensor for phase recognition can be built into the spindle to identify the phase during high-speed rotation, making it possible to complete the measurement with a minimum number of images. Furthermore, minimizing the number of shots enables shorter times required for image processing, allowing for faster processing. Fig. 5 shows the appearance of FormEye during measurement. FormEye can be installed and maneuvered in the same way as existing tool length measuring instruments, and no special treatment is required. Fig. 6 shows the measurement results for the tool contour. The measurement results show that even a brand new tool has an error of about 4 μm from the ideal round shape, which directly leads to a machining error. Also, this measurement function enables step-by-step monitoring of the detailed progression of damage to the tool edge due to wear or other factors after machining, enabling accurate tool life management.⁸⁾



Fig. 5 View of FormEye measurement

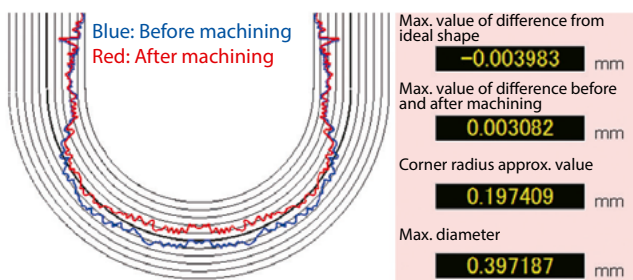


Fig. 6 Tool contour measurement results

4.2 | Tool Path Vector Correction

Even in ultra-precision milling, the machining process consists of (1) Model creation in 3D-CAD, (2) Machining path generation in CAM, (3) Actual machining, and (4) Measurement analysis. FormEye has made it possible to obtain accurate tool contour data, but currently, no matter how high the computational accuracy of 3D CAD/CAM, only an ideal shape of a perfect circle can be defined for tools. Therefore, if an error of 4 μm is found in the actual tool contour, as shown in Fig. 6, the error is directly transferred to the machined workpiece as a form error component. If the tool protrudes from the perfect circle, which is the ideal shape, the machined workpiece will be over-cut. However, if the tool is receded from the perfect circle, the machined workpiece will have uncut sections. In order to correct this error, information is needed on which direction and how far to retract or advance. Since FormEye provides information on the unevenness of the tool contour, it is only necessary to identify which position of the tool is acting at each selected machining point on the workpiece surface.

To solve this problem, we developed software which provides an error correction function called "tool path vector correction." In tool path vector correction, 3D CAD data is used to identify each contact point of the tool and provide information on which direction to move the tool. Fig. 7 shows a schematic diagram of tool path vector correction. In the conventional process, a tool radius value is input to the 3D model to calculate the NC data for machining. If the result does not pass the subsequent analysis, it can take nearly 100 hours to modify the 3D model and recalculate the NC data by inputting an optimum tool radius value. Furthermore, if the machining results are not satisfactory, this corrective machining routine must be repeated several times, resulting in a tremendous loss of production time. In contrast, the process using tool path vector correction automatically corrects the NC data coordinate values on the machine side based on the values measured by FormEye, making it a "method of error

correction not returning to CAM" where 3D model correction and NC data re-creation are unnecessary. This enables significant reductions in loss of production time from non-machining processes.

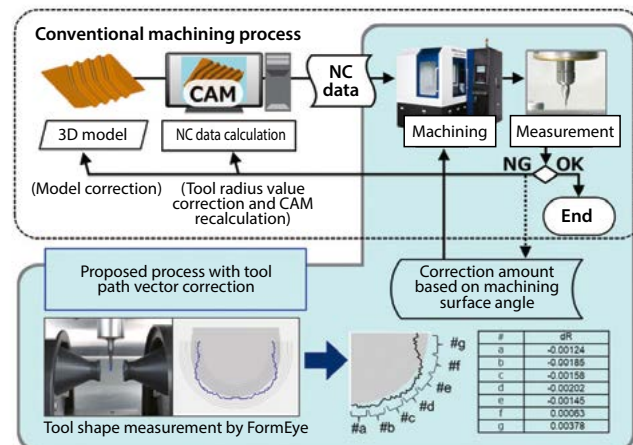


Fig. 7 Schematic diagram of tool path vector correction

5 | Machining Verification

Machining verification of the bipolar plate form was conducted with the aim of improving the form accuracy using FormEye and tool path vector correction. The 3D model and cross-sectional view of the bipolar plate form for machining verification are shown in Fig. 8. The workpiece material was stainless steel for molds (HRC52), and the tool was a cBN ball end mill (R 0.5 mm). Fig. 9 shows the contour accuracy of the ball end mill and the tool correction amount obtained by FormEye's tool shape measurement. The correction amount calculated from the tool contour is minimal around 0° at the tool rotation center, and increases toward the periphery, reaching a maximum of 2.5 μm around 90°. Therefore, when machining without correction, the form accuracy will be $2.5 + \alpha$ (effect of wear or disturbance) μm , and as the angle of the workpiece approaches the 90° vertical wall, over-cutting due to tool contour error is expected to occur. Using this tool, a machining test was conducted to compare the correction effects with and without tool path vector correction. The form accuracy of a cross section of the machined surface was measured by a FormTalysurf PGI850A (made by TAYLOR HOBSON). Fig. 10 shows the machining results without vector correction. The form accuracy is -3.2 to $+0.2$ μm (PV : 3.4 μm), which is a large error from the design value and does not meet the required accuracy. While the workpiece surface is cut without error near the 0° angle, excessive cutting is observed as the angle of the workpiece surface approaches 90°. Fig. 11 shows the machining results with vector correction. The results of machining with vector correction show

that the phenomenon of over-cutting seen without vector correction has been improved, and a form with almost no error relative to the design form was obtained. The form accuracy was -0.6 to $+0.7\ \mu\text{m}$ (PV : $1.3\ \mu\text{m}$), which is less than $\pm 1\ \mu\text{m}$, which is required for bipolar plate molds.

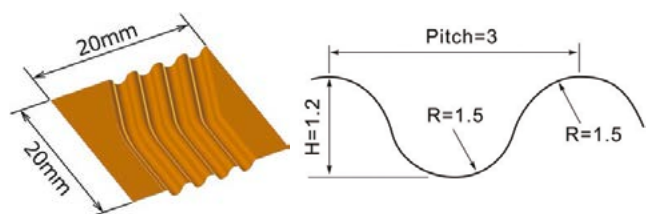


Fig. 8 3D model and cross-sectional shape

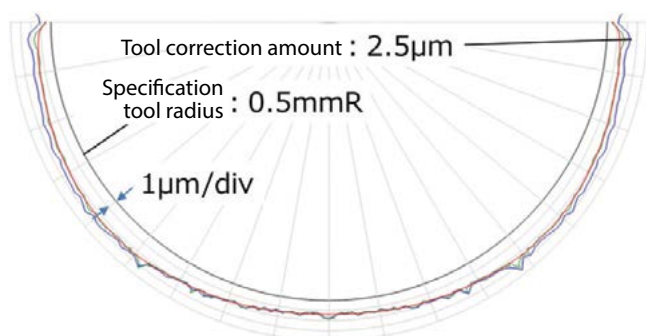


Fig. 9 Tool correction amount

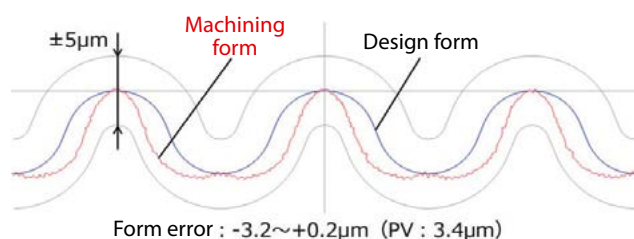


Fig. 10 Cross-sectional form accuracy without vector correction

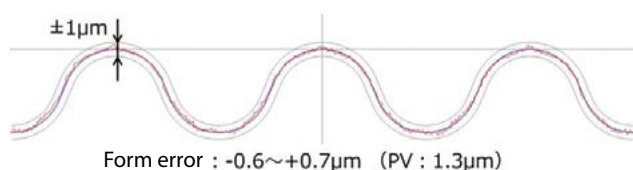


Fig. 11 Cross-sectional form accuracy with vector correction

6 Conclusion

This paper describes one example of the development of machining technology for high-precision forming of bipolar plates for fuel cell stacks. In addition to this case, many other industrial products are improving their performance at a remarkable pace, and the component parts are becoming significantly more precise and miniaturized. Consequently, while more and more markets will

be requiring nanofabrication technology, there will also be more areas where conventional manufacturing processes cannot be adapted, and so the production process itself needs to be examined beyond the existing framework. We will continue to identify needs from new perspectives and strive to expand the application scope of nanofabrication technology for manufacturing.

References

- 1) Japan Automobile Manufacturers Association, "Japan's Automobile Industry 2020," 30.
- 2) H. ONAKA, Development of Fuel Cell Vehicles at Toyota, *Hydrogen Energy Systems* 34, 2, (2009) 10-17.
- 3) A. MIYAZAWA et al., Development of a New Compact High-power and Low-cost Fuel Cell Stack, *Society of Automotive Engineers of Japan* 40, 5, (2009), 1267-72.
- 4) H. NAKAJI et al, Development of High performance and Low cost Fuel Cell stacks, *Production and Technology* 68, 2, (2016), 72-75.
- 5) Honda Motor Co., Ltd., CLARITY Fuel Cell https://www.honda.co.jp/tech/auto/CLARITY/five_seater.html (accessed Oct.18.2021)
- 6) Shibaura Machine Co., Ltd., ULC/ULG Series: http://www.toshiba-machine.co.jp/jp/product/nano/lineup/ulg_lg/index.html (accessed Apr.12.2021)
- 7) A. AMANO, Technology to Improve the Accuracy and Efficiency of Mold Machining Using Ultra-Precision Machining Centers, *Mold Technology*, February 2021.
- 8) Y. MUROFUSHI, Importance of On-machine Tool Shape Measurement and FormEye, a High Precision Tool Shape Measuring Instrument, *Mold Technology*, June 2021.

Extended Battery Life of the Resolver Multi-Turn ABS and its Contribution to the Circular Economy

In recent years, growing global interest in the SDGs has become a major trend, accelerating the effective use of resources and carbon-free initiatives in many countries. Our BS servo system has an absolute position detection system called the "Resolver Multi-Turn Absolute System" which applies a resolver to detect the position of the servo motor. However, since the circuit is driven by a battery during a power failure, power consumption determines the life of the battery. In this resolver multi-revolution ABS system, we have made efforts to save power, extend the maintenance period by extending the battery life, and reduce the number of primary batteries used. In this paper, we introduce our efforts.



Control Systems Company
Control Systems Engineering
Department

Narutoshi YOKOKAWA



Control Systems Company
Control Systems Engineering
Department

Kazuya WATANABE

1 Introduction

With the growing interest in the SDGs, practical ways to realize a "Circular Economy," have been attracting attention. A circular economy refers to efforts to minimize the input of new resources and raw materials, creating new value in what is already being used, and minimizing the generation of waste.

At present our BS servo system has an absolute position detection system called "Resolver Multi-Turn Absolute System" (hereinafter called "ABS"). This system maintains the machine home position by means of battery backup in case of power failure or when the power is turned off. The advantage of this system is the machine coordinates are remembered when the power is turned on again, so there is no need to search for the origin at startup. Since the circuitry which constantly monitors the motor movement continues to operate with battery backup in case the machine is moved during a power failure, this power consumption determines the life of the battery. Routine maintenance after machine operation requires replacement of the battery before it reaches the end of its life. For this reason, primary alkaline and lithium batteries are often used, which are inexpensive and readily available even overseas. Currently, most of the used batteries are discarded. According to an estimate by the Battery Industry Association of Japan, 49,000 tons of batteries are disposed of annually in Japan, which translates to 2.1 billion AA

batteries disposed of annually. The beneficial environmental impact of recycling is greater than that of general disposal, but the view remains general disposal of batteries is appropriate, so recycling has not been expanded.

Under these circumstances, one of our efforts to contribute to the recycling-oriented economy is to reduce the amount of battery waste by saving power. In this report, we introduce our efforts to date to reduce the power consumption of the resolver multi-turn ABS system.



Fig. 1 BS servo system

2 Past Activities

2.1 Resolver Multi-Rotational ABS System Features

We first introduce the resolver multi-revolution ABS system. The main feature of the resolver multi-revolution ABS system is the

construction of an absolute position detection system at low cost without external sensors, without compromising the overwhelming environmental resistance (heat resistance, vibration resistance, shock resistance, and long life). In other words, during a power failure, the resolver body continues to monitor the angle and number of rotations as it does when the power is turned on. In general, a separate magnetic sensor would be externally mounted and an electronic circuit provided in the sensor section, but the merits of the resolver are greatly diminished when an electronic circuit is added to the motor sensor because the environmental resistance performance is reduced. For the characteristics of the sensor alone, Table 1 shows the comparison with our serial encoder. The resolver's values for environmental resistance and long-distance transmission are based on the specifications, and its performance is even higher than the values.

Table 1 Comparison of sensor characteristics

Item	Resolver	Serial encoder
Allowable rotation speed	10,000 min ⁻¹	6,000 min ⁻¹
Resolution	24,000 P/rev	131,072 P/rev
Angular error	8 min	1 min
Vibration resistance	20 G	10 G
Shock resistance	100 G	20 G
Ambient operating temperature	-55 ~ 155 °C	-10 ~ 85 °C
Maximum transmission distance	120 m	30 m

With the latest BS servo system R series, it is possible to build a resolver multi-revolution ABS system by simply connecting a battery and changing some parameters, without adding any optional boards, by selecting a resolver compatible servo amplifier and motor.

Table 2 History of power consumption reduction in resolver multi revolution ABS system

Development Steps	Main approaches	Battery life ^{*1)}	
2003 Development of V series	• Pulse excitation power recovery • reverse excitation disconnection detection	3 parallel AA lithium battery	2 years
2008 Development of X series	• Ultra-low power consumption CPLDs adopted		4 years
2012 Development of S series	• Analog circuit reduction		4.5 years
2018 Development of R series	• Addition of electric double layer capacitor	1 AA lithium battery + capacitor	6 years

*1) The condition for calculating the service life is when the power of the servo system is turned on for 12 hours and off for 12 hours.

2.2 | History of Power Consumption Reduction

The history of power consumption reduction from the beginning of development in 2002 to the present is shown in Table 2. The development steps were carried out in conjunction with the development of the BS servo system series, and the battery life has been steadily extended. At the beginning of the development the optimal conditions were derived from the trade-off between the pulse width of the excitation pulse, the signal-to-noise ratio of the received signal, and the allowable power consumption. In addition, power recovery of the pulse excitation was implemented to reduce the power consumption within that range. At that time, it was extremely difficult to detect wire breakage within the limitations of low power consumption, but we cleared this problem by using reverse excitation pulses.

This was followed by improvements in the performance of capacitors and lithium batteries used in mobile information terminals, and the emergence of ultra-low power consumption CPLDs (Complex Programmable Logic Devices) and CPU devices, which we also adopted to further reduce power consumption. As a result, we were able to triple the maintenance period of the resolver multi-revolution ABS system from the initial development stage. We were also able to reduce the number of primary batteries from the original three to one, thus reducing the amount of primary battery waste to 1/9.

2.3 | Specific Approaches

The following sections describe concrete examples of implementation.

2.3.1 | Power Recovery for Pulse Excitation

A simplified diagram of the resolver excitation circuit is shown in Fig. 2. Our excitation system uses two-phase excitation and one-phase output, and two-phase excitation uses PWM (Pulse Width Modulation) excitation because the accuracy of the voltage amplitude and phase difference of 90 degrees affects the detection accuracy. For this reason, a bus transceiver is used to drive excitation. Normally, continuous PWM excitation is used for angle detection while the power is on to achieve high accuracy and high resolution, but when the power is off, intermittent pulse excitation is used because low power consumption is necessary. Fig. 3 shows an example of the

excitation voltage waveform. In the case of pulse excitation, the pulse width of driver S1 is set to a few μs , and S3 is set to half the width.

Since the resolver has a large inductance, widening the pulse width increases the current. As a result, current flows in the cable and the resolver itself, and the signal-to-noise ratio of the signal fed back from the resolver is improved, but power consumption also increases. To improve this situation we have devised and implemented a function to recover the excited energy to the power supply. Fig. 4 shows the mechanism of energy recovery. Each FET represents the output stage of the driver shown in Fig. 2.

(A) State before applying excitation pulse

Drivers S1 and S3 both output Low voltage, and FETs (Field Effect Transistors) Tr2 and Tr4 connected to the GND are turned ON, while Tr1 and Tr3 connected to the power supply are turned OFF.

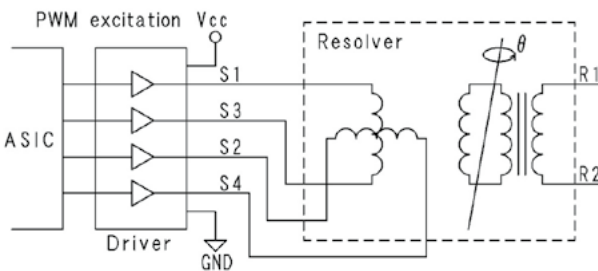


Fig. 2 Simplified diagram of resolver excitation circuit

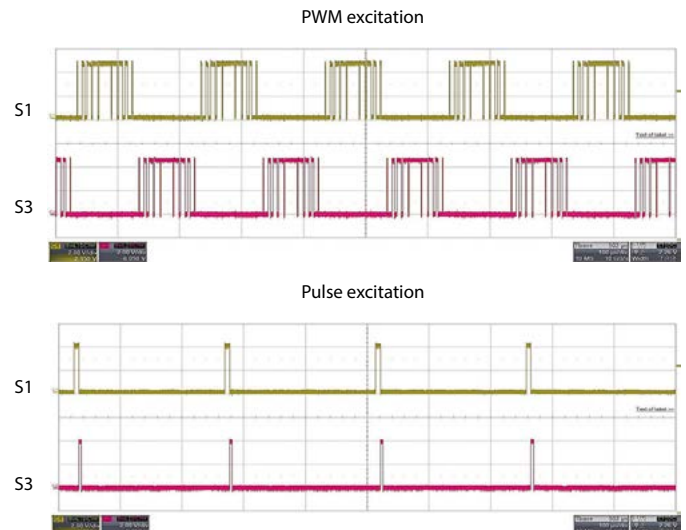
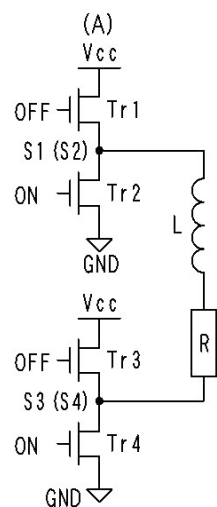
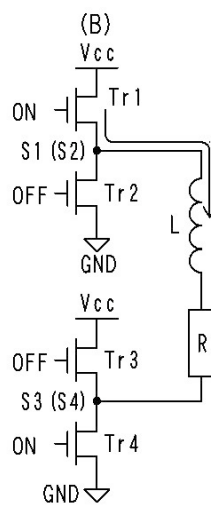


Fig. 3 PWM excitation and pulse excitation

(A) State before applying



(B) After applying excitation pulse



(C) When excitation pulse is OFF

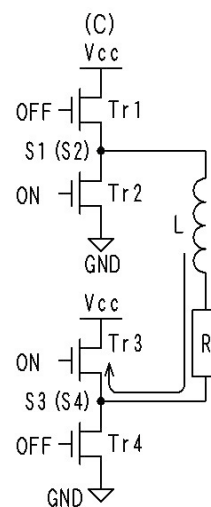


Fig. 4 Recovery of excitation energy

(B) State with excitation pulse applied

When Tr2 of driver S1 is turned off and Tr1 is turned on, a high voltage is output, voltage is applied to the resolver coil, and current begins to flow in the coil. At this time, energy U is stored in the coil.

$$U = \frac{1}{2} LI^2$$

U : Energy (J)

L : Inductance of the coil (H)

I : Current (A)

(C) State when the excitation pulse is turned off

After the pulse width time has elapsed, the driver S1 is set to LOW voltage to stop the application of voltage, but at the same time, Tr4 is turned OFF and Tr3 is turned ON to set the driver S3 to High voltage. Then, the current in the coil flowing in the state of (B) goes through Tr3 and returns to the power supply. This is equivalent to recovering the energy of the coil to the power supply. In fact, although there are losses such as resistance components of the coil and ON resistance of the FET, 70 to 80% of the excitation energy can be recycled by this recovery. By recycling the energy which would be lost in resistance and released as heat if left as is, we are implementing a circular economy.

2.3.2 | Application of Electric Double Layer Capacitor

When industrial machines operate 24 hours a day, they are always in operation except for a few weeks a year during year-end holidays and summer holidays, and the actual battery life is extended because the power supply from the battery is small during power outages, etc. On the other hand, if the power supply is turned on during the day and off at night, the battery power is used during the night. This power is supplied from an electric double layer capacitor installed in the amplifier.

Fig. 5 shows the application circuit of the electric double layer capacitor, and Fig. 6 shows a photograph of the implementation. Even when the power is turned off, provided the voltage of the capacitor remains, no power is supplied from the battery. The electric double layer capacitor is slowly charged while the power is ON to prepare for the next power OFF period. However, when the power supply is turned off for as long as 10 days during weekends, year-end holidays, and summer vacation, it is not possible to use the battery at all. However, the battery life of six years was achieved by reducing the number of lithium batteries from three in parallel to one. Although electric double layer supercapacitors have existed since the beginning of development, it was difficult to apply them, but the recent increase

in voltage resistance and capacity, low cost, miniaturization, and reduction of circuit current consumption made it possible. Currently, only a few users are equipped with these supercapacitors, but we will consider making them standard in the future.

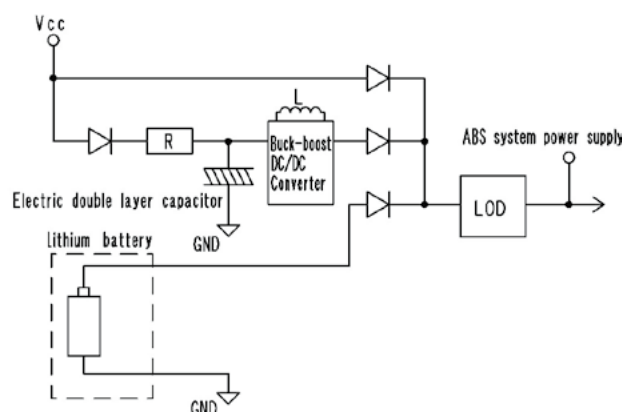


Fig. 5 Application circuit for electric double layer capacitor



Fig. 6 Electric double layer capacitor mounting board

3 Conclusion

In this report, we have described various measures to reduce the power consumption of the resolver multi-revolution ABS system to extend battery life. We believe we can continue to contribute to the circular economy by efficiently even with the energy of AA batteries, by using it with ingenuity and without waste. We have not been able to mention wire breakage detection and other technologies in this report, but please refer to the patent gazette for details. ^{1)~3)}

References

- 1) Patent No. 4364569: Resolver signal processing device
- 2) Patent No. 4364570 Resolver signal processing device
- 3) Patent No. 4364571, Resolver signal processing device

Training Junior Employees using Digital Technology : Standardized Documents in Video Format

In recent years, the widespread use of tablets and other mobile devices has made it possible to easily view large video files at worksites. We are using these tablets to give operators access to standardized documents (formerly text-only) in video format, featuring easy-to-understand photos, footage, and supplementary text to cover the same content as the original documents. These documents can efficiently convey nuances that are difficult to convey only in text format in a short time, and the technical terms that are used in the field of manufacturing can be recognized and understood. More than 50 standardized documents have been converted to video manuals so far through our efforts from 2017.



Production Center
Machinery & Production
Engineering Department

Ryosuke FUJIMOTO

1 Introduction

Seniors are expected to make up a third of Japan's total population by 2030¹⁾, eroding the nation's working population and causing severe labor shortages. The working population had already fallen by an average of 180,000 people over the previous year in fiscal 2020²⁾, so Japan is already facing labor shortage challenges. At the same time, employers must be willing to take on a workforce which is more diverse than ever before, lending critical significance to operating standards. The issues covered in this report are relevant to two Sustainable Development Goal targets: 4.3 (substantially increase the number of youth and adults who have relevant skills, including technical and vocational skills, for employment, decent jobs, and entrepreneurship) and 9.4 (greater adoption of clean and environmentally sound technologies and industrial processes).

One of the challenges we face in the Machinery & Production Engineering Department at our Production Center is transferring skills to junior operators. The specialized terms used at worksites have nuances which are difficult to communicate in written form or orally, so the junior employees vary widely in terms of their levels of understanding and how long it takes them to acquire this knowledge. There are also situations where technical skills are difficult to express in written words, making it essential to instruct people verbally. And yet, even oral communication ultimately only explains the actions themselves, with the purpose of the operation often lost. Once this happens, operations are subject to ad hoc shortcuts which are intended to support efficiency but run the risk of triggering quality issues which were never problems before.

At Shibaura Machine, we used to use written (text format) standardized documents and oral explanations to communicate

operating standards to junior operators. But with the widespread availability of tablets and other mobile devices which can be used at worksites, we have been able to show large video files on the floor. Our company has therefore begun using mobile devices to create video versions of our standardized documents (video manuals) which use pictures and video coupled with supplementary text explanations. This report describes the makeup of the video manuals we use at our worksites and our results.

2 Implementation

Our basic rules for creating video manuals include standards for ensuring safety, ease of use, and quality. We also include standards for target operation times to ensure efficiency. Fig. 1 shows our procedure for creating video manuals. We start by selecting a video to create (target operation), creating and revising a storyboard, recording the video, and then editing and revising the footage.



Fig. 1 Procedure for creating video manuals

2.1 Creating the Storyboard

Creating a storyboard is a critical part of the process, as it gives a clear picture of the overall flow of the video manual by visually indicating the screen configurations for each clip. Storyboards consist of a job (title), basic operations, required tools, detailed operations, and an inspection step. Storyboard creators also consider the amount of time needed for each clip. Fig. 2 shows an example of a storyboard for a video on how to maintain a digital dial gauge.

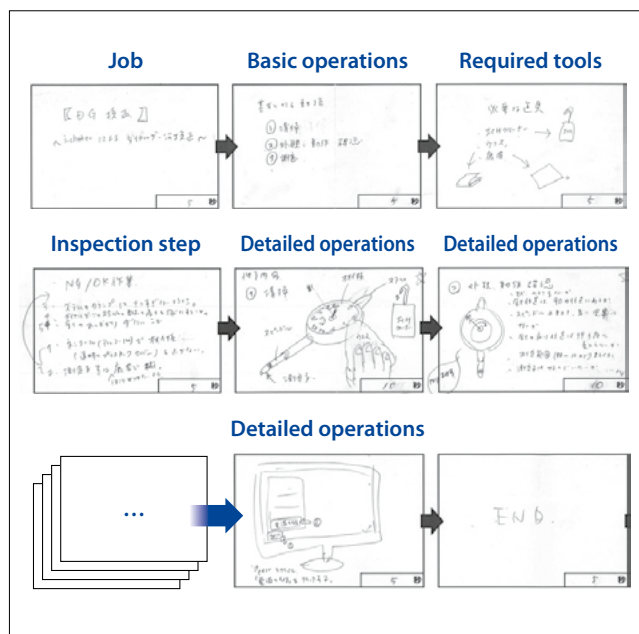


Fig. 2 Example of a storyboard

The basic operations clip divides the overall job into major steps. It also includes explanations of any technical terms used. In this example, the basic operations are cleaning, confirming external operation, and measurement. The required tools clip shows photos of all the tools needed for the operation as well as their names in text. In this example, the operator will need an ICH cleaner, shop cloth, and deerskin cloth. The detailed operations clips include detailed explanations designed for inexperienced operators. The inspection step explains how to inspect the work and provides pass/fail criteria along with a film of a perfectly-performed operation. In this example, the failed operation is “not wiping away with the ICH cleaner because it makes the transparent plastic cover foggy and makes the gauge hard to see.” The pass operation is “wiping the gauge head and other components with the deerskin cloth so dust does not adhere to them.” Each detailed operation describes the corresponding inspection step.

All members involved in the job participate in the making of the storyboard, which then serves as a springboard for discussion, revisions, and additions to make sure frontline workers are on board with the video and can use it on site.

2.2 | Recording the Video

The required footage is recorded quickly while consulting the storyboard. As shown in Fig. 3, an iPhone^{*1} or iPad^{*2} is used for the recording. Operators are consulted to determine the recording angles or distances which will best indicate the key points of each

operation or subject so the video is easy to understand. Both film and stills are used as needed, as still images make it easier to explain tools or other non-moving components of the operation.

(*1, *2 : iPhone and iPad are trademarks of Apple Inc.)



Fig. 3 Video recording

2.3 | Editing the Video

Next, an iPhone/iPad video creation and editing app (Photron's Mobile Video Creator) is used to edit the footage. Editing can take place at the worksite since the same iPhone or iPad used to take the videos is also used for the editing process (Fig. 4).



Fig. 4 Video editing

Video editing is also guided by the storyboard, with every effort made to keep the video to around three minutes total. The three-minute standard allows operators to focus on the video while they are on the job. For longer operations, content is split up into different scenes to keep the videos from dragging on. Fig. 5 shows the storyboard alongside the edited video.

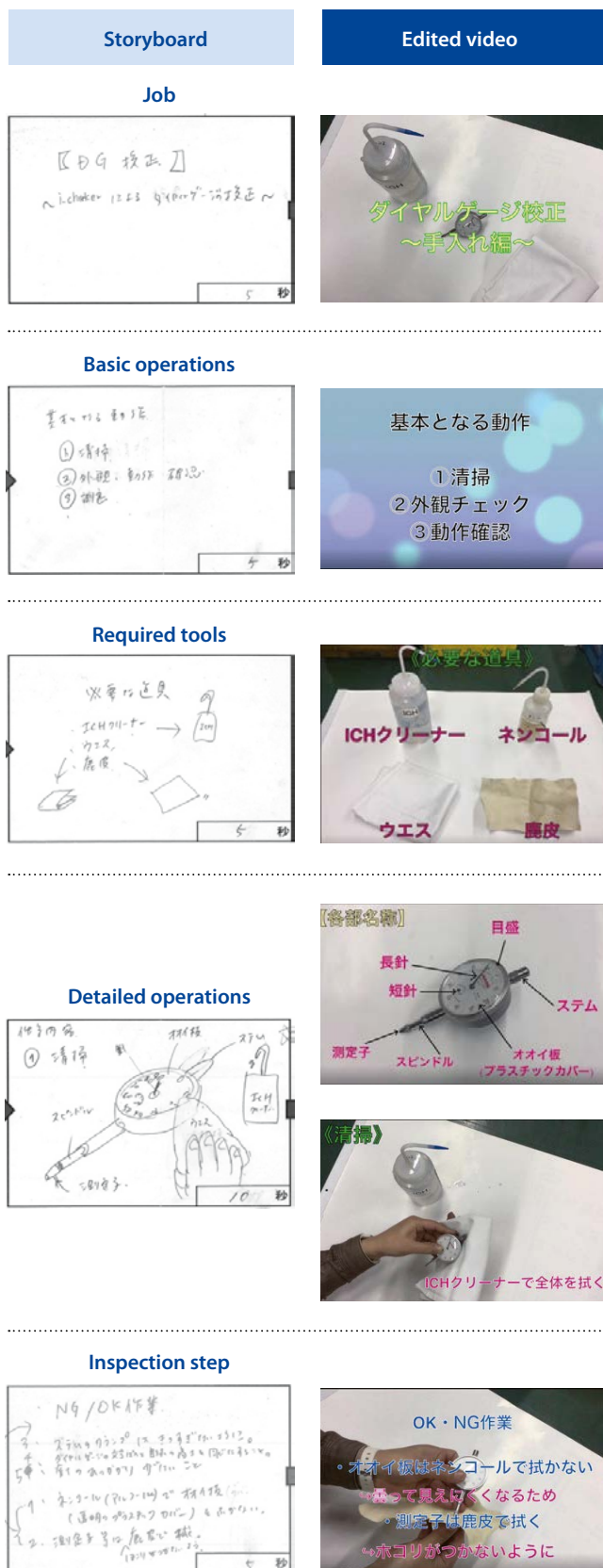


Fig. 5 The storyboard and edited video

As shown in Fig. 5, the edited video faithfully replicates the content in each storyboard clip. The editors select the footage which matches the parameters of the storyboard and then insert text and

images. They can also add music or narration tracks to effectively demonstrate key points. Once all editing tasks are complete, the final version is reviewed using a preview function and saved.

Videos are kept to an absolute minimum to speed up processing time and limit storage demands. Video manuals are saved at 960 x 540 and a bit rate of 4 Mbps. At this rate, the data load per second is 4 megabits/8, or 0.5 megabits per second.

3 Results and Outlook

Experienced operators use standardized documents to transmit skills to junior operators primarily at worksites during on-the-job training sessions. This means both those teaching and learning the material are often pressed for time. Use of the video manuals allows skills to be efficiently transmitted to multiple operators in a streamlined way when there isn't enough time to do so on the job. Fig. 6 shows operators using the video manual at a worksite.



Fig. 6 Watching a video manual at a worksite.

Prior to using iPhones and iPads to create video manuals, we used home video cameras coupled with desktop video editing software. The video manuals were still highly valued, but each one took about two days to create. Switching to the iPhone and iPad video creation and editing app, however, has allowed us to shorten video creation time to around three hours. And because the same device is used to edit and film the videos, revisions and additions can be made on the spot - further streamlining the process.

We can achieve quality management through the implementation stage of Total Quality Management (TQM), based on the Systems component of the ISO 9000 series. The Union of Japanese Scientists and Engineers (JUSE) has issued a list of action steps for TQM and

quality management activities related to the ISO and TQM standards.³⁾ According to this document, standardization is the key to taking operations from stage three to stage four within a total of five steps. The action items listed are (1) thorough education and training in all departments based on rules and standards, (2) clear enactment and revision of rules and standards, (3) seeking root causes (of both occurrence and outflow) and preventing recurrence, (4) implementing “go and see” management and change management, and (5) permeating standardization and daily management throughout the organization. The video manuals have proven to be an effective method of overcoming the hurdles to achieving these standardization-related targets at our worksites.

Casting and machining processes can involve fluctuations and sudden changes which must be swiftly addressed on the plant floor. The key here is standardized operations. If every operator has the same streamlined knowledge, then they should be able to properly implement the OODA Loop (Observe, Orient, Decide, Act)⁴⁾ even at worksites which undergo dramatic situational changes.

Our Production Center will continue to use digital technology to improve the quality of its manufacturing practices, aiming for efficient production which raises the bar on quality, cost, and delivery (QCD) with a small workforce.

4 Conclusion

We create video manuals using a four-step process: selecting the target operation, creating a storyboard, recording the video, and editing the video. Using mobile devices with a video creation and editing app allows us to move from filming to editing in a short period of time. Using these video manuals at worksites has allowed us to transmit skills to multiple operators in an efficient, streamlined way - even when we are pressed for time. In this way, video manuals powered by digital technology have proven to be an effective method of overcoming the hurdles to implementing standardized operations at worksites, thereby enabling high-level quality management and efficient production in line with ISO 9000 series and TQM standards.

References

1. Population Projections for Japan, National Institute of Population and Social Security Research (2017)
2. Labor Force Survey (Basic Statistics) 2020 Averages, Statistics

Bureau of Japan (2021)

3. Guide to Taking TQM and Quality Management Activities to the Next Stage, Union of Japan Scientists and Engineers (2014)
4. OODA Loop, Chet Richards (translated by Tsutomu HARADA), Toyo Keizai (2019)

Development of an AI-based Function to Monitor the State of Machining during Cutting in the Double Column Type Machining Center

Human senses play an important role in the processing field of the manufacturing industry. There are many craftsmen in Japan who have mastered the technique, called Takumi (master artisan), but it is almost impossible to pass on their technique to future generations in a nearly perfect state. This research was conducted with the aim of making AI (artificial intelligence) learn the senses of an operator to reproduce his/her discernment ability when operating a machine tool as a subject. In particular, much information is obtained from sound during cutting. Therefore, this research focused on 3-axis acceleration during machining. As a result, a high machining state accuracy has been achieved as evidenced by the data we received.



Research & Development Center
Research & Development
Department

Taku HOSHIYA

1 Introduction

In machining, the state of ongoing machining is judged based on the information from the operator's five senses including sight and hearing. However, the acquisition of a sense-based discernment ability is impossible in a day and requires enormous experience. This research focused on a supervised multiclass classification technique in deep learning to replace with AI the discernment ability of humans acquired through experience.

By making AI learn the discernment ability, even people without skills or experience will be able to perform stable processing, which improves productivity and leads to relaxation of employment conditions. The 8th item in the SDGs, "Decent Work and Economic Growth", aims at achieving "full and productive employment", protecting "labor rights", and promoting "safe and secure working environments" by 2030 for all workers including migrant workers irrespective of their age and gender. Therefore, it becomes possible to contribute to the above-mentioned SDGs if employment conditions are relaxed while ensuring a high-level of economic productivity as a result of this research.

2 Dataset Overview

2.1 Dataset

For supervised multiclass classification, input data to be given to AI and training data showing what kind of data the input data is, are necessary.

In this research, the object was machining by a double-column type machining center (MPF-2614FS). Certain data processing was performed for the acceleration data acquired from the 3-axis

acceleration sensor installed on the side surface of the spindle, and the processed data was input to AI.

2.1.1 Acquired Data

Fig. 1 shows an example of acceleration data acquired during machining. In Fig. 1, a difference is seen between the tool idle region (gray area), the machining introduction region (orange area), the stabilized machining region (blue area), and the machining closing region (green area).

In this study, first, a data set for the stabilized machining region (blue area) and a data set for the other regions (hereinafter referred to as unstable data) in Fig. 1 were created. Options for differentiating the three states during machining in the stabilized region; (i) normal state, (ii) chipping state, and (iii) chattering state, were set. AI needs to differentiate between the four options, including (iv) unstable data, to determine which machining acceleration data corresponds to which state.

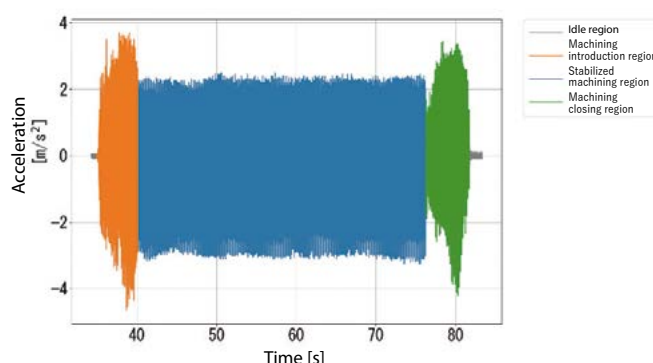


Fig. 1 Acceleration data during machining

2.1.2 Preprocessing of Data

As a method for analyzing acceleration data, the FFT (Fast Fourier Transform) was used in this research. This time, acceleration data per

second was analyzed, and binning was performed first. Binning is a method to calculate the representative value in a certain section (bin width). It is possible to extract the characteristics of the FFT result data (1 to 3.2 kHz) described above by performing binning for 100 sections for every 20 Hz (bin width). The analysis was performed for 1 to 2 kHz.

This time, it was thought that the characteristics of the FFT result could be maintained by using the maximum value as the representative value in the section.

The milling cutter, a tool used in a machine tool, has multiple parameters such as the number of blades, rotation speed, and machining direction. The nature of acceleration changes as the parameters fluctuate. To optimize the versatility of AI, preprocessing which absorbs the effects of parameter fluctuations is important. In this research, we performed binning and synthesis/normalization of binning results as pretreatment.

For binning, in expectation of improvement of general versatility, we focused on the forced vibration during machining, which depends on the rotational speed during cutting and the number of blades of the tool. The formula for calculating the forced frequency is shown as the equation (1).

$$\text{Forced frequency [Hz]} = \frac{\text{Rotational speed [min}^{-1}\text{]}}{60 [\text{s}]} \times \frac{1}{\text{Number of blades}} \quad (1)$$

It can be seen in the equation (1) that the forced frequency depends only on the rotational speed and the number of blades. In this research, reference values were set for the number of blades, rotational speed, forced frequency, and bin width to deal with fluctuating parameters. Table 1 summarizes the reference values.

Table 1 Reference parameters

Reference number of blades	8
Reference rotational speed	500 min ⁻¹
Reference forced frequency	66.67 Hz
Reference bin width	20 data items

As shown in Table 1, the reference forced frequency is 66.67 Hz. This means the value of the forced frequency will be stored in the fourth section (61 to 80 Hz) if binning is performed with a bin width of 20 Hz. In this research, the bin width was adjusted so the forced frequency would be stored in the fourth section under all conditions.

The process of adjusting the bin width is shown below.

a) Calculating the correction coefficient of the number of blades

The correction coefficient of the number of blades is a coefficient for correcting the difference in the number of blades which differs for each tool. The reference number of blades was set to eight according to Table 1. The formula for calculating the correction coefficient of the number of blades is shown as the equation (2).

$$\text{Correction coefficient of the number of blades} = \frac{\text{Actual number of blades}}{\text{Reference number of blades}} \quad (2)$$

b) Calculating the correction coefficient of rotational speed

The correction coefficient of rotational speed is a coefficient for correcting the difference in rotation speed which differs for each machining operation. The reference rotational speed was set to 500 min⁻¹ according to Table 1. The formula for calculating the correction coefficient of the rotational speed is shown as the equation (3).

$$\text{Correction coefficient of rotational speed} = \frac{\text{Actual rotational speed}}{\text{Reference rotational speed}} \quad (3)$$

c) Calculating correction coefficient of bin width

Based on the equations (2) and (3), the formula for calculating the coefficient for adjusting the bin width and the correction coefficient of rotational speed is shown as the equation (4).

$$\text{Correction coefficient of bin width} = \frac{\text{Correction coefficient of the number of blades} \times \text{Correction coefficient of rotational speed}}{\text{Correction coefficient of bin width}} \quad (4)$$

d) Adjusting the bin width

The bin width is adjusted using the equation (4). The equation used for the adjustment is shown as the equation (5).

$$\text{Bin width} = \frac{\text{Reference bin width} \times \text{Correction coefficient of bin width}}{\text{Correction coefficient of bin width}} \quad (5)$$

The above is the process of adjusting the bin width.

Since the object of analysis in this research is 3-axis acceleration, the same processing was performed for each axis. Fig. 2 shows an example of binning in the range of 0 to 200 Hz. The red dashed line in Fig. 2 indicates the bin width, and the maximum value therein is the representative value.

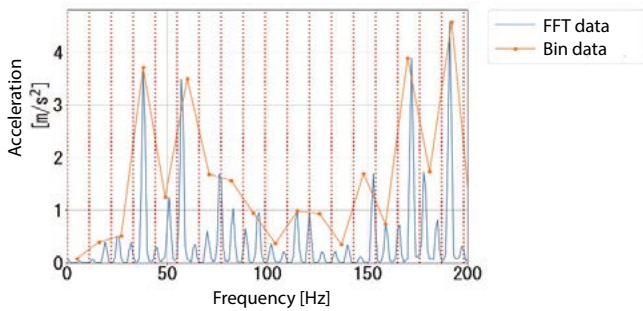


Fig. 2 FFT and binning

2.1.3 | Effect of Cutting Direction

Cutting process at a processing site is not only single-axis cutting such as single-plane cutting.

It is clear a huge amount of time is required to collect data in consideration of the cutting pattern. In this research, it was considered that highly generalized AI could be created by making AI learn created data obtained by reducing the effects of cutting direction by normalizing and synthesizing the X-axis, Y-axis, and Z-axis binning data. The process is shown below.

a) Normalization of 3-axis binning data

There is a wide variety of vibrations during machining, and the maximum acceleration recorded by each vibration type varies depending on the data. This may lead to AI recognizing the difference in the magnitude of the maximum value, which is a problem when considering generalization. In this research, it was decided that unifying the maximum acceleration for all data would solve this problem. The equation used for the normalization is shown as the equation (6).

$$\text{Normalized data } (x', y', z') = \frac{\text{(Binning data for each axis)}}{\text{(Maximum value of 3-axis binning data)}} \quad (6)$$

In this way, by using the equation (6), normalized data having a maximum acceleration of 1 is created. Since the amplitude was set to an absolute value in FFT, the normalized data is composed of a value of 0 to 1.

b) Synthesis of 3-axis normalized data

As described in this section, reducing the effects of direction leads to improvement of generalization. In this research, it was decided the effects of direction could be reduced by synthesizing the normalized data for each axis. The equation used for the synthesis is shown as the equation (7).

$$\text{Synthesized data } (r) = \sqrt{(x'^2 + y'^2 + z'^2)} \quad (7)$$

At this time, the maximum value of the synthesized data may differ depending on the machining direction. Therefore, by dividing the synthesized data by the maximum value as shown in the equation (6), the synthesized data was also normalized so it was composed of a value of 0 to 1.

Based on the above, in this research, deep learning was performed using 100 items of normalized synthesized data as input data. As an example, Fig. 3 shows a graph of synthesized data which has been normalized under normal conditions.

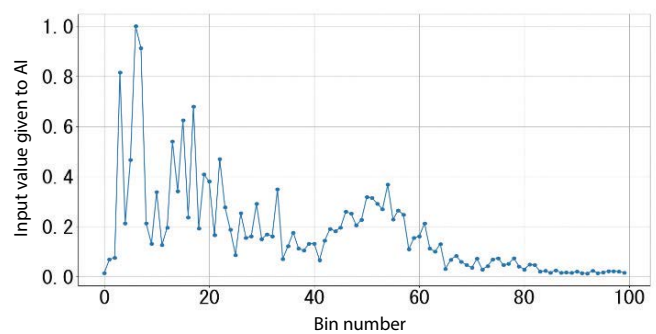


Fig. 3 Synthesized data

2.1.4 | Training Data

As explained in section 2.1, AI learning requires input data to be given to the AI as training data. First, the input data given to AI was normalized as described in section 2.1.3. With respect to training data, the classification of four states of machining was utilized in this research, and it was found from Fig. 1 that training-labeling of stable and unstable regions was relatively easy. The stable region was training-labeled based on the determination of the machining operator in execution of a cutting test.

3 Results and Consideration

Table 2 summarizes the relationship between the discernment results of an AI model using verification data and the training labels.

As shown in the thick frame in Table 2, all items of the stable region (normal, chipping, and chattering states) judged as mis-discernment are "unstable". This is because although current unstable data corresponds to the areas where the acceleration is unstable, the acceleration data in the stable state is mixed in during data processing in some cases; as a result, the characteristics of the

stable region are also included for learning. A possible solution to this is to exclude the range where the boundary between the stable region and the unstable region is ambiguous at the time of data extraction by combining such range with information such as spindle status from NC. By this, it is considered possible to reduce the number of misdetections.

4 Conclusion

This report described research showing it is possible to classify machining into four states by performing deep learning of

characteristic data which was extracted from 3-axis acceleration data and preprocessed to minimize the effects of parameters.

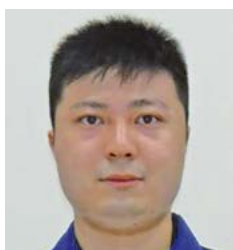
However, the discernment accuracy shown this time has been verified within the data we currently have, so it is necessary to verify the versatility by using more data in the future. In addition, trends of more complex data groups may be shown at the stage of verifying the generalization, so it is possible the final discernment accuracy will be lower than the current one. Although there are still issues to be solved, we intend to proceed with research on the added value of machine tools for making them more intelligent.

Table 2 Discrimination results

		Prediction result			
		Normal	Chipping	Chattering	Unstable
Training labels	Normal	1657	0	0	3
	Chipping	0	905	0	1
	Chattering	0	0	91	3
	Unstable	14	7	3	566

Column

Perspectives Gained from My Work



Metal & Plastics Industrial Machine Company
Metal & Plastics Industrial Machine Technology Department

Koichi KUMAKI

My assigned work is currently the development of hybrid core cylinders for die casting molds. Conventional core cylinders are controlled only by hydraulic pressure, but hybrid core cylinders are either electrically controlled or controlled by hydraulic pressure, and the control method can be changed depending on which is most suitable. Initially, my understanding of cores was that they only move in one dimensional direction, so I thought allowing simple back and forth movement would be enough.

However, as soon as I started my work, I realized my understanding of cores was naive. Since cores move to press against the mold and a hybrid core cylinder uses a ball screw, if the core is affected by an exterior effect such as pressing force, a positioning error will be caused. Therefore, it is not enough to simply move it back and forth, but countermeasures are needed. That is what I found. From this experience, I learned the importance of understanding the entire event from various perspectives, such as the action of forces when the machine moves and the characteristics of the machine, not to mention understanding the superficial aspects of machine operation. I will use this experience to carry out my future work.

Introduction of Large-Size Electric Injection Molding Machine EC1800SX III



1 Overview

Amid the background of a declining working population due to a decreasing birthrate and ageing population, improvements in the productivity of factories have long been a pressing issue. On the other hand, global interest in SDGs such as the suppression of energy consumption towards the realization of a low-carbon society is increasing. High productivity and labor-saving features in an injection molding machine are therefore important contributions towards resolution of these issues. We developed the large size electric injection molding machine EC1800SX III as a product to realize this goal.

2 Features

The EC-SX III series of electric injection molding machines employs a linear guide in the moving die plate support structure to achieve high productivity by high-speed mold opening and closing and is top of its class in the industry.

In addition to this feature, the EC1800SX III can be equipped with new high-speed mold thickness adjustment specifications as a special option to achieve even higher productivity.

2.1 Shortening of Mold Exchange Time

Resin parts which make up the end product are also becoming more diverse due to the diversification of consumer needs, and as a result, the increasing frequency of mold exchange is a significant trend. Mold sizes are also diverse, allowing molds with a thickness from 800 to 1500 mm to be mounted in the EC1800SX III. In a typical toggle-type mold clamping device, the mold thickness adjustment

speed when replacing the mold with one having a different mold thickness is extremely slow due to the mechanism. Therefore, when exchanging molds between thin and thick types, the downtime (non-productive time) increases, leading to a drop in production efficiency.

To resolve this problem, the mold thickness adjustment speed was improved in the EC1800SX III.

By supporting the link housing (a component of the mold clamping device) with a linear guide, the sliding resistance is reduced, and by high-speed rotation and high-precision positioning control of the servo motor, a drastic increase in the repeating speed and stability by the mold clamping force are achieved. A resulting increase in production quantity is one of the effects of increasing this mold thickness adjustment speed.

Fig. 1 shows a comparison of the mold exchange time for a difference in mold thickness of 700 mm.

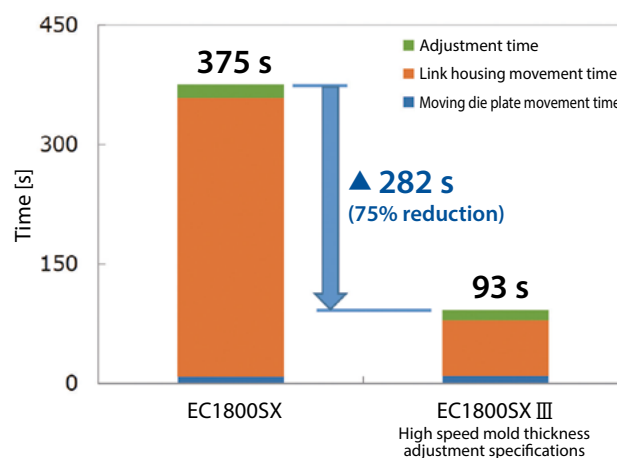


Fig. 1 Comparison of mold exchange time

Compared to EC1800SX, the time can be shortened by 282 s (75% reduction). Assuming the mold exchange count per day is 10, the

time is shortened by 172h¹ annually, and an increase in production volume by 20,680 shots^{*2} can be expected.

*1: Number of operating days 220 days/year

*2: Molding cycle 30 seconds

On the other hand, to immediately restart production once mold exchange is complete, the heater of the heating cylinder is on standby in a powered-up state even during mold exchange. The proportion of power consumed by the heater in an electric injection molding machine is high, so a shortening of the mold exchange time (standby time) is directly linked to a reduction in power consumption.

Fig. 2 shows the standby power consumption during mold exchange.

Compared to the EC1800SX, the reduction in power consumption is 1.6 kWh (56%) per hour in the EC1800SX III, so on a converted basis, an annual reduction of about 0.5 tons in CO₂ emissions can be possible.

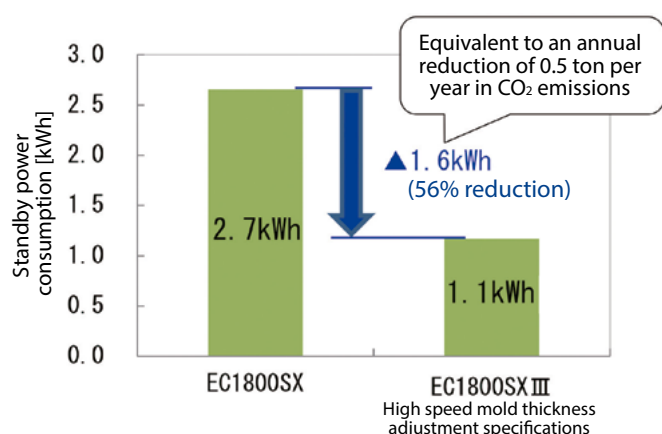


Fig. 2 Standby power consumption during mold exchange

2.2 | Automation of Set-up Work

Every time a molded part is changed, a “set-up operation” to exchange the mold and switch the type and color of the raw resin material needs to be carried out. Since operations and judgments are carried out by the operator, there is a potential risk of human error.

Fig. 3 shows a partial excerpt of the production process.

When production under molding condition A is completed, set-up operation (set-up condition 1) is carried out before the next production (molding condition B) is initiated. After production under molding condition B is completed, set-up operation (set-up condition 2) is executed.

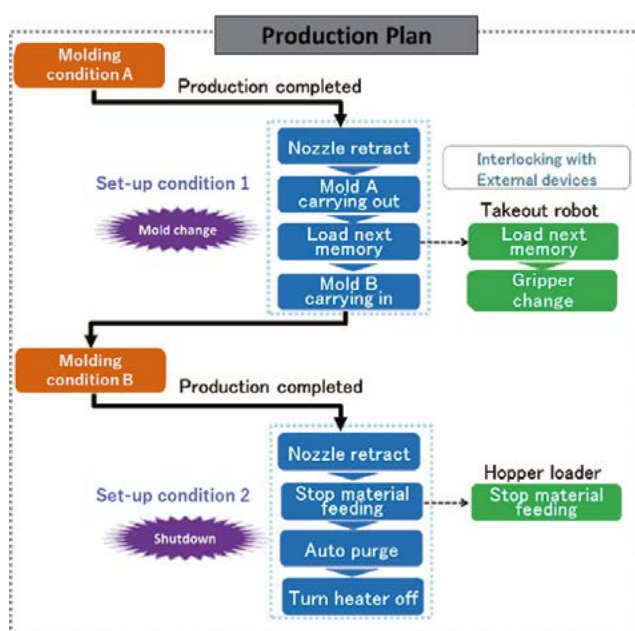


Fig. 3 Example of a production process

To support these tasks, the controller “INJECTVISOR-V70” is equipped with a production planning function called “INDUSTROL”. In the production plan shown in Fig. 4, a series of actions under multiple molding conditions and set-up conditions can be set. When production under molding condition A is completed, set-up condition 1 is automatically executed, and when it ends, production under molding condition B is started. Similarly, when production under molding condition B is completed, set-up condition 2 is executed.

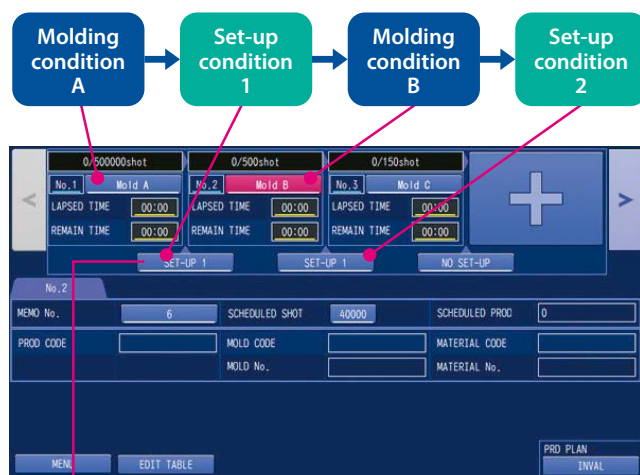


Fig. 4 Production plan



Fig. 5 Set-up condition settings

Fig. 5 shows the set-up condition settings. Each operation is visually represented by an icon, allowing the operator to freely create a work program by placing the operation icons in the work sequence. A feature of the system is the ability to intuitively check the settings in this way.

Being able to switch the molding condition and configure the set-up process beforehand allows the operator to reduce human error, shorten the work time, and carry out other tasks while the process is being automatically executed. Moreover, since this function is highly compatible with peripheral ancillary devices (automatic mold exchanger, auto coupler/connector), it can easily support automation and labor-saving for switching molded parts.

3 Summary

We developed the EC1800SXIII as a product which is capable of greatly contributing to higher productivity, labor-savings, and the realization of a low-carbon society as cited in our SDGs. Moving forward, we intend to continue developing injection molding machines which can meet the needs of the world.

Introduction of the Newest Die Casting Machine DC1300R-E



1 Overview

Die casting is more productive than other casting methods, and its ability is largely dependent on the die casting machine. This report introduces the die casting machine DC1300R-E, which we have developed for improving productivity.

The DC1300R-E is a large high-cycle die casting machine which operates at high speed by employing a servomotor to drive die-plate open and close and a pump which fills the accumulator (ACC) at high speed.

Equipped with the newest controller TOSCAST-999, the DC1300R-E offers improved display visibility and operability.

2 Features

1) By adopting a toggle mechanism driven by an electric servomotor, the die clamping time is shortened as compared with the conventional model. (Fig. 1) The DC1300R-E features higher response than hydraulic die clamping and stable operation by precise position control. As optional features of the DC1300R-E, core advanced return and spray position intermediate stop operations are available. (Fig. 2) In addition, a high cycle is realized by simultaneous operation of the electric die clamber and the hydraulic actuator.

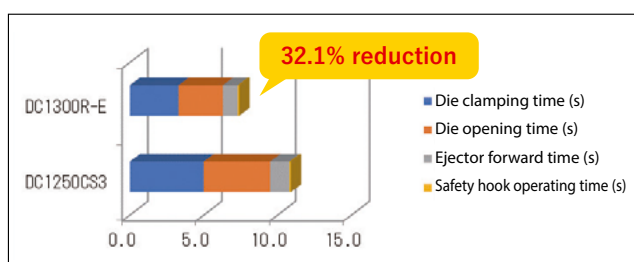
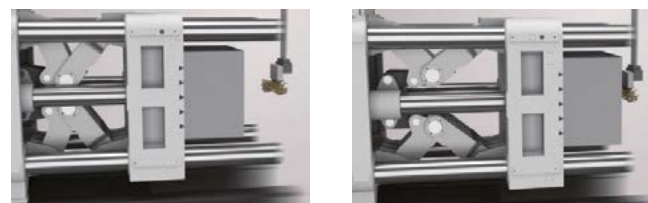


Fig. 1 Cycle comparison



Spray descending position
(die opening limit)

Die intermediate position

Fig. 2 Die opening / closing intermediate stop

2) Space saving has been achieved by reducing the size of the tank inside the frame, which was made possible by electrification of die-plate clamping and by modifying the layout of the hydraulic motor. The DC1300R-E can be installed in the same space as a machine one class-size smaller. (Fig. 3)

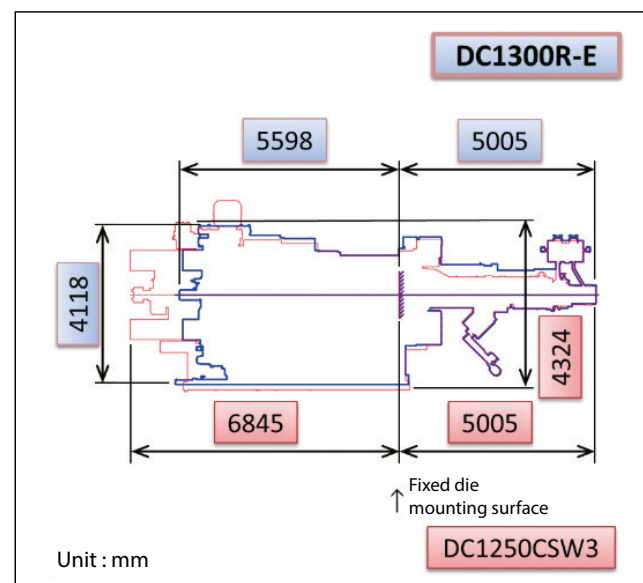


Fig. 3 Space saving

3) As the number of hydraulic parts decreased, hydraulic problems have decreased, failure time has decreased, and maintainability has improved.

- 4) By adopting a large-capacity hydraulic pump as standard, the speed of hydraulic operations, such as accumulator filling, has increased.
- 5) The upper 2-tie bar draw-out equipment is equipped as standard, making it easy to change dies.
- 6) Equipped with the newly developed large-screen TOSCAST-999 controller, the operability of the DC1300R-E has drastically improved. (Fig. 4)

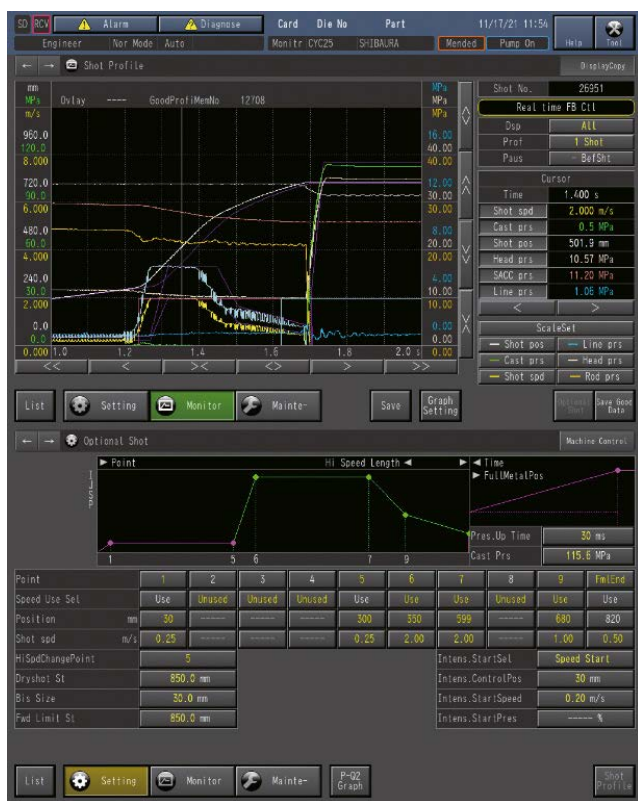


Fig. 4 TOSCAST-999 controller

Documents which are referenced by the user, such as ladder circuits, instruction manuals, and schematic diagrams, can be digitally displayed on the screen to reduce paper and improve workability.

7) Conformance to SDGs

The implementation of high-cycle technology for die casting machines that make products from highly recyclable aluminum alloys can improve productivity and contribute to society.

3 Specifications

Table 1 shows the specifications of the DC1300R-E. The specifications of the previous model DC1250CSW3 are also shown for comparison. The items colored in light blue indicate improved performance as compared to the DC1250CSW3.

Table 1 DC1300R-E specification table

Specification comparison

	Unit	DC1300R-E	DC1250CSW3
Clamping	Clamping force	kN 13000	12500
	Die plate dimensions (vertical x horizontal)	mm 1895x2205	1930x1800
	Space between tie bars (vertical x horizontal)	mm 1250x1525	1250x1120
	Tie bar diameter	mm 250	250
	Die height	mm 700 to 1500	600 to 1500
	Die stroke	mm 900	900
Injection	Maximum injection force	kN 1080	1080
	Intensifier ratio	1 : 2.56	1 : 2.56
	Injection plunger stroke	mm 950	950
	Plunger jog stroke	mm 400	400
	Injection opening position (downward from the center of the machine)	mm 300	300
	Injection speed	m/s 0.1 to 9.0	0.1 to 9.0
	Plunger tip diameter (standard)	mm 115	115
	Casting volume (standard insert diameter)	cm ³ 7375	7375
	Casting area (standard tip diameter)	cm ² 1250 to 3215	1251 to 3215
	Casting pressure (standard tip diameter)	MPa 40.4 to 104.0	40.5 to 104.0
Ejection	Ejection force	kN 615	616
	Ejector stroke	mm 150	200
Hydraulics	No. of movable cores	Set 3/4"x2	3/4" x2
	Movable core ports (per solenoid controlled valve)	Set 1"x2	1" x4
	No. of fixed cores	Set 3/4"x1	3/4" x1
	Fixed core ports (per solenoid controlled valve)	Set 1"x2	1" x2
	Operating hydraulic pressure	MPa 15	15
	Required hydraulic fluid amount	L 2100	2200
Cooling water	Hydraulic fluid oil tank capacity	L 1880	1900
	Die cooling water inlet connection pipe diameter	Rc 2"	1+1/2"
	Die cooling water outlet connection pipe	Rc 3"	3"
	Heat exchange cooling water inlet pipe	Rc 1+1/2"	1"
	Heat exchange cooling water outlet pipe	Rc 1+1/2"	1"
	Die cooling adjustment valve (fixed)	RcxSet 1/2"x10	1/2" x20
	Die cooling adjustment valve (movable)	RcxSet 1/2"x10	1/2" x20
	Plunger tip cooling water adjustment valve	RcxSet 1/2"x1	1/2" x1
	Required cooling water (for heat exchange)	L/min 50	50
	Required cooling water (for dies)	L/min 160 to 240	160 to 240
Machine size	Required floor area (length x width)	mm 10300x3800	11800x3500

4 Effects

By implementing electric die-plate clamping, the following three effects have been achieved.

- 1) Core return operation can be performed while the moving die-plate is being opened.
- 2) The spray operation and the moving die-plate operation can be linked to shorten the spray time. *Option
- 3) Electric servo control has made it possible to accurately approach the spray nozzle.

5 Conclusion

The DC1300R-E is the latest model designed to improve the operating rate and product quality.

We will continuously meet the needs of our customers by expanding our product lineup.

Introduction of the High-Shear Processing Machine HSE-48

1 Overview

As the need for plastics becomes more diversified, the functionality of extruders needs to be further extended. High-performance plastics are produced through the process of adding an inorganic filler or a polymer into another kind and kneading them in an extruder. However, if they are not sufficiently kneaded, the additive will not be dispersed properly in the polymer. As a result, expected functionality will not be demonstrated.

To solve this challenge, Shibaura Machine has developed the High-Shear Processing Machine HSE-48 (Fig. 1) through joint study with HSP Technologies Inc. HSE-48 features higher shear performance than the TEM Twin Screw Extruder Series. This report introduces the features of HSE-48 and example applications.



Fig. 1 HSE-48

2 Features

HSE-48 consists of three sections: the preliminary kneading section which is designed to melt resin, the high-shear section which is designed to apply high shear forces into resin, and the metering and pressurizing section. The Twin Screw Extruder TEM-26SX is used as the preliminary kneading section. Also, a single screw extruder with a barrel whose inside diameter is 48 mm is used as the metering and pressurizing section.

Adopted as the high-shear section is a single screw extruder with a barrel whose inside diameter is 48 mm with a maximum screw speed of 3600 min^{-1} . As illustrated in Fig. 2, a hole is drilled through the side of the screw. Directly behind the through-hole is a reverse

screw. This section is structured so excessive heat can be suppressed by intercepting resin, applying additional shear forces, and then passing it through the through-hole.

HSE-48 has a motor, a control panel, and an operation panel integrated in a single frame. In addition, the preliminary kneading section can be turned in the direction shown by the blue arrow in Fig. 3 so it can be compactly folded. This helps to transport the machine with ease. Also, translating the preliminary kneading section in the direction shown by the black arrow allows us to change the feed port in the high-shear section and then to adjust the length of the barrel in the high-shear section.

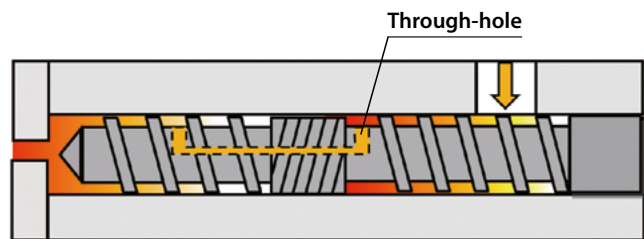


Fig. 2 Cross sectional view of the high-shear section

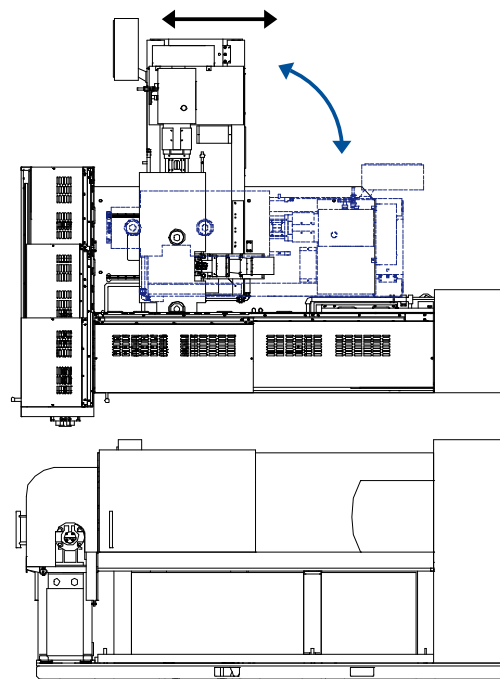


Fig. 3 When in operation (black) or being transported (blue)

3 Specifications

The mechanical specifications and the dimensions of HSE-48 are as shown in the tables below.

Table 1 Mechanical specifications

	Max. screw speed [min ⁻¹]	Motor power [kW]
Preliminary kneading section	745	30
High-shear section	3600	132
Metering and pressurizing section	207	5.5

Table 2 Outer dimensions and weight

H × W × H [mm] (When in operation)	2980×3590×1780
H × W × H [mm] (When being transported)	1910×3590×1780
Weight [kg]	4970

4 Effects / Application Examples

• High-density recycled CF (hereafter called RCF) compound

At first, the use of commercially available carbon fiber (hereafter called CF) compound was considered when the high-shear processing machine was developed. However, this resulted in shorter fibers due to high shear forces as well as low mechanical strength. Therefore, we decided to increase the tensile rigidity of the base material rather than increase the tensile strength by exerting high shear forces to break CF into pieces and charging more compound.

Typically, a commercially available CF compound has a CF content of 30 to 40wt%. But in this study, we considered charging a compound with a CF content of 40wt% or higher (50 to 70wt%). Also, low-priced RCF was adopted. As a comparison, it was discussed whether a CF compound with a CF content of 40wt% or over could be charged into a twin screw extruder. But when content was 50wt% or over, scattered spots of CF were found, and CF could not be continuously pelletized. On the other hand, when using the high-shear processing machine, the diameter of the through-hole, the number of through-holes in the screw, and the screw speed in the high-shear section were adjusted to find the optimum condition. As a result, material which was stiffer than an Al alloy or as stiff as a Mg alloy (with a CF content of 60wt%) was successfully produced. (Fig. 4) In addition, from the view of mill cost, the use of an RCF compound may be more cost competitive than that of a commercially available CF compound. For this reason, we will test the marketability and physical properties (blockage of electromagnetic waves and heat radiation) of this material.

• Lowering the molecular weight of general-purpose polypropylene (PP)

The production volume of a very low-viscosity resin, which is used to manufacture meltblown nonwoven fabric, is so low it is dealt with at a higher price than general-purpose resin. Therefore, if the molecular weight of general-purpose resin can be reduced, the raw material cost can also be reduced. In addition, if the molecular weight of resin can be adjusted as desired, it is expected meltblown nonwoven fabric with a variety of physical properties will be manufactured.

For this reason, we tested how much the molecular weight of general PP (melt flow ratio of 30 g/10 min) could be lowered using HSE-48. The test was performed with a throughput of 2 kg/h and a screw speed of 3600 min⁻¹ in the high-shear section and a barrel temperature of 260 °C with 4 barrels. As a result, the test demonstrated the melt flow ratio (hereafter called MFR) of the PP was approximately 1500 g/10 min. Typically, MFR required to manufacture PP meltblown nonwoven fabric is approximately 1000 g/10 min. Therefore, the requirement was successfully met.

In addition, in this study, the PP with MFR of approximately 1100 g/10 min, which was produced using the high-shear processing machine, was actually made into meltblown nonwoven fabrics. With respect to the physical properties of the nonwoven fabric, the mass per unit area was 30 g/m², and the average fiber length was 1.6 μm. The produced nonwoven fabrics looked white, became free from discoloration, and felt flexible. Furthermore, the fibers were so densely packed no gaps were found. When the produced nonwoven fabrics were observed using SEM, there were no significant variations in the fiber diameters. Also, no residual resin was found. These results have proved it will be possible to perform melt blown extrusion at a lower cost while maintaining the quality of the conventional products.

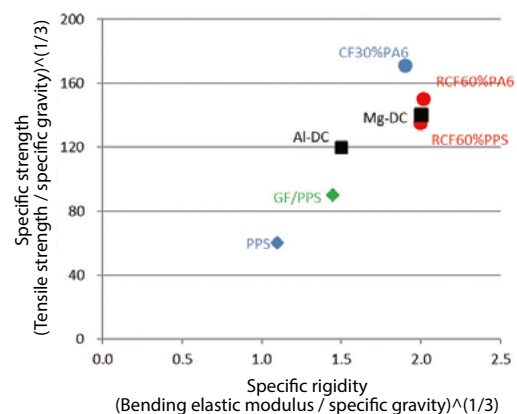


Fig. 4 Physical properties of the high-density RCF compound

Introduction of Real-time Collision Check Function to Prevent Machine Collisions and Interference

1 Overview (Background and Purpose of Development)

Damage caused by machine tool collisions and interference can lead to major damage, including the following:

- Damage to machines, jigs, materials, and tools
- Increase in costs due to repairs and repurchases
- Lower production efficiency due to downtime

Currently, to prevent collisions and interference, the program is visually checked by the operator. However, there is a lot of dependence on the operator's sense and experience, and many human errors are caused by inability to see, lack of attention, or other simple mistakes. Therefore, as an aid to operators, we developed software for a Real-Time Collision Check (RTCC) function which detects collisions and interference before they occur and stops the operation.

With this function, the following effects can be expected.

- Reduction of time and cost loss due to damage
- Reduction of operator's work time
- Reduction of unnecessary cutting fluid and hydraulic oil consumption as well as electricity consumption

2 Features

2.1 System Configuration

Fig. 1 shows the system configuration. The Real-Time Collision Check function connects the CNC machine to an external PC via LAN cable to perform 3D simulations in advance. This function prevents collisions and interference by detecting interference through simulation using coordinates which precede the actual machine tool movement and stopping the operation. Since this function does not require a specific operation mode, it can detect tool interference and machine interference other than cutting in addition to MDI (Manual Data Input) operation and automatic operation, thereby reducing failures.

The Collision Avoidance Software (CAS) consists of our relay application Shiba CAS and VERICUT CAS, which is a machine collision check function extracted from the NC simulation software VERICUT provided by CGTech. At this time we are building our own CNC machine TOSNUC and Shiba CAS, so possible collisions can be checked in real time.

In order to use this function, it is necessary to prepare 3D shape models of machines, jigs, materials, and tools.

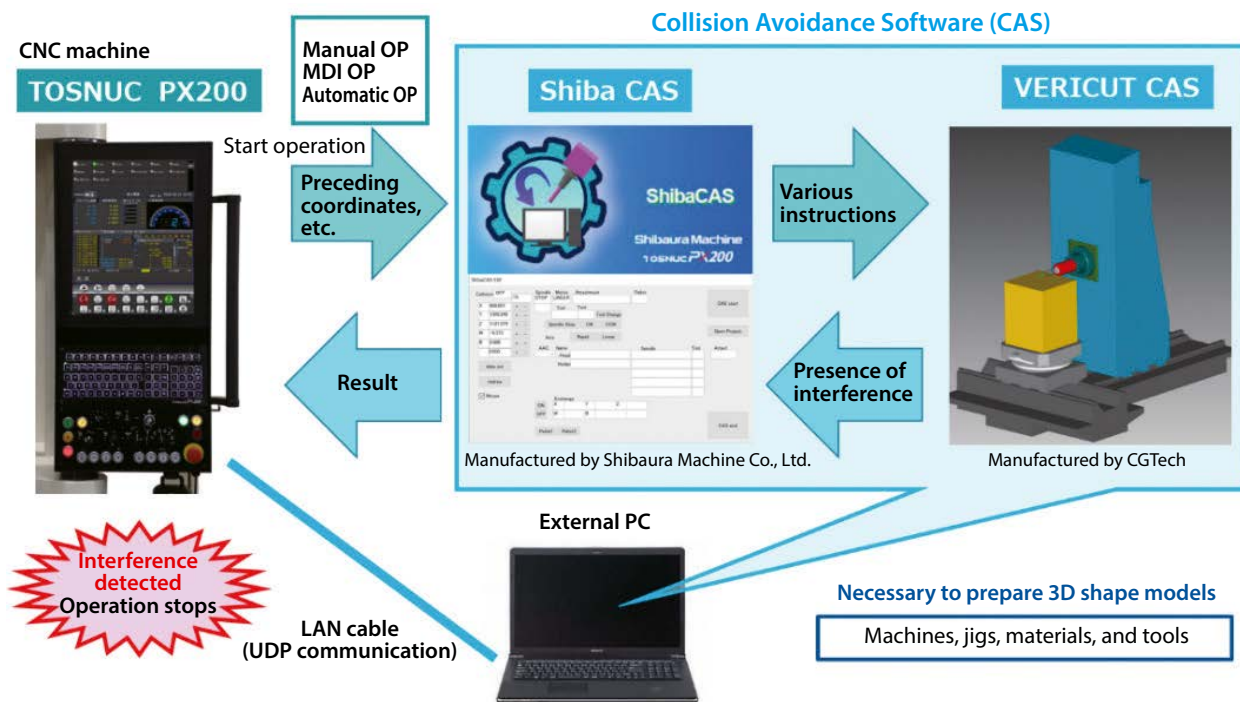


Fig. 1 System configuration

2.2 | Sequence Axis Motion Support

The sequence circuit is mainly used to create the data transfer part for the angle indexing (AAI: Auto Attachment Index) of the attachment.

Our double column machining centers have special attachments with virtual axes (B-axis and C-axis) depending on the model. These two axes are controlled by the C-axis control function of the NC spindle, unlike the normal servo axes. Since the data of the B- and C-axes under control cannot be sent directly from the NC to the CAS, the angle data is written in the data table determined by the sequence circuit and then sent to the CAS.

Also, if interference is identified during AAI, the machine will stop in the middle of operation. In this case, complex operations will be required for recovery, and much time will be consumed. Therefore, as shown in the sequence axis operation flow in Fig. 2, the sequence circuit has been changed so as to perform the collision check before the start of the operation while this function is running and perform the operation only when no possible collision is detected.

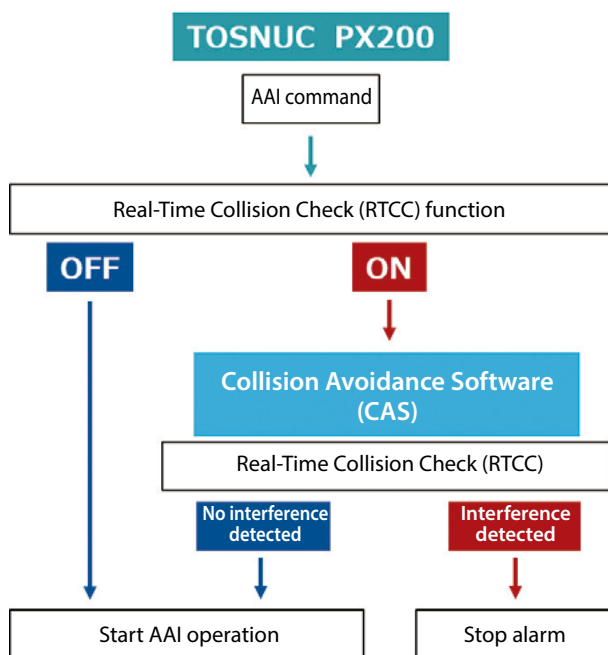


Fig. 2 Sequence axis motion flow

Furthermore, when the CAS starts communication with the NC at the time of system startup, it can read the data of the servo axis, but it cannot read the data of the tools and attachments on the spindle. For this reason, the circuit has been created so the tool number, attachment number, and AAI angle on the spindle are read into the CAS when communication with the NC is established, such as when the CAS is started or the system is restarted.

3 Specifications

Table 1 Specifications

CNC machine		TOSNUC PX200
Collision Avoidance Software		Shiba CAS
		VERICUT CAS (Version 8.2)
External PC	CPU	Intel® Xeon® processor 3.5 GHz or more
	Memory	32 GB or more
	HDD	M2 SSD 500 GB or more
	GPU	OpenGL RX4000P or more

* An external computer and a VERICUT CAS license need to be provided by the customer.

4 Effects and Examples

In MDI operation and automatic operation, the operation stops one block before possible collision is detected. In manual mode, operation can be stopped before collision occurs by controlling the interference area with the machine travel speed (sensitivity can be changed by a parameter).

Example: Fast forward 100%; stop at short of 70 mm

Manual pulse generator (quick rotation); stop short of 30 mm

Manual pulse generator (slow rotation); stop at range short of 0.1 mm

The Real-Time Collision Check function can contribute to cost reduction and energy saving by utilizing the digital twin to reduce the time and energy consumed by repeated trial and error.

5 Conclusion

In the future, we plan to support pre-machining collision checks with machine locks, collision checks for finished shapes, and automatic input of compensation values for workpieces and tools by on-machine measurement.

Introduction of the USM-20B(H) High-Precision Grooving and Cutting Machine

1 Development Objectives

In 2020, the prime minister pledged Japan would be carbon neutral by 2050. To achieve a decarbonized society, the use of IoT technologies, such as remote operations and monitoring, is essential, but this requires the development of a communication infrastructure. Optical fibers used for optical communication are connected to each other using optical connectors in repeaters and distributors. Because misalignment in fiber connections can lead to significant transmission loss, optical connectors are key components and high-precision V-groove machining is used for these components.

Also, ceramic-made scintillators, power semiconductors, and piezoelectric parts are used for sensors and actuators in the latest X-ray CT systems in medical equipment for enabling higher precision, in automotive parts for greater automation, and in commercial inkjet printers for higher resolutions. Even though these ceramic materials are difficult to cut, they are required to have high precision, and their machining processes must be highly efficient due to growing demand.

The USM-20B(H) has been developed specifically for this high-precision grooving and cutting of parts which will be key to the above-mentioned efforts to achieve the Sustainable Development Goals (SDGs) in such fields mentioned above as optical communications, medical care, automated driving, and printers. The appearance of the USM-20B(H) is shown in Fig. 1.

2 Features

1. V-V type dynamic pressure guideway for the workpiece feed axis (X-axis)

The V-shaped guideway surface is hand-finished by scraping and polishing to ensure smoothness and high straightness over long periods of time.

2. Linear motor drive and special low-waving linear guide for wheel positioning (Y-axis)

This design reduces waving motion compared to the ball screw drive and linear guide used in conventional machines. Also, the scale resolution is 1nm, compared to 2nm for the previous model,

for delivering more precise positioning.

3. Equipped with an ultra-precision aerostatic bearing spindle

The USM-20B(H) is equipped with a high-rigidity aerostatic bearing spindle developed in-house. Three types of spindles are available, optimized for each grinding wheel diameter of 2, 3, and 4 inches.

4. Bed made of cast metal

The bed is made out of cast metal for providing high rigidity and stable machining over a long period of time.

5. Touch panel operation

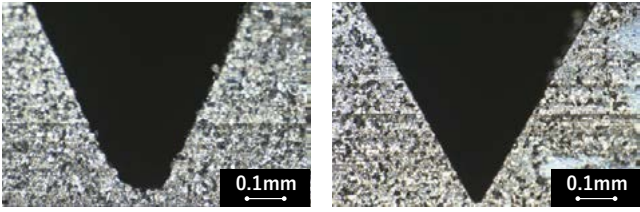
The design minimizes the number of operation buttons, and microscope screen operations and selection of machining programs are performed from a touch panel for greater ease of operation and reducing the workload of machining operators.

6. Electrical discharge truing option available

The electrical discharge truing option can be used to correct grinding wheel shaking and to optimize the wheel tip angle when the wheel is mounted. Also, with this option, grinding wheels which have been worn by machining can be reshaped to enable further use to the end for minimizing waste. An example of electrical discharge truing is shown in Fig. 2.



Fig. 1 Appearance of the USM-20B(H)



Worn grinding wheel After electrical discharge truing
Fig. 2 V-groove bottom shape before and after electrical discharge truing

3 Specifications

The specifications are shown in Table 1.

Table 1 Main specification values

Travel amount	X-axis (Workpiece feeding)	300 mm
	Y-axis (Grinding wheel positioning)	160 mm
	Z-axis (Grinding wheel height)	80 mm
	C-axis (Workpiece rotation)	Unlimited
Maximum feed rate	X-axis	2400 mm/min
	Y-axis	1000 mm/min
	Z-axis	1000 mm/min
Minimum command unit	X-, Y-, and Z-axis	0.00001 mm
Spindle	For 2 inch grinding stone	4000 to 40000 min ⁻¹
	For 3 inch grinding stone	3000 to 30000 min ⁻¹
	For 4 inch grinding stone	2000 to 20000 min ⁻¹

4 Results and Examples

1. V-grooving on low thermal expansion glass substrates

V-grooving (0.25 mm pitch x 20 grooves for 10 sets) for optical connectors was performed on low thermal expansion glass (100 x 100 x 1 mm). Fig. 3 shows the V-grooving appearance, and Fig. 4 shows the cumulative pitch error measurement results. The cumulative pitch error was found to be 1/2, which was significantly better than the previous model.

2. Deep grooving of ceramic blocks

As an example of machining on ceramic materials, grooves of 0.7 mm width, 3.7 mm pitch, and 15 mm depth were machined on an alumina block (50 x 50 x 20 mm), and its appearance is shown in Fig. 5. A normal machine tool would have required multiple cuts to machine a single 15 mm deep groove. By contrast, with this machine tool, a 15 mm deep groove was achieved in a single cut.

Also, if the workpiece to be machined is thin, multiple workpieces can be stacked and cut for significantly improved productivity.

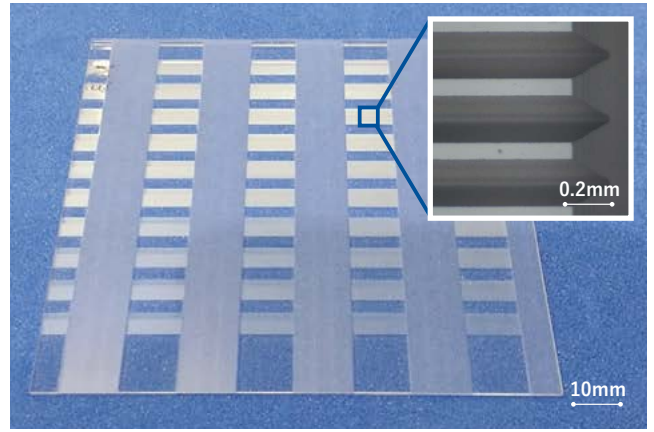


Fig. 3 V-grooving of low thermal expansion glass substrate

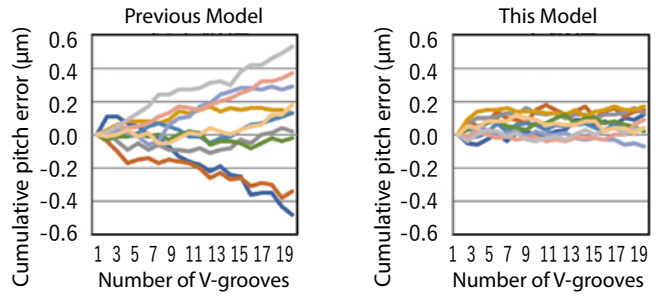


Fig. 4 V-grooving: Cumulative pitch error measurement results

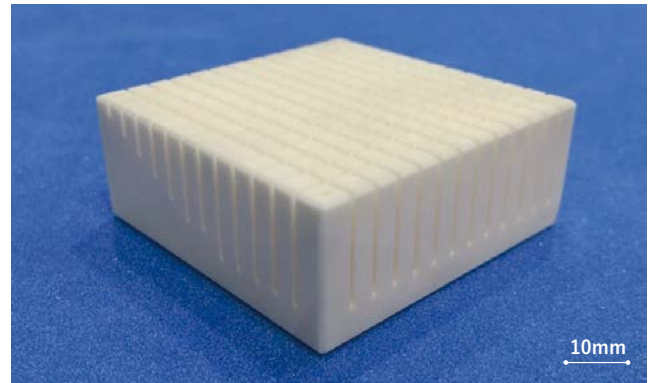


Fig. 5 Grooving on an alumina block

5 Conclusion

Looking forward, we intend to utilize the newly-developed USM-20B(H) to provide high-precision and high-efficiency machining for achieving the SDGs.

Introduction of the TCmini TC12 Series

1 Overview

The TCmini is a microcontroller board which can be programmed in ladder logic (PLC language) and can be optimized in function, size, and cost to meet specific customer needs.

The current TC3 series has been adopted in a wide array of fields such as air conditioners, electrolytic water systems, and milking machines. To meet further market needs, we have developed the TC12 series, which uses the latest MCU^{*1} and has improved control performance.

The TC12-02, the first model in the TC12 series, provides control functions with higher performance while maintaining the installation and functional compatibility of the TC3-02 (previous model).

*1 MCU (Micro Controller Unit): A microprocessor for embedded applications which incorporates a wide range of peripheral functions, such as ROM, RAM, and I/O, in a single integrated circuit.

2 TC12 Series Features

1) Control performance: Half the ladder processing time of the previous model

2) Ladder program capacity: Double the capacity of the previous model

Data register capacity: 12 times the capacity of the previous model

3) Enhancements to communication functions

CAN ^{*2}: Installable^{*3} without dedicated IC

USB I/F: Installable^{*3} without dedicated IC

SD card I/F: Installable^{*3} without dedicated IC

Serial communication: Max. 13 (10 more than previous model)

*2 CAN (Controller Area Network): Serial communication protocol developed by Bosch

*3 Installable through customization options

3 Specifications

Table 1 TC12 Series Main Specifications

Item	TC12	TC3 (Previous model)
Processing time (1k words)	5 ms or less	10 ms or less
Program capacity	24k words	12k words
Number of commands	Basic	16
	Applied	74
Internal Relays / Timers	7296	1160
Data registers	3978 words	309 words
USB I/F	Available ^{*Option}	Unavailable
SD card I/F	Available ^{*Option}	Unavailable
CAN	Available ^{*Option}	Unavailable
Serial communication	Max. 13	Max. 3
Analog input	12bit(Max. 24 in)	10bit(Max. 8 in)
Analog output	12bit(Max. 2 out)	8bit(Max. 2 out)



Fig. 1 Appearance of the TC12-02

4 Results and Examples

The TC12 series not only provides higher control performance, but also can be easily customized with a USB I/F, CAN, and other communication functions, which have been requested by many customers, for supporting their shift to smart factories. The number of parts has also been reduced compared to the previous model, which was already an environmentally-friendly product.

4.1 Application Examples

Dairy machinery: Milking machines, Milk cooling systems

Kitchen equipment: Electrolytic water systems

Air conditioning equipment: Bio-toilet



Fig. 2 Milk cooling system



Fig. 3 Electrolytic water system



Fig. 4 Bio-toilet

Inspire Children's Interest in Science!! Activity Report from a Retired Member



Kuramae Science Class
Fushigi-fushigi(KURARIKA)
<http://kurarika.net/>

Fumio KAMAHORA

Representative of KURARIKA
Shizuoka (Retired in 2008)

My university alumni started a science and handiwork school in the Tokyo area with the aim of providing children opportunities to experience fun and interesting science through handiworks and experiments. My friends and I organized the same school for the eastern area of Shizuoka prefecture. We are providing school sessions in many places, such as;

elementary schools, children's homes, after-school kids clubs, and also at Mt. Fuji children's world (Fujisan Kodomo-no Kuni).

Our activities are based on the policy that; (1) all participants experience handiworks and experiments using materials on hand, (2) scientific principles and laws and the mechanisms of behavior in a specific theme should be explained in an easy-to-understand way using a projector or demonstration device, and (3) one assistant should be assigned to each five or six children to provide detailed guidance. It is important children make, move, and observe things for themselves and we hope our school can help participants find interest in science and also become talented people who will support future science and

technologies in Japan.

There are now 12 members including 3 Shibaura Machine retirees. We are funded by donations from companies and gratuity from classroom organizers. In particular, we are very grateful for the support we have received from Shibaura Machine since the establishment of our program.



Ooka Elementary School 4th grade "Cartesian diver class"

History of Ultra-Precision Machine Tools and Contributions of Shibaura Machine to the Development of Ultra-Precision Machining Technology

This paper introduces the history of ultra-precision machine tools which and machining technology and Shibaura Machine's role in this development.



Machine Tools Company
Machine Tools Engineering
Department

Katsutoshi TANAKA

1 Introduction

Computers, smartphones, the Internet, and optical communications have become an integral part of our lives, making our lives faster, richer, and more convenient than we could ever have imagined. Optical communication, PCs, flash memory, digital cameras, smartphones, printers, LCD monitors, and other devices have become common in many households as the entry and exit points for information, forming a huge market. In the industrial world, not a day goes by without the use of these devices, and with the spread of COVID-19, the scope of their application has expanded significantly. The magnetic disk substrates, V-groove substrates, magnetic heads, aspheric lenses, diffraction gratings, light guide plates, optical films, and polygonal mirrors used in these devices are ultra-precision parts which can only be produced through ultra-precision machining, and they are the key parts which determine the functions, performance, and popularity of the devices.¹⁾ Also, with the spread of safe and automated driving for cars, security, high-speed communication, 4K/8K, and IoT, the demand for ultra-precision machining is expected to grow, enabling even more advancements.

Ultra-precision machining has been utilized and developed to meet the demand for features strongly desired in these devices, namely, more compact size, lighter weight, multi-functionality, higher precision, higher density, mass production, and lower costs. For example, the Schmidt corrector plate was invented in 1930 to eliminate aberrations in aspheric lenses, but its use was limited to equipment such as astronomical telescopes and special cameras because no viable production technology was available. It was not

until the 1980's, when NC-controlled ultra-precision machining became possible that the technology was applied to consumer products such as cameras and CD players. In this way, ultra-precision machining technology has become indispensable for the production and development of the devices which support the information society²⁾⁻³⁾.

In this paper, we will introduce the historical background leading to the development of ultra-precision machining technology and the role Shibaura Machine has played in this development.

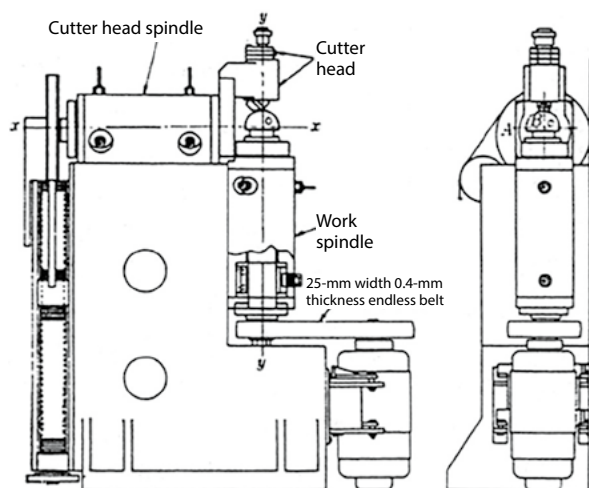
2 The Process of Developing Ultra-Precision Machining

2.1 The Process of Developing Ultra-Precision Machining Overseas

In the 1950's and 1960's in the U.S., research and development on machine tools capable of ultra-precision machining by motion transfer was conducted by Union Carbide, LLNL, Polaroid, DuPont, and others to improve the machining accuracy and productivity of military-related ultra-precision parts without relying on the skill of machine operators. Research was conducted on aerostatic bearings as bearings for spindles and guideways, which are the main components of machine tools, and the Ultra-precision Hemisphere Turning Machine (Fig. 1) was developed as the first ultra-precision machine tool for machining of high-precision spherical surfaces. This machine used aerostatic bearings in the workpiece spindle, which holds and rotates the workpiece, and in the cutter head spindle, which swivels the diamond bit.⁴⁾⁻⁶⁾

Aerostatic bearings have been researched and developed since the 1960's, but their use was focused on high-speed

turbomachinery, gyroscopes, grinding wheel spindles of internal grinders, centrifuges, and other applications because these bearings could deliver high-speed rotation due to the low friction caused by the low viscosity of the air interposed between the shaft and bearing. However, spindles for ultra-precision machining which require surface roughness and form accuracy require high precision, high rigidity, and low vibration, and development proceeded on aerostatic spindles which could satisfy these requirements. Fig. 2 shows the aerostatic spindle for the work spindle used in DuPont3, which is a larger version of DuPont1 shown in Fig. 1, and was designed for machining of spherical surfaces 400 mm in diameter. In this work spindle structure, hemispheres are facing each other and the spherical surface supports radial and axial loads, and the bearing material uses porous restrictors made of porous carbon. For rotational accuracy, the measurement method is not specified, but it is said to be $0.3 \mu\text{m}$ or less, and the rigidity is $117.6 \text{ N}/\mu\text{m}$.⁷⁾



Machine configuration and machining accuracy
(1) Runout of aerostatic spindle: $0.125 \mu\text{m}$
(2) Hemisphere form accuracy: $0.6 \mu\text{m}/101.6 \text{ mm}$
(3) Surface roughness: 25 nm CLA

Fig. 1 Ultra-Precision Hemisphere Turning Machine (DuPont1)⁴⁾

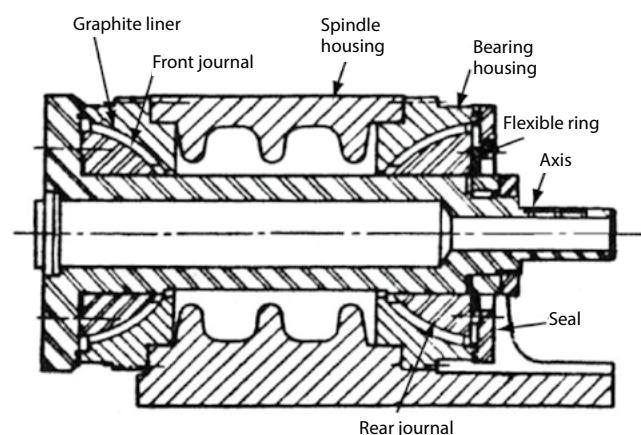


Fig. 2 Porous aerostatic spindle⁴⁾

In the 1970's, aerostatic spindles, aerostatic guideways, and other machine elements for ultra-precision machining were developed for practical use, and these elements were used to achieve mirror-like machining of flat, cylindrical, and spherical surfaces by motion transfer. However, the resolution of the numerical control was $1 \mu\text{m}$ to $10 \mu\text{m}$, and it was not possible to perform ultra-precision machining of spherical and parabolic surfaces (submicron form accuracy and mirror surfaces) with simultaneous two-axis control. To compensate for this poor numerical control resolution, an ultra-precision machine tool with mechanical circular interpolation, which combined linear and rotary motion, was developed. Fig. 3 shows an ultra-precision machine tool named the Omega-X Nanometer Machine Tool developed by Battelle Pacific Northwest Laboratories in 1978, which combines two linear guideway axes and two swivel axes. This machine could obtain a surface roughness of 1.23 nm rms and a form accuracy of $75 \text{ nm}/50 \text{ mm}$.

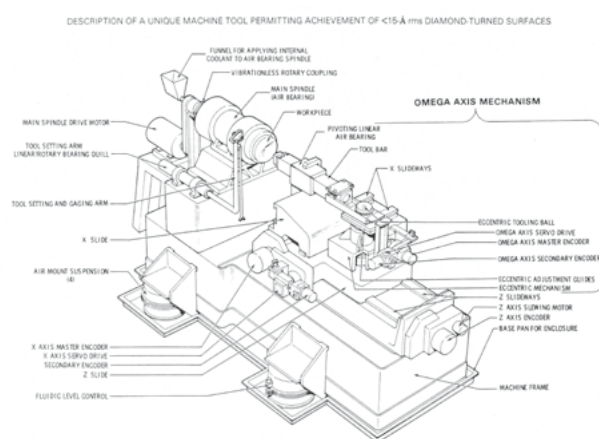


FIGURE 1. Omega-X Nanometer Machine Tool

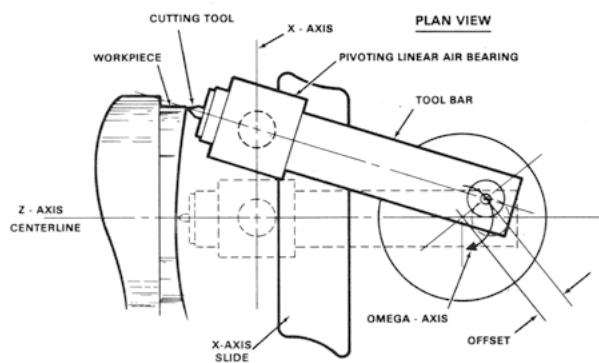
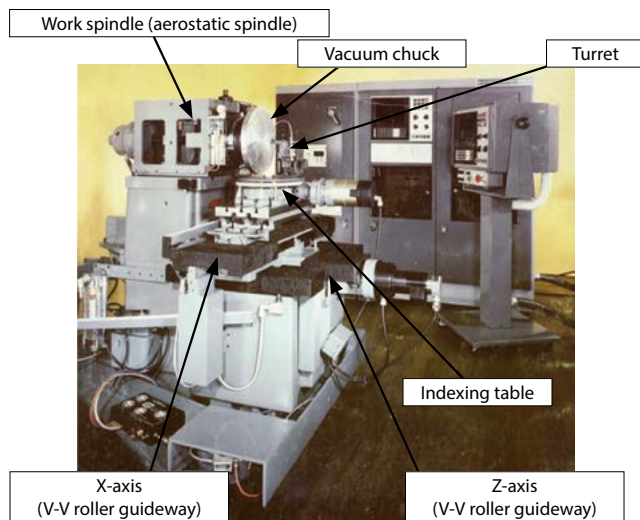


FIGURE 2. Omega-X Tool Motion

Fig. 3 Omega-X Nanometer machine tool (1978) Battelle Pacific Northwest Laboratories⁸⁾ (Aspheric machine tool using a link configuration for the aerostatic bearings)

In the latter half of the 1970's, high-resolution NC devices (25 nm resolution) were developed, and in response to requests from DuPont and LLNL, NC-controlled ultra-precision lathes were developed by Moore Special Tool and PNEUMO PRECISION, which had amassed tremendous technological capabilities in ultra-precision machine tools. Fig. 4 shows the ultra-precision CNC lathe (M-18AG) developed by Moore Special Tool in 1975. The machine uses the V-V roller guideway and precision feed screw technology used in the company's jig grinders and measuring machines, a Professional Instruments aerostatic spindle as the work spindle, and a laser interferometer for position detection. The structure is made of cast iron and is carefully finished to the precision required for ultra-precision machining by employing highly skilled work such as scraping and lapping.⁹⁾⁻¹²⁾



Machine configuration and accuracy
(1) Aerostatic spindle, V-V roller guideway
(2) Control resolution: 25 nm

Fig. 4 Ultra-precision lathe M-18AG (1975)
Moore Special Tool⁹⁾⁻¹⁰⁾

Fig. 5 shows the ultra-precision CNC lathe (MSG-325) developed by PNEUMO PRECISION in 1977. In this machine, the X and Z axes of the aerostatic guideway are arranged in a T-shape on a granite surface plate, the work spindle of the aerostatic bearing is placed on the Z-axis, and a feedback system using a laser interferometer is employed.¹³⁾⁻¹⁴⁾

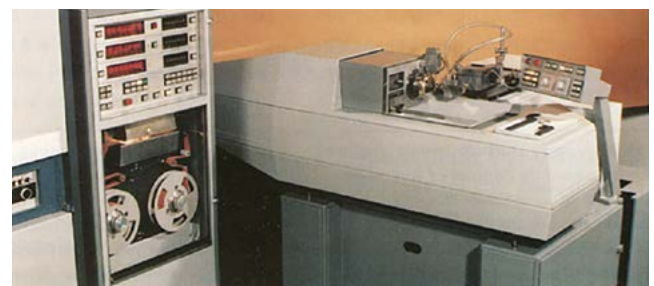
With the advent of these machines, highly efficient and ultra-precision machining of axisymmetric spherical, parabolic, ellipsoidal, and aspherical surfaces by numerical control became possible. On the other hand, in Europe, PHILIPS of the Netherlands developed a unique ultra-precision CNC lathe in 1980 which employed hydrostatic bearings (linear guideway and work spindle), a hydraulic servo feed mechanism, and laser feedback (Fig. 6).



Machine configuration and accuracy
(1) Aerostatic spindle: Runout accuracy = 0.1 μm
(2) Aerostatic guideway
(3) Control resolution: 25 nm

Fig. 5 Ultra-precision lathe MSG-325 (1977)
PNEUMO PRECISION, INC.¹³⁾

While the purpose of the development of ultra-precision machining technology in the U.S. was to improve the accuracy and productivity of ultra-precision parts used in military, energy, and space development, PHILIPS pursued the development of magnetic disk substrates, reflectors for carbon dioxide lasers, plastic aspheric lenses, and injection molds for plastic aspheric lenses for consumer and industrial use. This was groundbreaking research and development which spearheaded the mass production of plastic aspheric lenses using the injection molding method¹⁵⁾.



(a) Ultra-precision CNC lathe



(b) Machining examples



(c) Plastic lens formed by
ultra-precision mold

Machine configuration and accuracy
(1) Hydraulic servo and laser feedback
(2) Control resolution: 16 nm
(3) Machining form accuracy: 0.5 μm
(4) Machining surface roughness: 0.02 μmRy

Fig. 6 Ultra-precision CNC lathe COLATH (1980) PHILIPS¹⁵⁾

2.2 How Ultra-Precision Machining Was Developed in Japan

In the 1970's, the active research on ultra-precision machining in Europe and the U.S. prompted Japan to conduct research on this technology as an essential cornerstone of Japan's efforts to build a technological powerhouse. However, in the 1970's, there was no budding industry in Japan which required ultra-precision machining, and research was limited to universities, public research institutes, and corporate laboratories.¹⁶⁾⁻¹⁷⁾ Under these circumstances, the author and colleagues started to work on ultra-precision machining as a fundamental technology for developing higher accuracy and unique machine tools.

2.2.1 Development of Spherical Aerostatic Spindles and Mirror Surface Machining with Flat Surface Machining Equipment

To tackle ultra-precision machining, which requires an accuracy two to three orders of magnitude higher than normal machining accuracy (flatness, roundness, surface roughness, etc.), and to achieve ultra-precision in the machine components, in 1977, we acquired the technology for a spherical aerostatic spindle with an inherent restrictor (Fig. 7) from the Manufacturing Engineering Research Center of Toshiba Corporation. Table 1 shows the performance of various spherical aerostatic spindles. The runout was measured by the Lissajous method using a capacitance-type non-contact micro-displacement sensor.¹⁸⁾⁻²⁰⁾

Table 1 Specifications of spherical aerostatic spindle

Spindle diameter (spherical diameter) mm		60 mm	100 mm	120 mm
Runout nm	Radial direction	50	50	50
	Axial direction	50	50	50
Rigidity N/ μ m Supply air pressure 0.6 MPa	Radial direction	15	50	60
	Axial direction	30	60	70
Allowable load capacity N Supply air pressure 0.6 MPa	Radial direction	90	300	350
	Axial direction	180	360	400
Rotation speed min ⁻¹	Max.	10000	6000	5000

By combining a $\phi 100$ mm spherical aerostatic spindle with our newly developed aerostatic guideway, we fabricated a prototype of the flat surface machining equipment shown in Fig. 8, and studied the mirror surface machining of soft metals (aluminum alloy and oxygen-free copper) by fly cutting using a single-crystal diamond bit, and we obtained a flatness of $0.79 \mu\text{m}/\phi 100$ mm and surface roughness of 20 nmRz .²¹⁾

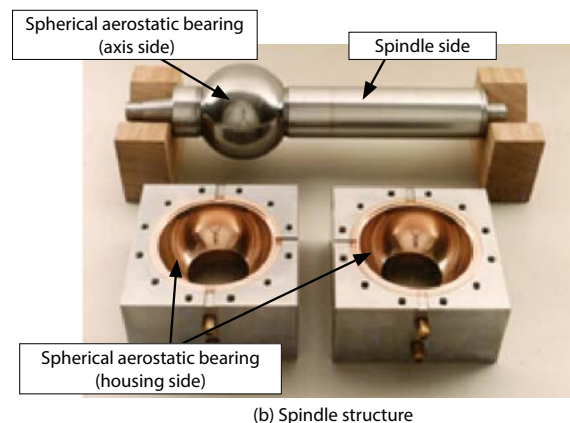
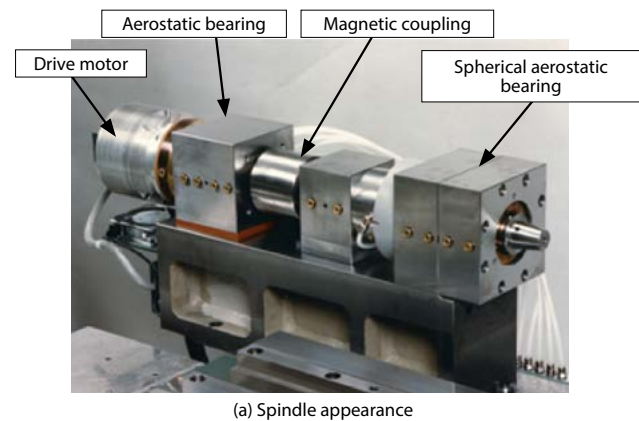


Fig. 7 Spherical aerostatic spindle and component parts
ABS-10 (1978)¹⁸⁾

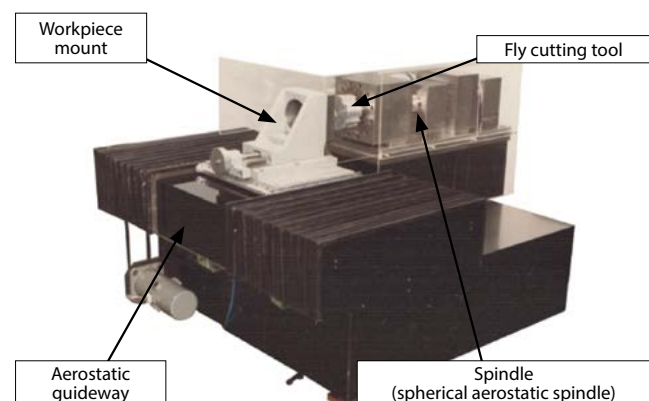


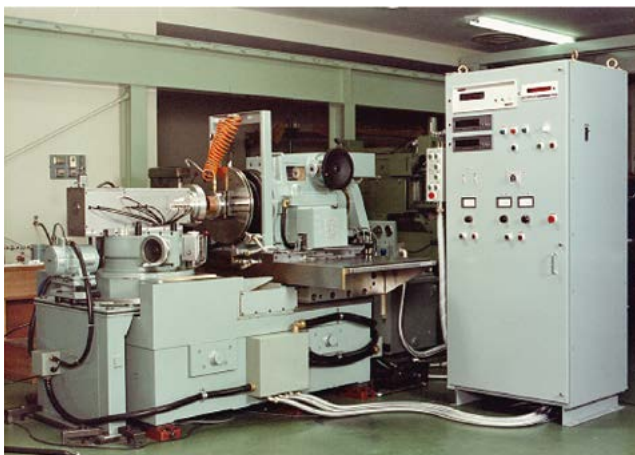
Fig. 8 Flat surface machining equipment (1979)
Mirror surface machining of soft metals by fly cutting²¹⁾

2.2.2

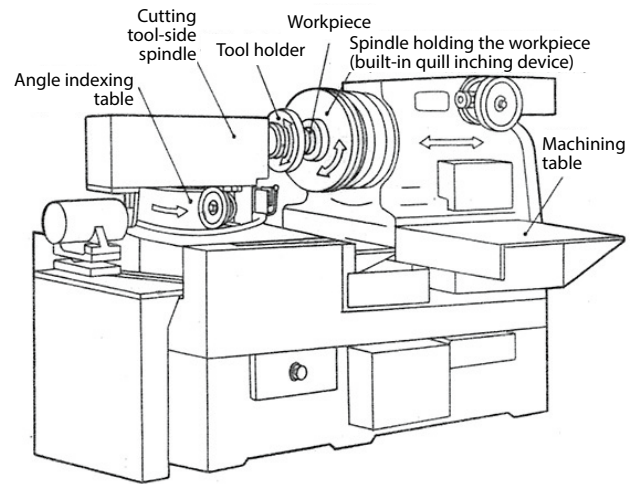
Development of Metal Mirror Machining Equipment (SPM-4)

As a part of the research commissioned in 1978 by the Industrial Technology Agency of the Ministry of International Trade and Industry (MITI) under the project "Research and Development of Complex Production Systems Using Ultra-High Performance Lasers", research and development was conducted for seven years from 1977, and the Manufacturing Engineering Research Center of Toshiba Corporation and Toshiba Machine Co., Ltd. jointly developed the metal mirror machining equipment (SPM-4) shown in Fig. 9(a) to supply metal mirrors machined for high-power laser generators of the target system.²¹⁾⁻²⁴⁾

Due to schedule constraints and the performance of NC equipment at the time, we decided to use the spherical surface generating method to cut the flat, concave, and convex mirrors, resulting in the structure shown in Fig. 9(b). The spindle for the cutting tools used a spherical aerostatic spindle with 100mm diameter, and the spindle which holds the workpiece used a hydrostatic spindle due to the diameter of the faceplate and the weight of the workpiece, and because the machining table was the feed axis for plane mirror machining, a hydrostatic guideway was used to enable smooth feeding. The rotation of each spindle and the X-axis feed drive motor were installed at locations away from the machine body to reduce the effect of motor vibration. The flatness of the machined plane mirror was $0.3 \mu\text{m}/\phi 150 \text{ mm}$, as shown in Fig. 10. This metal mirror machining equipment (SPM-4) is still in use today after 40 years, maintaining its initial performance.

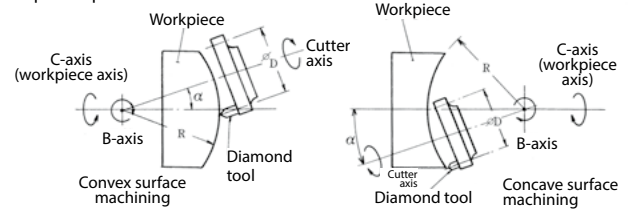


(a) Equipment appearance



(b) Equipment structure

Principle of Spherical Surface Generation



(c) Principle of spherical surface generation

Fig. 9 Metal mirror machining equipment

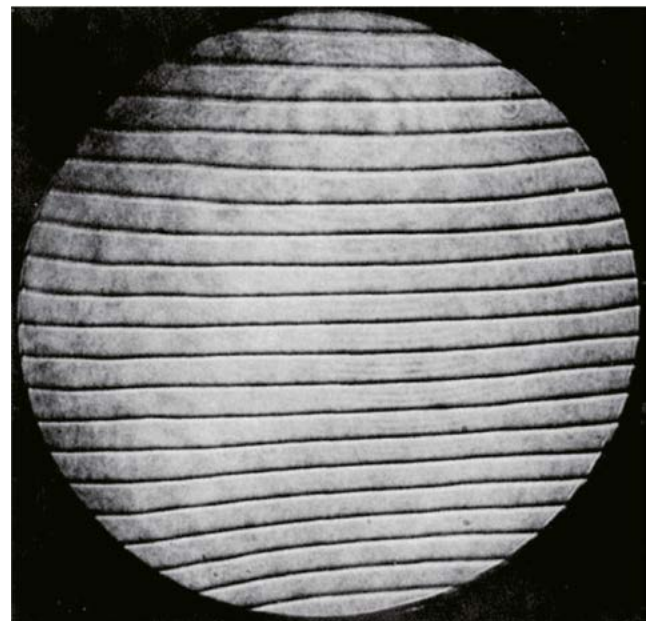


Fig. 10 Machining result from metal mirror machining equipment
(Flatness: $0.3 \mu\text{m}/\phi 150 \text{ mm}$) ($\lambda=632 \text{ nm}$)²¹⁾⁻²⁴⁾

2.2.3

Development of Polygonal Mirror Machining Equipment

In the 1980's, mirror machining of soft metals started, including photoreceptor drums for copiers, diamond turning of magnetic disk substrates (aluminum alloy) for HDDs, and fly cutting of polygonal

mirrors for laser printer scanners, which required ultra-precision machining technology. Previously, mirror machining using single-crystal diamond cutting tools had been called diamond cutting, and the mirror surface was intended for decorative purposes such as rings, necklaces, watch dials, and audio knobs. Magnetic disk substrates and polygonal mirrors, on the other hand, require geometrical tolerances for optical surfaces such as flatness and surface roughness, and research and development (R&D) for achieving these tolerance targets was conducted on ultra-precision mechanical elements such as spindles, guides, and feed mechanisms, and on single-crystal diamond cutting tools, materials, and evaluation methods.

As a part of this R&D, applications for polygonal mirrors (rotating polygonal mirrors) for laser printer scanners were studied based on the results of mirror machining by fly cutting using the flat surface machining equipment shown in Fig. 8. Previously, polygonal mirrors had been used as angle standards to measure the indexing accuracy of rotary tables and other equipment and were manufactured by optically polishing glass. Consequently, the large weight and high cost of glass was not conducive for use in scanners which required mass production.²⁵⁾⁻²⁹⁾

The typical form and accuracy of a polygonal mirror used in a scanner for a laser printer is shown in Fig. 11. These polygonal mirrors are used at high rotational speeds (7000 to 40000 min^{-1}) and require mass production. To meet these requirements, the polygonal mirror machining equipment shown in Fig. 12(a) and (b) was developed. The system uses a 100mm diameter spherical aerostatic spindle as the cutter axis and uses an aerostatic table as the feed axis. As shown in Fig. 12 (c), the aerostatic table is divided into a drive table with a fixed female screw and a main table, and the structure is designed so only the force in the feed direction acts on the main table through a non-contacting aerostatic joint.

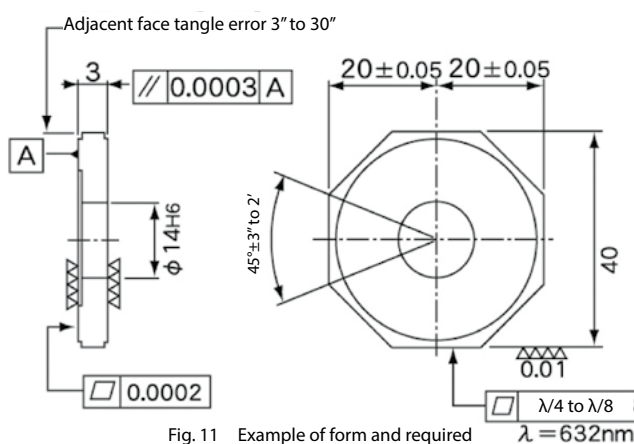
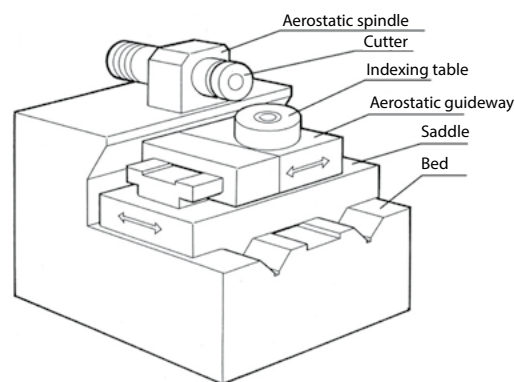


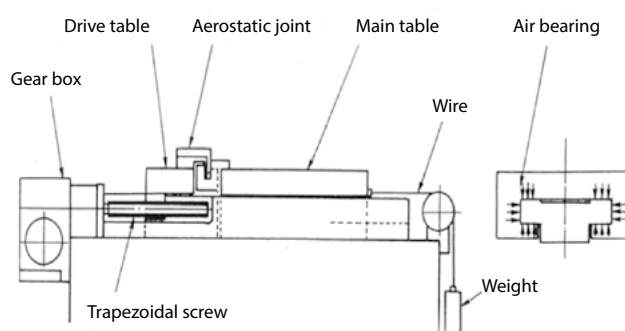
Fig. 11 Example of form and required accuracy for polygonal mirror



(a) Equipment appearance



(b) Equipment structure



(c) Structure of aerostatic bearing table using aerostatic joints
Fig. 12 Polygonal mirror machining equipment

Angular indexing is performed by an indexing table using a curvic coupling with 360 teeth. The workpiece holder is preset with 10 to 20 workpieces stacked on top of each other, and this workpiece holder is mounted on the indexing table and machined at a feed rate of 50 to 200 mm/min ³⁰⁾.

The cutter holder has four cutting edges for roughing (two), medium finishing, and finishing, and the four cutting edges are arranged in the radial and axial directions at different depths of cut and feed rates, making it possible to complete the finishing process in a single cut for a finishing allowance of about 0.1 mm , making this method suitable for mass production (Fig. 13). The cutter holder was used to fly-cut the polygonal mirror, and a surface roughness

of 5 nmRz was obtained (Fig. 14). The measuring instrument was the Taylor Hobson Talystep, an ultra-precision surface roughness and film thickness device which employs a probe.

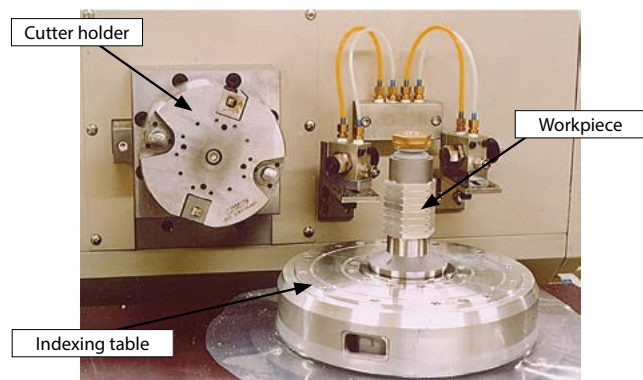


Fig. 13 Cutter holder and workpiece



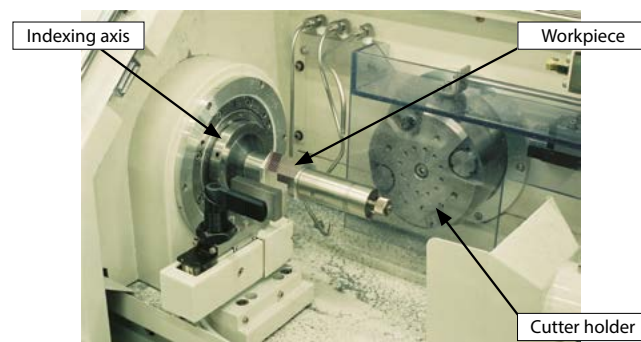
Fig. 14 Surface roughness of polygonal mirror machined by fly cutting

Since the development of the polygonal mirror machining equipment shown in Fig. 12, we have been able to meet the demand for polygonal mirrors, and with the advancements in ultra-precision technology, we have developed the polygonal mirror machining equipment shown in Fig. 15, which incorporates a new structure and mechanism to achieve more stability, more compact size, and higher efficiency at a lower cost. The aerostatic guideway is a special V-V sliding guideway designed for accuracy and stability, and the infeed axis, which used to be a V-V sliding guideway, is a linear guide for enabling improved positioning accuracy. The indexing axis, which is the horizontal axis, has a bearing structure and supports the workpiece holder at the center, enabling the number of stacked workpieces to be increased. A high-resolution encoder is used for detection of the indexing angle.

The market for laser printers is still just under 40 million units per year, with sales of almost 5 trillion yen, accounting for over 80% of all printers in terms of sales. Looking forward, demand is also expected for polygonal mirrors in scanners for automated and safe driving of automobiles.



(a) Equipment appearance



(b) Cutter holder and workpiece

Fig. 15 Polygonal mirror machining equipment UFG-80C(P) designed with more compact size, higher efficiency, and more stability

2.2.4 | Development of Disc Lathe

As the recording media for computers shifted from magnetic tape to magnetic disks, we developed an ultra-precision front lathe (Fig. 16) in 1982 for mirror-finishing aluminum alloy disks used as material for magnetic disks.³³⁾

Magnetic disk substrates required an accuracy of 25 nmRa for surface roughness, a runout of 0.051 mm at 3600 min⁻¹, and an acceleration of 38.1 m/sec² at that runout (the current ANSI standard in 1985). Discs had to be machined with high efficiency to have outer diameters of 14 inches, 8 inches, 5 1/4 inches, and a thickness of 1.905 mm±0.025 mm.³¹⁾⁻³³⁾ Even so, most of the specifications for machine tools were 5 1/4 inches or less in outer diameter due to the demand for increased recording density and miniaturization. Because of the required machining accuracy, aerostatic bearings were used for the spindle, and magnetic couplings were used to drive the spindle and to block motor vibration. The disc substrate was held by a vacuum chuck, and urethane rubber was bonded to the surface of the chuck faceplate to reduce scratches and inaccuracies (micro-waviness) caused by trapped dust and chips, but the soft urethane rubber made it extremely difficult to cut with high accuracy. Aerostatic bearings

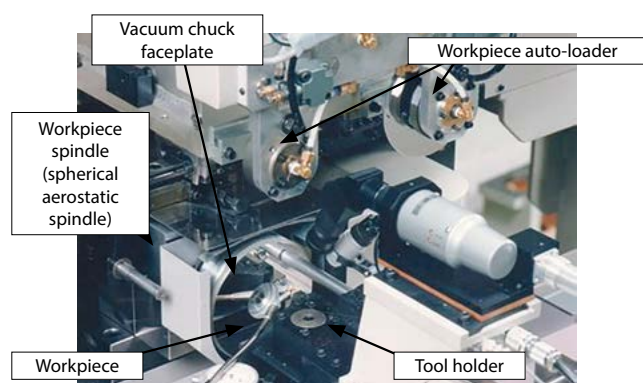
were used for the guideways, and aerostatic joints and friction drive were used for the feed mechanism to prevent disturbance to the table.

Mass production was the basis of parts machining, and cutting was performed using a single-crystal diamond flat bit with a cutting edge width of 1.5 mm to 2.5 mm. The machining time for a 5 1/4 inch substrate was 20 to 30 seconds, and automatic attachment, removal, and transfer of the mirror-finished disk substrate, thickness measurement, and complete chip removal were required for enabling production by unmanned operation.

This diamond turning of magnetic disk substrates was eventually replaced by less costly lapping in the late 1980's and had a short life of less than ten years.



(a) Equipment appearance



(b) Appearance of automation mechanism

Fig. 16 Automated disc lathe³³⁾

2.2.5 | Development of Ultra-Precision Slicer

From around 1980, the demand for video heads increased, and a high-precision surface grinder was required for the fine machining of single-crystal ferrite. However, no suitable machine tool was

available for these machining processes, and performance was unsatisfactory, so a "dicer" for dicing silicon wafers was used.

The machining of magnetic heads involves cutting, grooving, and surface grinding of the single-crystal ferrite material. Thin, all-round, and cup-shaped ultra-fine diamond grinding wheels are used in this high value-added machining process, during which 95% of the material is ground into chips. Development was carried out with the expectation the resulting solution would become a high value-added product because an ultra-precision surface grinder "slicer" with high rigidity and high accuracy would generate higher demand than a "dicer" for meeting the increasing demand for magnetic heads and for machining magnetic heads (heads for magnetic disks and 8 mm video heads) with even higher accuracy. The USM-300A(NC) ultra-precision slicer we developed earned a reputation for high accuracy and performance, but its price and equipment size (four times larger than a dicer) prevented its mass adoption.

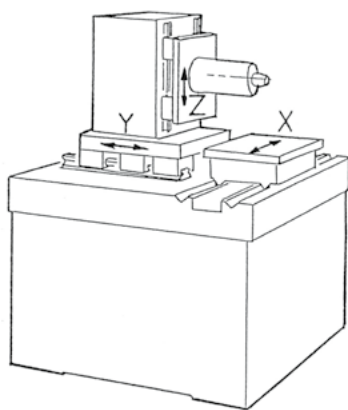
When a magnetic head manufacturer receives an order inquiry for a head, it examines how to fill the order using its existing equipment capacity, work system, and outsourcing, and if it still cannot fill the order, the manufacturer will then consider installing new equipment. The quality and delivery time of the equipment are absolute requirements, and when an order for a head is determined, the order is placed with a machine manufacturer which can satisfy these requirements to produce the head. However, because the recording density of magnetic disks is constantly growing, equipment which was recently installed cannot be reliably used for the next head order inquiry, and further new equipment will need to be considered. Under these circumstances, we developed the CNC ultra-precision slicer USM-200A(NC) in 1984 (Fig. 17(a) and 17(b)) to meet user requirements.

For the grinding of ferrite, which is a hard and brittle material, a cylindrical aerostatic spindle with a radial diameter of 60 mm was used for the grinding wheel spindle to achieve high speed, high accuracy, and low vibration. Measures were taken to obtain thermal stability, such as designing a restrictor with low heat generation to reduce the heat generated at high-speed rotation (12000 min^{-1}), using a low thermal expansion material for the spindle, and controlling the temperature with a constant supply of warm water. Fig. 18 shows an example of an aerostatic spindle with measures for preventing thermal deformation. In addition to the use of low thermal expansion materials and water-cooling of the

motor, the housing mounting position was modified. This was done by proportionally dividing the distance A from the spindle end to the reference surface and the distance B from the reference surface to the housing mounting surface by the inverse ratio of the linear expansion coefficient of the material used. When the temperature is stable, the reference surface moves backward with respect to the housing mounting surface by $B \times \text{Linear expansion coefficient of the housing material}$, and the spindle moves forward by $A \times \text{Linear expansion coefficient of the spindle material}$, resulting in zero elongation at the axis end with respect to the mounting surface. The spindle is made of Invar (coefficient of linear expansion: $16 \times 10^{-6}/^{\circ}\text{C}$), and the housing is made of stainless steel (SUS420J2, coefficient of linear expansion: $9.7 \times 10^{-6}/^{\circ}\text{C}$).



(a) Equipment appearance



(b) Equipment structure

Machine structure
(1) X-axis: V-V sliding guideway
(2) Grinding wheel spindle: Cylindrical aerostatic spindle
Fig. 17 Ultra-precision slicer USM-200A(NC)³⁴⁾

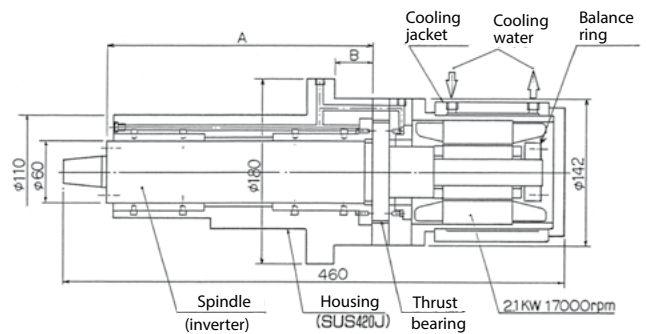


Fig. 18 Structure and thermal deformation prevention measures for cylindrical aerostatic spindle for ultra-precision slicer³⁵⁾

The X-axis (table) guideway for creep grinding is a V-V sliding guideway, which provides high precision, high rigidity, and smooth motion. The straightness of the table motion of the V-V sliding guideway, which has a carefully scraped finish (Fig. 19), is less than $0.3 \mu\text{m}/400 \text{ mm}$, contributing to high precision. The Y and Z axes are positioning axes and are linear guides with a small coefficient of friction and a scale feedback system with a command unit of $0.1 \mu\text{m}$.

With the demand for higher productivity in machine tool manufacturing and the decline in the skills of scraping and lapping, which is demanding and inefficient work, it was a great achievement to successfully improve, transfer, and maintain the skills which are considered essential in the manufacture of ultra-precision machine tools.



Fig. 19 Scraping work

The USM-200A(NC) ultra-precision slicer earned a high reputation among many magnetic head manufacturers, and four models with simplified functions were added to the series, resulting in the delivery of about 1,200 units over a six-year period from 1984 to 1990. The success of the ultra-precision slicer contributed to making

Japan the world's leading production base for magnetic heads, and the recognition of ultra-precision machining within Toshiba Machine (now Shibaura Machine) became the driving force behind its expansion within the company from a section to a department, and to a business unit. However, as magnetic heads became miniaturized as recording densities increased, thin-film heads using wafer processes were developed and became widespread due to their suitability for process shortening, miniaturization, and higher density. Ferrite heads were barely able to compete with thin-film heads through their efforts to improve performance, but once a certain line was crossed, they instantly lost the market to thin-film heads.

With the shift to thin-film heads, the number of ultra-precision slicers dropped to 1/10, new equipment could no longer be expected, and the era of ultra-precision slicers for magnetic heads came to an end in the early 1990's. Subsequently, although the number of ultra-precision slicers is not expected to be as large as it once was for magnetic heads, demand is expected to grow for grooving of inkjet heads, cutting of SiC substrates for power semiconductors, cutting of optical materials, and grooving of V-groove substrates for 5G.

2.2.6 Performance Improvements for Aerostatic Spindles and Development of High-Speed Ultra-Precision Machining Centers

We have manufactured various types and large quantities of aerostatic spindles by producing ultra-precision slicers and other magnetic head-related grinders. This experience has enabled us to improve the performance of the aerostatic spindles through higher speeds, higher accuracy, and toughness, and has expanded their range of applications. Let us present an interesting application here.

By varying the supply air pressure before and after the opposing thrust bearings of a cylindrical aerostatic spindle, the spindle can be moved back and forth within the range of the bearing clearance (bearing clearance is 16 μm per side) during rotation and positioned with an accuracy of 0.1 μm . For the purpose of simplifying the mechanism in a horizontal spindle surface grinder which uses a cup grinding wheel, a high-speed retract mechanism was developed which does not have a controllable feed axis, but allows the grinding wheel to be released by 3 to 5 μm and the wheel to be positioned in the forward position by simply switching a solenoid valve. This mechanism has eliminated the need for a

high-precision guideway, feedback scales, and NC control.

By using carbon as their bearing material, the cylindrical aerostatic spindles are more resistant to seizure due to overload and other causes, and measures for preventing heat generation enable a spindle with a radial diameter of 60 mm to achieve a rotational speed of 17000 min^{-1} and a rigidity of 35 $\text{N}/\mu\text{m}$ in the radial direction (load capacity: 300 N) and 60 $\text{N}/\mu\text{m}$ in the axial direction (load capacity: 600 N). Previously, aerostatic spindles had been used for ultra-precision machining, such as mirror surface machining, where the load is small, but we thought if the above performance could be obtained, they could also be used for small-diameter end milling. And so, a cylindrical aerostatic spindle with a diameter of 60 mm was mounted on the milling machine of the equipment for cutting tests (Fig. 20).

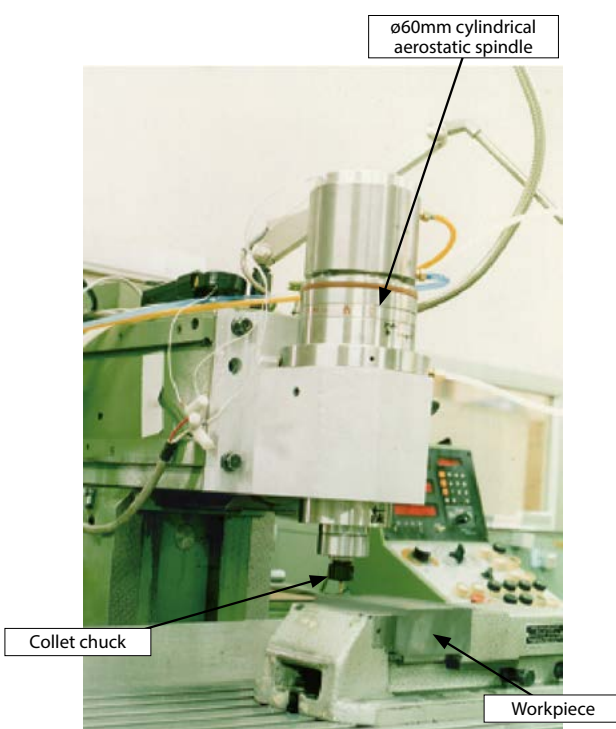


Fig. 20 End mill machining test using aerostatic spindle

The use of aerostatic spindles enables high-speed rotation, which in turn enables the selection of a cutting speed suitable for the tool material, enables faster feed rates, longer tool life due to less vibration, improved machined surface roughness due to less center runout, more stable feed rate per cutting edge due to less center runout, and longer tool life. Also, the temperature rise of the workpiece is minimized due to adequate chip evacuation and the carrying away of the cutting heat by the chips. Using this milling machine, grooving of workpiece material FC200 was carried out

using an end mill with a diameter of 6 mm (two flutes, material grade ME-10) under the machining conditions of a rotational speed of 12000 min^{-1} , a feed rate of 493 mm/min (maximum speed of the milling machine used), and a depth of cut of 5 mm. As a result, the cutting force was 114 N in the X-direction (feed direction), 98 N in the Y-direction (perpendicular to the feed direction), and 28 N in the Z-direction, which was well within the capacity of the 60 mm diameter cylindrical aerostatic spindle. Because the center runout is small, the variation of the cutting force in the X-axis direction is small and stable (Fig. 21).

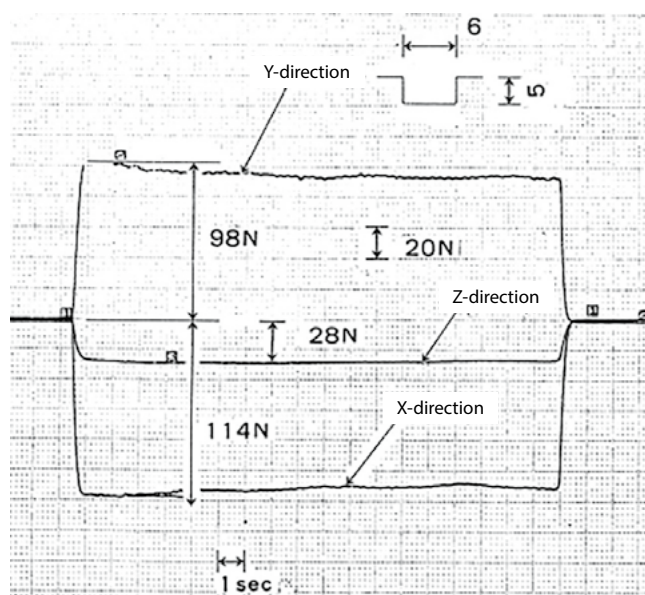


Fig. 21 Cutting force in X, Y, and Z directions for end mill machining using aerostatic spindle

Based on these results, a cylindrical aerostatic spindle with a diameter of 60 mm was mounted on the spindle of a vertical machining center (JRV-40S), which was exhibited at JIMTOF in 1992 (Fig. 22). At that time, the die and mold industry was looking for a way to directly machine shapes by high-speed cutting (direct engraving) instead of EDM-based machining processes for reducing costs and shortening lead times. Mr. Etsuo TAKEOKA of the Industrial Research Institute of NIIGATA Prefecture installed this machine, which was exhibited at JIMTOF, and studied the effectiveness of direct engraving using a small-diameter end mill for hard steel such as forging dies (reducing machining time, simplifying NC machining data, skipping the polishing process, and improving machining accuracy). He received his degree for his thesis, "A Study on End Milling of High-Hardness Materials by High-Speed Aerostatic Spindles."³⁶⁾

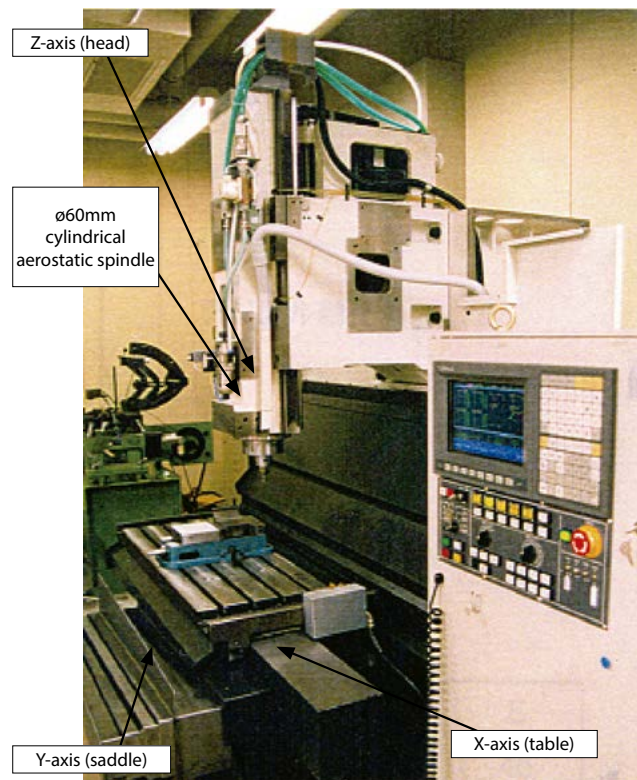


Fig. 22 High-speed machine tool with aerostatic spindle JRV-40S was delivered to Industrial Research Institute of NIIGATA Prefecture

Once Mr. TAKEOKA proposed his new machining method, Toshiba Machine worked to develop a high-speed machine tool product specialized in aerostatic spindles and further increased the spindle speed to 60000 min^{-1} at a radial diameter of 40 mm and to 80000 min^{-1} at a radial diameter of 21 mm. The market did not easily grow due to a lack of compatible applications, but demand for LED-related optical components was born. Therefore, in 2008, the machine was redesigned as an ultra-precision machining center with linear motor drive for all linear axes to improve machining accuracy and mirror surface quality, an ATC, and various attachments for diversification.

In recent years, the halogen lamps and other light sources in automobile headlights have been replaced by LEDs, and lenses and reflectors have become plastic components. As a result, molds are required to have high accuracy (form accuracy and surface roughness), complex shapes, and large sizes. Because the number of parts which cannot be polished as before has increased, we developed the ultra-precision machining center with 5-axis control shown in Fig. 23. Fig. 24 shows an automobile lamp reflector mold machined by this machining center.



Fig. 23 Ultra-precision machining center UVM-700E(5AD)
Simultaneous 5-axis control

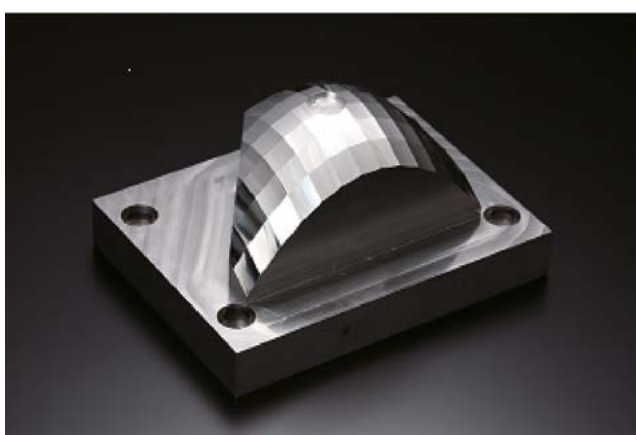


Fig. 24 Lamp reflector mold for automobile

2.2.7 Development of Ultra-Precision Aspheric Machine Tools and Opening New Markets

(1) Background to the development of the ultra-precision aspheric machine tool

As mentioned before, NC-controlled ultra-precision lathes were developed in Europe and the U.S. between 1975 and 1980, and I was impressed when I saw Moore Special Tool's M-18AG and PNEUMO PRECISION's MSG-325 at the Chicago Machine Tool Show in 1980. At that time, there was already a demand for CD pickup lenses in Japan, and the first ultra-precision CNC lathe (MSG-325) was introduced into an optical manufacturer in 1982. With this background and the fact Toshiba Machine was already able to machine flat and spherical optical mirror surfaces with its metal mirror and polygonal mirror machining equipment, it was only natural we would want to expand into the machining of spherical, parabolic, and aspherical surfaces by controlling two axes, and in 1984, we began the development of an ultra-precision aspheric

machine tool which could outperform the M-18AG and MSG-325.

The machine configuration is based on the MSG-325 with a T-shaped aerostatic bearing table on a cast iron base, a turret on the X-axis, a spherical aerostatic spindle on the Z-axis, and a table feed mechanism with laser feedback using a ball screw and servo motor by INLAND. Because it was not possible to outperform the M-18AG and MSG-325 so long as we used Allen Bradley's controller, we decided to develop what is now called the personal computer (PC) NC unit. However, in 1984, PCs were not reliable, and it was not possible to put a spherical aerostatic spindle weighing nearly 100 kg on a table with aerostatic bearings, and so this first development model was almost never used and had to be scrapped.

Then, based on the failure of the first development model, we selected a high-stability PC with the same machine configuration and enlarged the aerostatic guideway to better withstand the load, and proceeded with development of the second model. This made the machine bigger, but we were able to achieve cutting. Even so, the machining surface was unstable due to the lack of rigidity in the aerostatic guideway, fluctuation of the laser beam running in the air, and other factors. We tried test machining at the customer's site, but could not obtain satisfactory results, and so this ended in failure like the first machine (Fig. 25).



Fig. 25 Second prototype of ultra-precision CNC lathe UAG-150A(NC)

The main reasons for this failure were the instability of the controller, including bugs, the instability of using a laser length measuring device as a feedback scale in a factory environment, the low rigidity of the X- and Z-axis moving components using aerostatic guideways (especially for unbalanced loads), and the resulting scoring on the guideway surface.

(2) Development of limited V-V roller guideway

After the failure of the machine using the aerostatic guideway, we began to study the best guideway for an ultra-precision

machine tool. At the time, Toshiba Machine had an extensive track record of using hydrostatic bearings in large machine tools, and so we used them in the linear guideways of a large ultra-precision machine tool with a moving weight of 4 tons. However, the pressurized oil became a source of heat, and thermal stability in the ultra-precision range could not be obtained even when the oil temperature was controlled to $\pm 0.01^{\circ}\text{C}$. This is because oil pressurized at 0.3 to 0.5 MPa is supplied to the guideway surface as pocket pressure, and heat is generated by the pumping action when it is opened to atmospheric pressure, and so the oil temperature at the outlet is measured and pressurized oil at a lower temperature than the machine body temperature is supplied, resulting in a thermal imbalance. For these reasons, we thought that a hydrostatic bearing was inappropriate as a linear guideway for an ultra-precision aspheric machine tool.

Although the ultra-precision, high-rigidity, compact, and low-cost features of the V-V sliding guideway had been proven in the ultra-precision slicer, the sliding bearing had a large coefficient of friction of 0.2 to 0.3, making it impossible to handle fine positioning and low-speed movement due to the stick-slip problem. Moore Special Tool's M-18AG had a V-V guideway with aligned rollers for eliminating this problem through rolling friction. We examined this guideway system, made some improvements, and evaluated the coefficient of friction, rigidity, motion accuracy, and micro-waviness using the experimental apparatus shown in Fig. 26, in which a needle is inserted between the cast iron bed and table. The results showed the coefficient of friction was 0.003 to 0.005, and the rigidity was 10 to 20 times higher than that of aerostatic bearings. The guideway surface was finished by scraping, and the unevenness of the scraping caused micro-waviness of 0.3 to 0.5 μm , but we found the micro-waviness could be reduced by using hand lapping to remove the unevenness from the scraping.

In addition, we reduced the surface pressure by arranging many small-diameter needles at a pitch of 5.6 mm as guideways for the ultra-precision machine tool with expectations for positive effects in averaging and longer life. To simplify the structure and increase the rigidity, the V-V guideway surface was installed directly on the cast iron bed and table. Although the material was cast iron, cold metal was applied to the guideway surface area during casting, and so the hardness of the guideway surface was formed as Hv280.

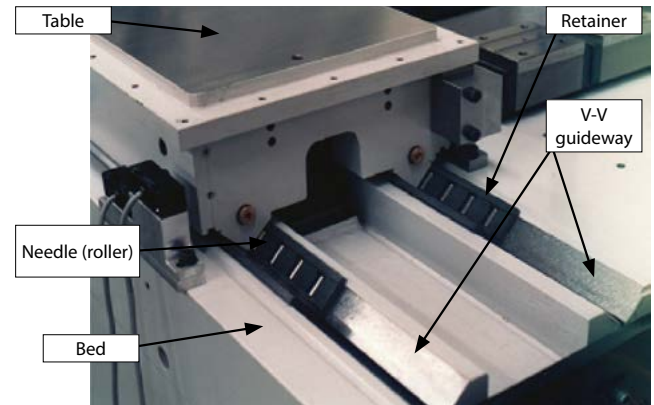


Fig. 26 Experimental apparatus for limited V-V roller guideway

(3) New concept for ultra-precision aspheric machine tools

In Japan, the demand for aspheric lenses in CDs and cameras increased, and Moore Special Tool's M-18AG and PNEUMO PRECISION's MSG-325 were imported to meet this demand. However, among domestic machine tool manufacturers, in 1985, Toyoda Machine Works (now JTEKT Corporation) released a CNC ultra-precision aspheric surface machine tool (AHN10), and Nachi-Fujikoshi released an ultra-precision aspheric surface machine tool (ASP-10). Later, in 1991, Toshiba Machine enhanced the peripheral equipment such as a limited V-V roller guideway, a cylindrical aerostatic spindle driven by a synchronous motor, a controller (FANUC FS15-MA, control resolution: 10 nm), and an optical scale (HEIDENHAIN LIP401, minimum gradation: 10 nm) and promoted the development of an ultra-precision aspheric machining tool with a new concept utilizing the experience of our two failed attempts.

From early on, Toshiba Machine had been researching glass lens production methods using the heat press method and had developed a high-accuracy optical glass element molding system which enabled rapid and uniform heating using infrared lamps, precise control of heating and cooling temperatures, and control of mold position and press force. Unlike resin molding, the pressing temperature of glass is as high as 400°C to 750°C . Therefore, heat-resistant cemented carbide and ceramics were used as mold materials, and machining had to rely on grinding. In addition, as digital cameras and camera phones gained higher performance features, the number of glass aspheric lenses was also expected to increase. Against this backdrop, we began development of an ultra-precision aspheric grinder (ULG-100A) based on the concept of ultra-precision, high rigidity, high stability, compact size, and low cost, with a focus on grinding functions.

In ultra-precision machining of lens molds, the machining results include errors in relation to the commands in the machining program, and these errors were caused by machining conditions, workpiece centering, tool wear, tool shape, deformation due to machining force, and thermal deformation. For this reason, we adopted a method of measuring the machining results and repeating the re-machining several times with a compensation program which corrects the error between the machining results and the command value to converge to the target value. Because this compensation method assumes the machine, tools, and environment do not change between the pre-machining and the compensation processes, we decided to use a highly stable limited V-V roller guideway, a high-resolution glass scale, and full temperature control at each location. (Incidentally, Toshiba Machine was the first company to use a high-resolution glass scale for the feedback scale of an ultra-precision aspheric machine tool, and other companies have since adopted high-resolution glass scales for their feedback systems.) For this reason, the machine was designed with a highly rigid integrated-structure cast iron bed with X and Z guideways arranged in a T-shape to eliminate overhangs caused by movement and reduce the effect of deflection caused by moving loads. The reason for the emphasis on making the machine compact is so the machine can be configured as small as possible since most workpieces were 100 mm or less in diameter, and high rigidity can be easily obtained with compact machine sizes. It also has the advantage of reducing the volume of the thermostatic chamber, leading to more precise temperature control and higher energy savings. In addition, this machine aimed to reduce the size of the table and other moving components by using limited V-V roller guideways with high rigidity and load capacity.

Expensive ultra-precision CNC lathes were imported from the U.S. for the purpose of making aspheric lenses which would satisfy the performance requirements during the development stage of cameras, CDs, and DVDs. The applications for aspherical lenses were consumer cameras, camera phones (which did not exist in the 1980's, but developed into a phenomenal market in later years when it became possible to manufacture compact, high-performance, low-cost lens units), CDs, DVDs, and other products for which prices were expected to decline as product volumes increased, and it was only natural the molds and machining equipment used to manufacture aspheric lenses would also need to be greatly reduced in cost. The new machine was designed to be

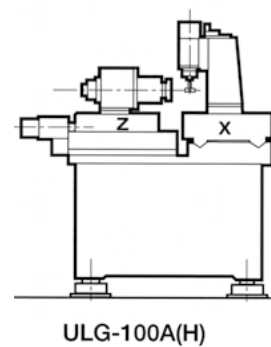
1/2 to 1/3 the price of existing machines and incorporated the following features: (1) Simplified structure, (2) Utilized established elemental technologies such as spindles and guideways, (3) Employed high-resolution scale feedback system, (4) Eliminated hydraulic units by employing a limited V-V roller guideway, and (5) Reduced installation area with a compact design.

The development phase proceeded smoothly due to our past experience with failures and improved technological capabilities, and so, after less than a year of development, the first model (ULG-100A(H)) (Fig. 27) with two-axis control (X and Z axes) was completed in June 1992 and delivered to the lens manufacturer who had been waiting for its completion. After 28 years, this machine is still in use at universities for research on ultra-precision machining.

As shown in Fig. 27, the control panel is integrated into the back of the bed for compactness and greater ease of operation. The control panel is a heat source and a 50 mm gap was provided to avoid heat conduction, but it was found the bed was deformed by radiant heat when the machine was used for long periods of time, and so unfortunately, the design was changed to a separate control panel. From our experience with the ultra-precision slicer, we realized humbly incorporating user requests and opinions would lead to the development of machines and new models which would sell well, and so we gradually increased the number of delivered units while adding improvements.³⁷⁾



(a) Equipment appearance



ULG-100A(H)

(b) Equipment structure

Fig. 27 First model of ultra-precision aspheric grinder ULG-100A(H)

(4) Training and supporting advanced researchers through ultra-precision machining and industry-academia collaboration

In the 1990's, the machining equipment, machining technology, software, elemental technology, control technology, and measurement related to ultra-precision aspheric machining were searching for direction, and I believe research in industry-academia

collaboration contributed greatly to subsequent development.

In November 1992, Dr. Toshiro HIGUCHI asked us to develop an ultra-precision aspheric machine tool with simultaneous 4-axis control, as shown in Fig. 28, as a tool for his research on ultra-precision machining at the Kanagawa Academy of Science and Technology (KAST). We used the same X and Z axes as those of the ultra-precision aspheric grinder provided the work spindle on the Z-axis with a built-in FANUC servomotor with C-axis function, and located the Y-axis on the X-axis. The limited V-V roller guideway is a mechanism where the table and the weight on the table applies a preload to the guideway surface, but this cannot be applied to vertical guideways. As a last-ditch effort, we adopted a structure where the moving component was clamped from both sides and mechanically preloaded as shown in Fig. 29. However, because of the wide-guide structure, orientation changes occurred during movement, and we could not obtain the same motion accuracy as the X and Z-axes. Later, this was developed into a method where the V-V roller guideway was situated for the Y-axis in the same way as for the X- and Z-axis and the reaction force of the aerostatic bearing, or the attractive force of the magnet of the linear motor, was used to apply a preload. Mitutoyo Corporation developed a feedback scale with a resolution of 1 nm, and we decided to use this scale. Dr. HIGUCHI told us, "We are developing a machine which has never existed before, so let's incorporate new mechanisms and elemental technologies even if it means taking risks."

Dr. Yutaka YAMAGATA of RIKEN has contributed to the development of ultra-precision machining by using this machine to create special free-form surfaces and developing software.

Dr. Toshimichi MORIWAKI and Dr. Eiichi SHAMOTO of Kobe University (as of 2021, Nagoya University) were involved in ultra-precision machining since early on, and we delivered ultra-precision aspheric grinders, mirror machining equipment, and aerostatic spindles for their research. Dr. SHAMOTO continued his research on ultra-precision cutting of hardened steel with single-crystal diamond tools using the elliptical vibration cutting method and expanded the application of ultra-precision machining as a new machining method for use in lens mold machining and automotive lighting-related mold machining. Later, Dr. Hirofumi SUZUKI (now at Chubu University) joined him and pioneered numerous applications for ultra-precision machining and has trained many engineers and researchers.³⁸⁾

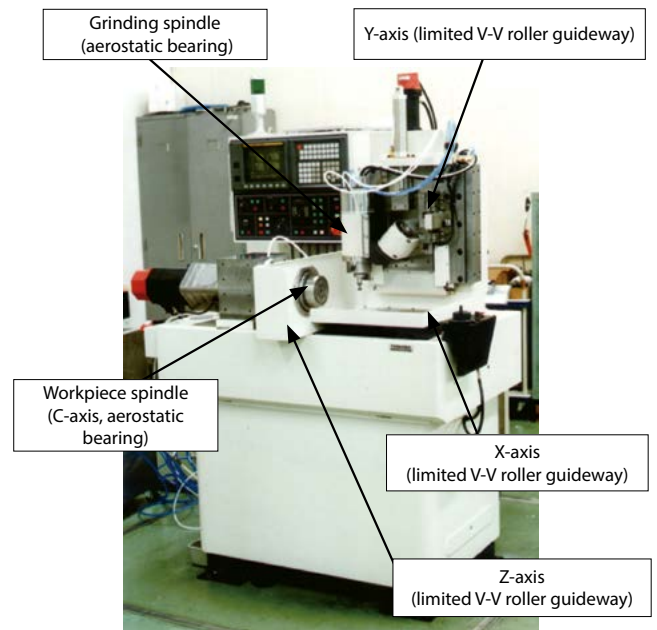


Fig. 28 Ultra-precision aspheric machine tool with 4-Axis control ULG-100A(H3) delivered to KAST

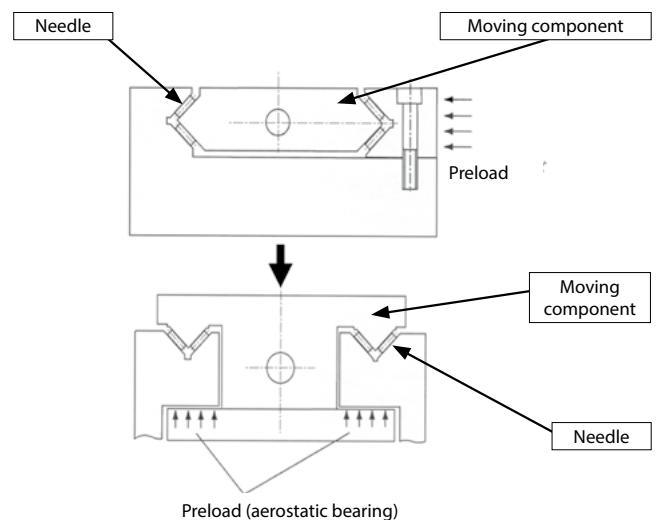


Fig. 29 Change in structure of Y-axis guideway surface

Dr. Katsuo SHOJI and Dr. Tsunemoto KURIYAKAWA of Tohoku University introduced an ultra-precision aspheric grinder and clarified the relationship between ultra-precision machining of new workpiece materials, machine behavior, and machining accuracy. They also proposed the parallel grinding method as a new grinding method, and we were able to build a prototype of a specialized machine for this process (Fig. 30). Dr. Gao WEI of Tohoku University has been implementing the use of ultra-precision machining technology in the field of measurement, such as the creation of large-area three-dimensional micropatterns on edge and cylindrical surfaces using an ultra-precision aspheric machine tool and conducting research and development on a surface encoder

for position and orientation detection with five degrees of freedom.

In addition, we have delivered more than a dozen ultra-precision aspheric machine tools and aerostatic spindles to universities and research institutes such as the University of Hyogo, Kumamoto University, Hiroshima University, Toyo University, RIKEN, and the Fukuoka Institute of Technology. And over the past twenty years, several research results using Toshiba Machine's ultra-precision aspheric machine tools have been presented in the ultra-precision machining sessions at scholarly conferences of the Japan Society of Mechanical Engineers, the Japan Society for Precision Engineering, and the Japan Society for Abrasive Technology. I believe the research at these universities has contributed to the application of ultra-precision machining technology to optical components, which has developed significantly since the late 1990s.

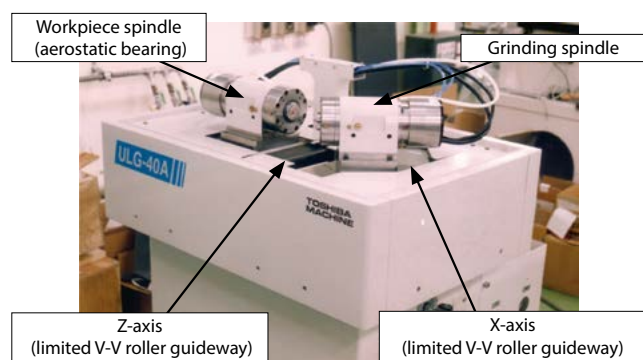


Fig. 30 Ultra-precision aspheric machine tool for parallel grinding of aspheric lens molds

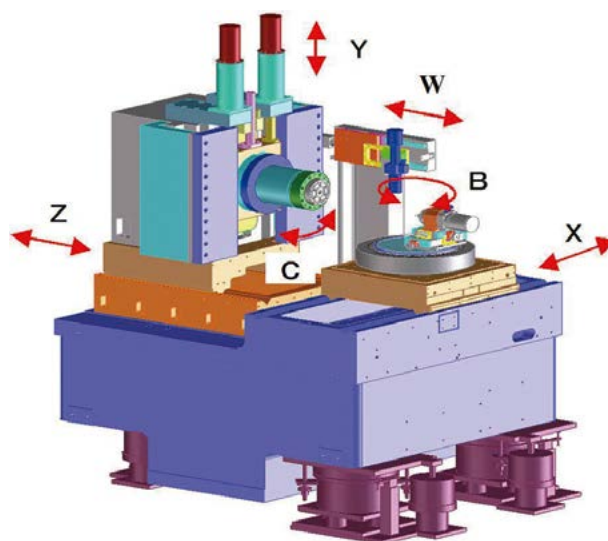
(5) Evolving ultra-precision aspheric machine tools by adding new elemental technologies

Since the first machine in 1992, the variations of ultra-precision machine tools have expanded to nine models in the range of 2-axis control to 5-axis control in response to user demands for higher accuracy, changes in workpieces, and lower prices, and the technical improvements made during this period will be described.

Fig. 31 shows the ULG-100D(5A), a 5-axis controlled ultra-precision aspheric machine tool, which is the top-of-the-line machine among ultra-precision aspheric machine tools. In addition, the ULC-100F(S), an ultra-precision aspheric machine tool specialized for cutting, has made it possible to obtain a smooth machined surface by reducing the instruction unit of the program from the usual 1 nm to 0.1 nm. Fig. 32 shows the excellent tracking performance of this machine at a step feed of 0.5 nm.



(a) Equipment appearance



(b) Equipment structure

Machine configuration and accuracy
 (1) X, Y, and Z-axis: Limited V-V roller guideway
 (2) X, Y, and Z-axis drive: Cored linear motor
 (3) C and B-axis: Aerostatic bearing
 (4) C and B-axis drive: Synchronous motor
 (5) Control resolution (X, Y, and Z-axis): 1 nm

Fig. 31 Ultra-precision aspheric machine tool ULG-100D(5A)
 5-axis (X, Y, Z, C, B)

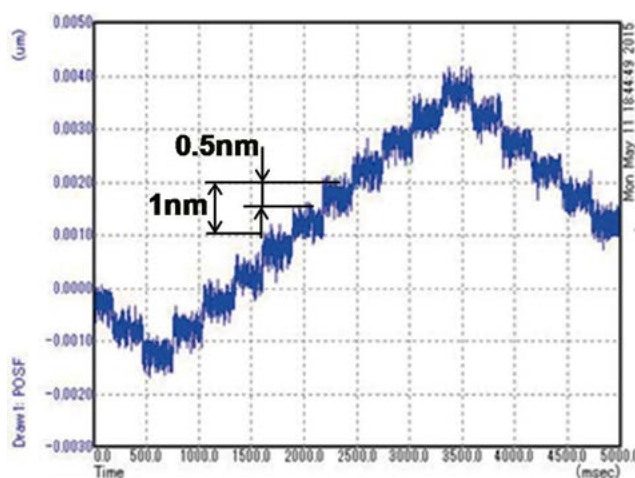


Fig. 32 Tracking performance of ULC-100F(S) at step feed of 0.5 nm

① Evolved limited V-V roller guideway

In the grinding process using a grinding wheel with a large number of random cutting edges, the surface roughness is limited to about 20 to 30 nmRz, and no effect is observed for the micro-waviness caused by the limited V-V roller guideway. However, Toshiba Machine's product was inferior to competing hydrostatic bearing machines in cutting with single-crystal diamond tools, and users evaluated Toshiba machines as unacceptable because of their roller guideways. Consequently, by devising the shape of the needle insertion area on the moving side and improving the finishing method on the guideway surface, a value of 10 nm or less for the micro-waviness was obtained, and a surface roughness of 2 to 3 nmRz was easily achieved in the cutting results. This product received high marks from users because of its high rigidity, excellent stability without a heat source like hydrostatic bearing machines, and energy savings (only 0.4cc of lubricant per axis per day was required). The limited V-V roller guideway was supported by a large number of rolling elements, and the load per needle was 10 N or less. Since many rolling elements are in contact, the damping effect is large, and the position deviation is stable at 0.5 nm during stopping as shown in Fig. 33 due to the suitable contact friction.³⁹⁾

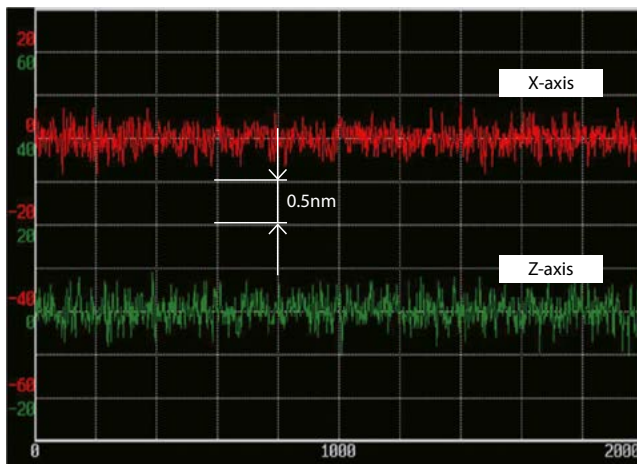


Fig. 33 Position deviation at X and Z-axis stoppage

② Development of porous restrictor aerostatic spindle

The work spindle employs an aerostatic bearing with an inherent restrictor. The inherent restrictor system has a large bearing clearance, high air flow rate, and low heat generation for high-speed rotation. The maximum speed of the work spindle in the ultra-precision aspheric machine tool is 3000 min⁻¹, and so there is little concern about heat generation. However, the mirror surface machined by the work spindle with the inherent restrictor has a

distorted pull line caused by the vibration generated by a large amount of air flowing through the pipe, and as shown in Fig. 34, this adversely affects the quality of the machined surface. For this reason, we developed a porous restrictor type aerostatic spindle which can narrow the bearing clearance, reduce the air flow rate, and increase the bearing rigidity (Fig. 35). Porous metal is used for the porous restrictor, and the surface is clogged with solid lubricant metal, which is removed by machining so the air flow rate reaches the target value. Although it takes more time and effort than the inherent restrictor system, this results in 1/8th the air flow rate, 2.3 times the axial rigidity, and 1.7 times the radial rigidity. The center runout (SPAM) of the work spindle is also 2 to 3 nm. As shown in Fig. 36, the results of machining with this spindle show no distortion in the pull line and the feed pitch per turn can be clearly seen. Furthermore, the work spindle has a C-axis function, which enables smooth speed changes by issuing the speed command in units of 0.01 min⁻¹, thereby contributing to improved efficiency and machined surface quality through constant peripheral speed machining even in the field of ultra-precision machining.⁴⁰⁾

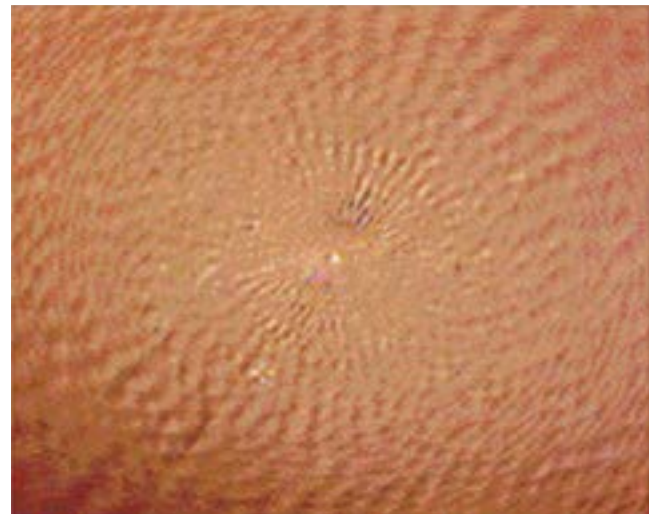


Fig. 34 Machined surface with inherent restrictor bearing

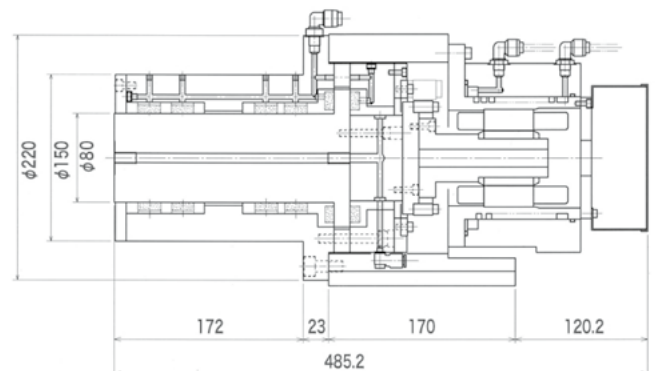


Fig. 35 Porous restrictor work spindle

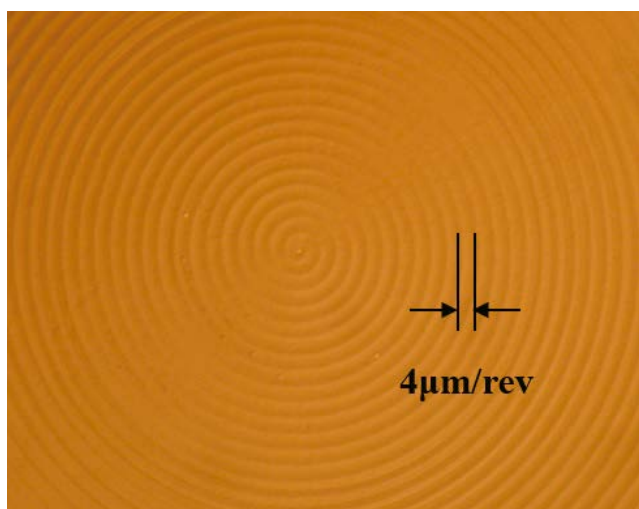


Fig. 36 Machined surface with porous restrictor bearing

③ New Technology for Feed Drive System: Cored Linear Motor Drive

AC servomotors and ball screws have been used for the feed mechanisms of ultra-precision machine tools, but bends and misalignments in the ball screws affect the behavior of the moving components and mechanisms have been implemented to absorb these errors. Parallel spring joints with rigidity in the feed direction and degrees of freedom in the direction perpendicular to the feed direction have been developed and used for ultra-precision aspheric machine tools. However, the rigidity of the feed system is low because the ball screw drive consists of many parts, including the servo motor, coupling, ball screw, nut, and parallel spring joint, and quadrant protrusion due to lost motion always occurs at the quadrant switching point in simultaneous 2-axis machining. Even by changing the machining conditions, such as slowing down the feed at the quadrant switching point, or by machining with a compensation program to predict the quadrant protrusion, it was not possible to eliminate the penetration caused by the quadrant protrusion. Therefore, there was no other way but to remove it by polishing after machining, which took time and caused loss of form accuracy. Also, the ball screw needed to be replaced after about three years of operation because wear of the ball screw directly affected lost motion. And so, we studied the application of linear motors, which have fewer parts and a simpler structure than ball screw drives, as a new feed mechanism for ultra-precision machines.

Coreless linear motors are used in ultra-precision machines and light-load machining centers to avoid the effects of cogging and magnet attraction, but they have the disadvantage of low

thrust and high heat generation. Toshiba Machine decided to use a cast iron bed with high rigidity, a limited V-V roller guideway featuring high rigidity and high stability, and a FANUC cored linear motor with high thrust (high efficiency) and low heat generation for compatibility with the controller. In addition to the strong attachment of the magnet and coil and the placement of the magnets opposite each other to cancel the attractive force, we devised a mechanism to continuously change the position of the linear motor and feedback scale and the magnetic field lines, improved the function of the servo system, and adjusted the control parameters for building a complete feed mechanism which is not affected by cogging (Fig. 37).

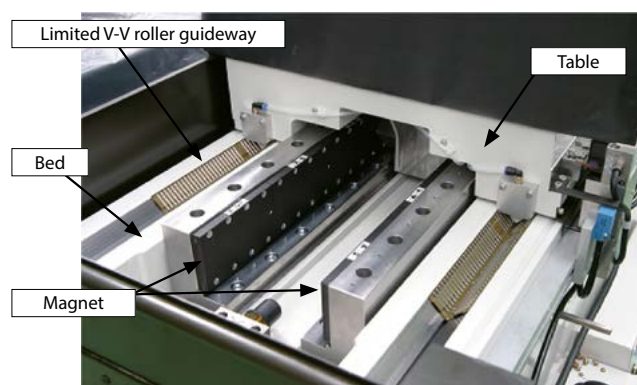


Fig. 37 Limited V-V roller guideway of linear motor drive
Magnets are placed opposite each other to cancel the attractive force

As a result of employing a cored linear motor, the coil and guideway do not need to be cooled in the ultra-precision aspheric machine tool, where the maximum feed rate is about 1000 mm/min, contributing to energy-saving operation. The high level of perfection of the limited V-V roller guideway and the linear motor drive have enabled us to achieve 10 nm or less for the micro-waviness, tracking performance within 0.5 nm or less with movement commands, and no lost motion when switching quadrants, making the term "quadrant protrusion" a thing of the past.

In the limited V-V roller guideway used for the X and Z axes, the needle is preloaded by the weight of the moving component, but as shown in Fig. 38, a method to reduce the weight of the moving component is also employed by using the attractive force of the magnet as a preload. In Fig. 29, the method of applying a preload to a limited V-V roller guideway for a vertical guideway was described earlier. However, the latest machines have employed a method which uses magnetic attraction instead of aerostatic bearings

in order to simplify the structure, reduce costs, and improve performance. Thus, the use of cored linear motors has greatly contributed to the accuracy, performance, and stability of ultra-precision aspheric machine tools.⁴¹⁾

Since 2010, the addition of digital cameras, smartphones, security cameras, industrial cameras, and in-vehicle cameras has created a huge demand for aspherical lenses (glass and plastic). Toshiba Machine has responded to this demand by expanding the specifications and functions of its ultra-precision aspheric machine tools (on-machine measurement system, 0.1 nm commands, etc.), improving accuracy, and developing machining methods (elliptical vibration cutting, constant peripheral speed control, etc.) and machining software for contributing to the delivery of more than 1000 units to date.

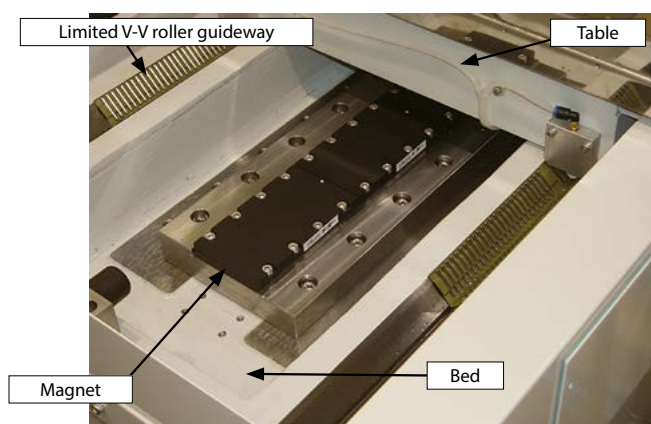


Fig. 38 Limited V-V roller guideway of linear motor drive
Attractive force of magnets is used to apply a preload

3 Conclusion

Our company has been involved in ultra-precision machining since 1977, with the aim of differentiating and adding value to our products by improving machine tool accuracy. In this context, we introduced high-precision machine tools (lathes, cylindrical grinders, surface grinders, jig borers, etc.) and a constant-temperature factory at $\pm 0.1^\circ\text{C}$ as machining equipment, improved the scraping and lapping skills (production of three-face sliding surface plates), and introduced capacitance-type non-contact micro-displacement sensors, roundness meters, surface roughness meters, differential interference microscopes, and Fizeau interferometers as measuring instruments. As elemental technologies to achieve submicron accuracy, we have developed aerostatic spindles, aerostatic guideways, V-V sliding guideways, limited V-V roller guideways, and more.

Through the production of these elemental technologies, we have developed improvements to machining and measurement technologies and come to better understand the hurdles presented by sub-micron technology. The breakthrough for ultra-precision machining was not the upgrading of conventional machine elements, but the challenge of completely new technologies such as aerostatic spindles, aerostatic guideways, limited V-V roller guideways, and cored linear motor drives.

In 1977, there was almost no need for ultra-precision machining in Japan, and we simply supplied aerostatic spindles to research institutes for research purposes. However, as mentioned earlier, we demonstrated optical mirror surfaces can be produced by cutting with an experimental device combining an aerostatic spindle and an aerostatic guideway, and the results were applied to machine tools for polygon mirrors and magnetic disk substrates, and the improved performance and accuracy of the aerostatic spindle and V-V sliding guideway were used in ultra-precision slicers. The limited V-V roller guideway and cored linear motor drive have been used in the ultra-precision double-column machining centers (light guiding sheet metal machining). The limited V-V roller guideway, cored linear motor drive, and porous restrictor aerostatic spindle have been used in ultra-precision aspheric machine tools, and the ultra-precision hydrostatic spindle and limited V-V roller guideway, and cored linear motor drive have been used in ultra-precision grooving lathes (roll machining for prism sheets).

Laser printers, hard disk drives, liquid-crystal displays, digital cameras, camera phones, smartphones, security cameras, and in-vehicle cameras involving these machine tools were unimaginable in 1977. It is not clear whether ultra-precision machining technology made these products possible, or whether the requirements for these products drove the development of ultra-precision machining technology, but I believe the above products are the result of ultra-precision machining technology being able to meet the requirements of the products.

Although we were not able to make much of a contribution to the upgrading of machine tools which we had envisioned at the start of ultra-precision machining in 1977, it has been a great pleasure to be involved in and contribute to the birth of completely new industries and product groups over the past 40 years.

References

- 1) Katsutoshi TANAKA: Ultra-precision machining contributing to information-oriented society, *Journal of the Japan Society for Abrasive Technology*, 50, 10 (2006) 563.
- 2) Isao HARUMOTO, Kunio WATANABE: Manufacturing technology of aspheric lenses, *Science of machine*, 28, 9 (1976) 1071.
- 3) Kazuo NAITO: Ultra-precision technology in camera production-Mass-production technology of high-precision aspheric lenses - *Journal of the Japan Society of Mechanical Engineers*, 87, 791 (1984) 1152.
- 4) Akira KOBAYASHI: Recent ultra-precision cutting technology, *Science of machine*, 33, 1 (1981) 97.
- 5) Masakazu MIYASHITA: Overseas trends in ultra-precision technology, *Journal of the Japan Society of Mechanical Engineers*, 87, 791 (1984) 1109.
- 6) Yoshitaro YOSHIDA, Kimiyuki MITSUI, Yuichi OKAZAKI: Ultra-precision machine tools and their elements, *Journal of the Japan Society of Mechanical Engineers*, 87, 791 (1984) 1116.
- 7) Yorikazu SHIMOTSUMA: Outlook for hydrostatic gas bearings in foreign countries, *Journal of Japan Society of Lubrication Engineers*, 15, 9 (1970), 544.
- 8) D. M. Miller, G.H. Hauver, J.N. Culverhouse, E. N. Greenwell: Description of a Unique Machine Tool Permitting Achievement of <15-Årms Diamond-Turned Surfaces, *SPIE Vol.163 Advances in Optical Production Technology* (1979) 55.
- 9) Akira KOBAYASHI: Recent Development of Ultra-Precision Diamond cutting Machines in Japan, *Special Lecture on Ultra-Precision Diamond Cutting*, Japan Society for Precision Engineering, (1984) 1.
- 10) Akira KOBAYASHI: Ultra-Precision Machining Technology - Historical Development and Future Expectations, *Special Lecture on Ultra-Precision Diamond Cutting*, Japan Society for Precision Engineering, (1984) 9.
- 11) J. W. Pearson: Precision Machining Commercialization, Japan Society for Precision Engineering, *Special Lecture on Ultra-Precision Diamond Cutting*, (1984) 31.
- 12) Floyd E. Johnson: Diamond Turning at Honewell, Japan Society for Precision Engineering, *Special Lecture on Ultra-Precision Diamond Cutting*, (1984) 39.
- 13) PNEUMO PRECISION, INC., Micro-Surface Generating Pneumo Model MSG-325 Catalog.
- 14) P. Donald Brehm: Diamond Machining of Metal & Plastic Optics, Japan Society for Precision Engineering, *Special Lecture on Ultra-Precision Diamond Cutting*, (1984) 23.
- 15) T. G. Gijssbers, COLATH, A Numerically Controlled Lathe for Very High Precision, *Philips Mechanical Review*, 39, 9 (1980).
- 16) Hideo TSUWA: The present and future of ultra-precision machining, *FOP*, 4, 8 (1979) 1.
- 17) Norio TANIGUCHI: Development of ultra-precision machining technology and its future issues -Relation to nanotechnology, *Journal of the Japan Society of Mechanical Engineers*, 87, 791 (1984) 1101.
- 18) Katsutoshi TANAKA: Air bearings and ultra-precision machining, *Science of machine*, 34, 12 (1982), 1304.
- 19) Mitsuo SUMIYA, Katsunobu UEDA, Tameyasu TSUKADA: Performance and Application of Developed Ultra Precision Air Bearing Spindle, *Journal of the Japan Society of Precision Engineering*, 45, 10 (1979) 1231.
- 20) Akira KOBAYASHI: History of the development of high-precision air bearing rotating axes and their applications, *Japan Society of Precision Engineering*, 45, 10 (1979), 1159.
- 21) Toshiba Machine Technical Report: Air bearings and mirror finishing for ultra-precision machining (1980).
- 22) Katsunobu UEDA, Mitsuo SUMIYA: Diamond cutting of metal mirrors for carbon dioxide laser equipment, *Toshiba Review*, 40, 10 (1985) 857.
- 23) Katsutoshi TANAKA: Machining by SPDT, Edited by Naoharu KINOSHITA, *Diamond Tools, Nikkei Gijutsu Tosho* (1987) 764.
- 24) Mitsuo SUMIYA: Planar and spherical mirrors, Edited by Naoharu KINOSHITA, *Diamond Tools, Nikkei Gijutsu Tosho* (1987) 771.
- 25) Masao USUKI, Masaomi KUBO, Yoshio MAKIMOTO, Takashi ONOGI: Applications for static pressure elements, *Fujikoshi Engineering Review*, 38, 2 (1982) 49.
- 26) Japanese Industrial Standard, Optical Polygons for Angle Standards, JIS B7432.
- 27) Etsuji MINAMI: Diamond cutting of polygonal mirrors for laser printers, *Machine Tool & Machine Technology*, 7 (1985) 116.
- 28) Nippon Light Metal Technical Report, Special Aluminum Alloy Material for Laser Scanner Mirror (Polygon Mirror).
- 29) Katsutoshi TANAKA: Mirror machining of polygonal mirrors, *New Machining Tool Encyclopedia*, Sangyo Chosakai (1991) 629.
- 30) Katsutoshi TANAKA: Structure, accuracy and application examples of aerostatic guideways, *Machine Tool & Machine Technology*, 8 (1987) 110.
- 31) Yujiro AKECHI: Spindle Head Design for Ultra-precision Lathe, *Journal of the Japan Society of Precision Engineering*, 45, 10 (1979) 1182.
- 32) Bryant Symons, *Fine Diamond Tool Lathes*, Catalog.
- 33) Katsutoshi TANAKA: Chapter 11, Ultra-Precision Lathes, Edited by Hiroshi EDA, *Ultra-Precision Machining Technology*, Triceps No. 2 (1986) 307.
- 34) Katsutoshi TANAKA: Current state of grooving and cutting by ultra-precision slicers, *Journal of the Japan Society for Abrasive Technology*, 46, 11 (2002) 544.
- 35) Katsutoshi TANAKA, Seiji KIMURA, Kiyoshi SUZUKI, Tetsutaro UEMATSU: A Study on achieving high accuracy in ultra-precision machine tools: 1st report: Improvement of performance of an aerostatic bearing spindle with an annular restrictor, *Journal of the Japan Society for Abrasive Technology*, 51, 5 (2007) 302.
- 36) Etsuo TAKEOKA: A Study on End Milling of High-Hardness Materials by High-Speed Aerostatic Spindles, Thesis (1998).
- 37) Katsutoshi TANAKA, et al., A Study on achieving high accuracy in ultra-precision machine tools: 3rd report : A Study on an ultra-precision aspheric generating machine and its performances, *Journal of the Japan Society for Abrasive Technology*, 51, 9 (2007) 553.
- 38) Hirofumi SUZUKI: Research on Ultra-Precision Machining of Aspheric Optical Components, Thesis (1997).
- 39) Yoshiaki KAI: A Study on the Analysis and Evaluation of the Dynamic Characteristics of Ultra-precision Machine Tools, Thesis (2015).
- 40) Rei SEKIGUCHI et al.: Higher Efficiency for Ultra-Precision Grinding of Glass Lenses by Controlling the Tool Feed and Workpiece Peripheral Velocity, *Proceedings of the 2015 Japan Society for Abrasive Technology*, 332-337.
- 41) Katsutoshi TANAKA, et al., A Study on achieving high accuracy in ultra-precision machine tools: 2nd report: Investigation on the performance of the V-V roller guide-way table driven by a linear motor with cores, *Journal of the Japan Society for Abrasive Technology*, 51, 8 (2007) 482.

Introduction to Patents

Establishing the "respect for intellectual property rights" as one of its corporate policies, SHIBAURA MACHINE protects the results of technological development by establishing intellectual property rights, and also respects the intellectual property rights of third parties. SHIBAURA MACHINE strives to promote the development of technologies to offer products, systems, and services which can satisfy customers. As a result, the company holds approximately 1,800 domestic and overseas patent rights. Of those patents, SDGs-related patents will be introduced herein. Such patents are highly evaluated by the patent score provided by Patent Result Co., Ltd. (Patent score: an evaluation index for scoring the level of attention to individual patents based on historical information)

1 Deep ultraviolet LED and method for manufacturing the same

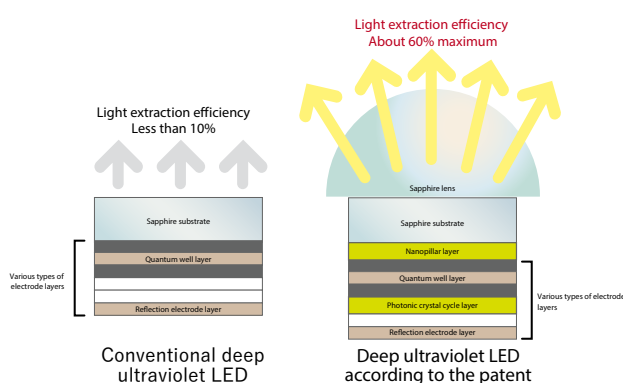
Patent number: Patent No. 6230038

Inventors:

Mitsunori KOKUBO, Takaharu TASHIRO (SHIBAURA MACHINE), Yukio KASHIMA, Eriko MATSUURA (Marubun), Hideki HIRAYAMA (RIKEN), Ryuichiro KAMIMURA, Yamato OSADA (ULVAC), Toshiro MORITA (Tokyo Ohka Kogyo)

Deep ultraviolet LEDs are expected to be widely used for sterilization in food, water purification, medical, and home electronics industries. However, power conversion efficiency of the product is only 2% to 3%. To put the deep ultraviolet LED into practical use in the above industries, a power conversion efficiency of 10% or higher is required. Major factors contributing to low power conversion efficiency are; <1> 50% or more of deep ultraviolet light is absorbed and disappears in the contact layer of the LED, and <2> light extraction efficiency is sometimes less than 10% because deep ultraviolet light is converted to heat due to total internal reflection. To improve power conversion efficiency, improvement of light extraction efficiency is required.

With respect to this LED patent, light extraction efficiency of up to about 60% has been achieved by adopting an appropriate stacking sequence of substrate electrode layers, periodic photonic crystal structure, nanopillar structure, and semispherical lenses.



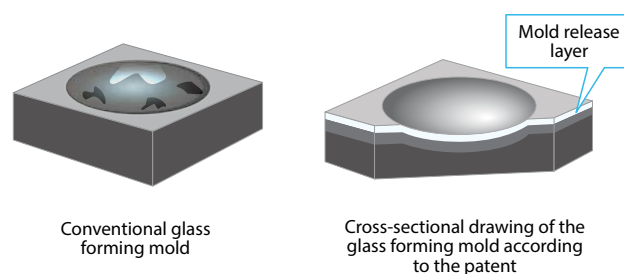
2 Glass forming mold

Patent number: Patent No. 5376984

Inventors: Hisanori FUWA, Jun MASUDA

In order to prevent reaction with glass, mold release film is applied to the mold during glass lens manufacture by means of press forming. Typical mold release film uses noble-metal based alloys, such as oxidation-resistant platinum and iridium. However, depending on the glass type combination, such mold release film has low mold-release properties, causing the glass to fuse in a short amount of time. Therefore, a mold release agent was applied to the mold on which an iridium-rhenium alloy mold release film was formed before molding the glass, or mold release coating was applied to the glass preform.

The glass forming mold according to the patent has a mold release layer containing carbon inside the mold. Because carbon contained in the mold release layer works similarly to the mold release agent, excellent mold release performance can be achieved without applying a mold release agent to the mold and glass preform. The mold use cycle is generally between 100 and about 500 times. However, SHIBAURA MACHINE's mold can now be used even more than 2000 times.

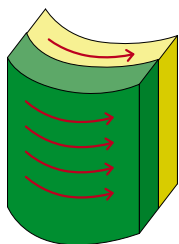


Patent number: Patent No. 6522456

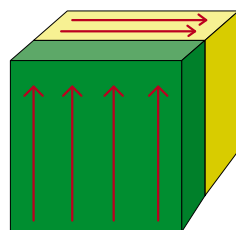
Inventors: Masamichi MOMONO, Takamitsu YAMASHITA

Fiber reinforced plastic is widely used for aircraft, automobiles, and other vehicles, housing equipment including modular baths, and recently, robots and drones. However, fiber reinforced plastic has a problem where reinforced fibers tend to be oriented to the direction of resin flow, causing molded products to warp, reducing strength in a specific direction. To solve this disadvantage, materials with mixed reinforced fibers have been used for forming plastic. However, such fibers easily break when the material is packed in a mold because the fibers of such materials are originally short, thus losing a primary advantage of reinforced fibers.

In the molding apparatus according to the patent, <1> it is possible to continuously load reinforced fibers, and <2> it is possible to laminate layers so the direction of resin flow varies. Accordingly, long reinforced fibers remain in the final molded product without breakage, and long reinforced fibers in the first layer and the second layer are formed in opposite orientation. As a result, it is now possible to obtain high-strength molded products having significantly improved bending strength and modulus of elasticity independent of the direction.



Conventional injection-molded article



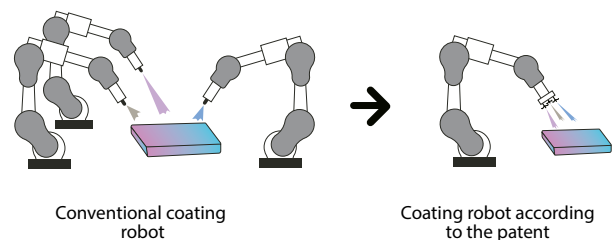
Injection-molded article according to the patent

Patent number: Patent No. 5437301

Inventor: Yuji NEGISHI

In the general coating system, various types of robots are disposed according to a plurality of different processes, such as basecoat, middle coat, and overcoat. One resulting problem is the system requires a large installation area. Since two or more robots are used for coating, it is necessary to program each robot to learn the details of the coating procedures.

In the coating robot system according to the patent, the arm of one robot is equipped with several spray guns, which enables one robot to perform multiple coating processes. As a result, it is possible to reduce the installation area of the entire system and reduce the learning tasks of the robot.



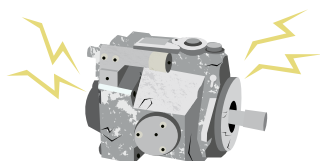
Conventional coating robot

Coating robot according to the patent

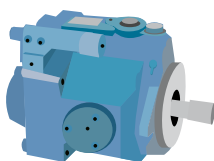
Patent number: Patent No. 6131322**Inventors: Ryosuke FUJIMOTO, Takumi HAREYAMA**

Currently, complaints about noise rank high among the seven typical environmental pollution types. Specifically, noise coming from construction work in urban areas is a big problem, and it is an urgent matter to reduce noise generated from urban-type construction machines. To reduce noise from construction work, is advantageous to increase the vibration damping performance of hydraulic component materials in heavy machines. For example, flake graphite cast iron has vibration damping performance but its strength is too low to be applied to the cast iron hydraulic components of heavy machines. For this reason, cast iron having strength equivalent to conventionally-used spheroidal graphite cast iron is required.

As the result of SHIBAURA MACHINE's research and development, it was found adding an appropriate amount of specific elements to cast iron can promote both the formation of iron-aluminum carbide and the spheroidization of graphite. Thus, both high strength and low vibration cast iron has been successfully achieved. The casing (blue-colored part in the below figure) of the hydraulic component (piston pump) of heavy machines made of SHIBAURA MACHINE's high-strength, high-damping capacity cast iron is irrefrangible (high strength) and makes quiet (low vibration) construction work possible.



Conventional cast iron
pump



Pump made of vibration
damping cast iron
according to the patent

My Expectations for Shibaura Machine



Emeritus Professor
University of Tokyo

Toshiro HIGUCHI

My relationship with Shibaura Machine (I will refer to it as Toshiba Machine hereafter because much of the following is about my time at Toshiba Machine) began about 50 years ago. I took a design exercise class in the Department of Precision Mechanics, Faculty of Engineering at The University of Tokyo. Since it was a small department, they asked engineers from companies with a considerable amount of practical experience to teach the class. A lecturer at Toshiba Machine who was also a senior member of the department taught me design drafting in an exercise with a positioning table for feeding using ball screws, and I learned Toshiba Machine manufactured large machine tools.

When I was appointed as a professor in the Department of Precision Mechanics in 1991, I requested Toshiba Machine send lecturers to my department, a relationship which continued for an extensive period of time. In April 1992, I concurrently started working on the Higuchi "Extreme Mechatronics" project at KAST, the Kanagawa Academy of Science and Technology. We built a laboratory at KSP in Mizonokuchi, Kawasaki City, where we worked on the project with a budget of one billion yen over five years. One of the tasks of the project was to research electrostatic motors, and we succeeded in developing a powerful electrostatic motor with a performance comparable to that of electromagnetic motors. In the course of investigating various electrostatic motor systems, we realized we needed a device capable of processing 3-row screws with a pitch of several micrometers in order to process electrodes. However, such a device did not exist, so we decided to create one ourselves using our ample research funds. We happened to come across an article in an industrial newspaper reporting Toshiba Machine had developed a small aspheric processing machine. On a hunch we would be able to develop a machine which could achieve

the desired functions if we used this processing machine as a basis, we asked Mr. Takahiko INOKUMA (director and manager of the Sales Department at the time), who was the instructor for our design seminar, to manufacture the device. After repeated discussions between the project laboratory members and Toshiba Machine, we designed an ultra-precision machine with 4-axis control capable of not only processing micro screws, but which could also be used in research on ultra-precision machining for various applications. The resulting ultra-precision machine was not only used for research on various types of ultra-precision machining, it also contributed to the development of excellent human resources playing important roles in ultra-precision machining.

In the KAST project, we collaborated with Toshiba Machine to promote the development of a device capable of obtaining 3D images of organs and insects by sequentially acquiring cross-sectional images of frozen samples by feeding them on a per-minute distance basis and cutting them with a rotating blade. The result of this research, a 3D internal structure microscope, was delivered by Toshiba Machine to RIKEN and other research institutions. In parallel with this joint research, we also succeeded in developing an automatic preparation device for tissue sections used in pathological examinations, which was put on the market by Toshiba Machine (the technology has since been transferred to Dainippon Seiki).

The success of this joint research was due to Toshiba Machine's ability to design and manufacture high-precision, robust machines which reliably fulfill their functions based on proven technology and abundant achievements. This is the DNA of Toshiba Machine. The new company name, Shibaura Machine, not only represents a brand name in machine tools, it also stands as a reminder of our

company's origins with Toshiba. Although Shibaura Machine is no longer part of Toshiba Corporation in terms of capital, we trust it will play a role as a successor to Toshiba's production machinery business, which has supported the development of Japanese industry.

This Technical Bulletin is the first to be published since our rebranding as Shibaura Machine. Fresh from the field of industry, the information contained in the Technical Bulletin is valuable for researchers and students at universities and other educational institutions. I hope the Technical Bulletin will continue to be published for years to come and contribute to advancements in science, technology, and engineering education.

As can be seen from this Technical Bulletin, Shibaura Machine has a number of uniquely distinctive technologies in the fields of large machinery, ultra-precision, injection and die casting machines, and control equipment. In addition to aiming at further growth in these existing areas, it will be important to develop new businesses which make use of these technologies, and for that, it is vital to interact with people from different fields. This Technical Bulletin is an important medium in making the technology of Shibaura Machine widely known to people in different fields. I hope the contributors to this bulletin will devise descriptions which can be readily understood by people from different specialties, and thereby convey the content and appeal of the developed technology to as many people as possible.

Publish : June 17, 2022
Not for sale : All Rights Reserved Reproduction
or quotion without permission is
prohibited.
Publisher : Mitsunori KOKUBO
Press : SHIBAURA MACHINE CO.,LTD.
Research & Development Center
R&D Department
4-29-1,Hibarigaoka,Zama-shi,
Kanagawa-ken,252-0003,Japan

Shibaura Machine Engineering Review Editonal Commission

Chairman	Mitsunori KOKUBO		
Members	Jun FUJITA	Toshihiro IGARASHI	Satoshi SUMIDA
	Hiroshi OKUYAMA	Toshiaki NAKANO	Takehiro YAMAMOTO
	Takato BABA	Masahiko IIDA	Shoichi SATO
	Takuro KAZAMA	Ryosuke FUJIMOTO	Hiroyuki ONUMA
	Kouichi USAMI	Hyo USAMI	
Coordinator	Kazuhito SATO	Masayuki YAMAMOTO	Takafumi OKAWA
	Akihide OKUBO	Shinichi NIKAI DOU	Hiroki AMEZAWA
	Itaru SETO		

Offices and Manufacturing Sites	Domestic Group Companies	Major Sites outside Japan	
Tokyo Headquarters 2-2, Uchisaiwaicho 2-chome, Chiyoda-ku, Tokyo 100-8503, Japan TEL: [81]-(0)3-3509-0200 FAX: [81]-(0)3-3509-0333	SHIBAURA MACHINE ENGINEERING CO., LTD. 267-2, Nishi-sawada, Numazu-shi, Shizuoka-ken 410-0007, Japan TEL: [81]-(0)55-921-7800 FAX: [81]-(0)55-921-7831 https://www.shibaura-machine.co.jp/smeng	< East Asia >	* : HEAD OFFICE
Numazu Headquarters 2068-3, Ooka, Numazu-shi, Shizuoka-ken 410-8510, Japan TEL: [81]-(0)55-926-5141 FAX: [81]-(0)55-925-6501	TOEI ELECTRIC CO., LTD. 131, Matsumoto, Mishima-shi, Shizuoka-ken 411-8510, Japan TEL: [81]-(0)55-977-4111 FAX: [81]-(0)55-977-4110 http://www.toei-electric.co.jp/index_J.htm	SHANGHAI SHIBAURA MACHINE CO., LTD. 4788, Jin Du Road, Xinzhuang Industry Zone, Shanghai, 201108, PEOPLE'S REPUBLIC OF CHINA TEL: [86]-(0)21-5442-0606 FAX: [86]-(0)21-5866-2450 SHANGHAI*, BEIJING, TIANJIN, DALIAN, CHONGQING, NINGBO	SHIBAURA MACHINE VIETNAM COMPANY LIMITED. 2nd Floor, VIT Tower, No. 519, Kim Ma Street, Ngoc Khanh Ward, Ba Dinh district, Hanoi, VIETNAM TEL: [84]-(0)24-2220-8700,1 FAX: [84]-(0)24-2220-8702 HANOI*, HO CHI MINH
Tohoku Branch 2-11-2, Yaotome, Izumi-ku, Sendai-shi, Miyagi-ken 981-3112, Japan TEL: [81]-(0)22-374-6111 FAX: [81]-(0)22-374-6118	FUJI SEIKI MACHINE WORKS,LTD. 840 Shimotogari, Nagaizumi-cho, Sunto-gun, Shizuoka-ken 411-8730, Japan TEL: [81]-(0)55-988-1001 FAX: [81]-(0)55-988-1027 http://www.fujiseiki-machine.co.jp/	SHIBAURA MACHINE (SHANGHAI) CO., LTD. 4788, Jin Du Road, Xinzhuang Industry Zone, Shanghai, 201108, PEOPLE'S REPUBLIC OF CHINA TEL: [86]-(0)21-5442-5455 FAX: [86]-(0)21-5442-5466	SHIBAURA MACHINE INDIA PRIVATE LIMITED No. 65 (P.O. Box No. 5), Chennai-Bangalore Highway, Chembarambakkam, Poonamallee Taluk, Thiruvallur, Chennai, TN 600123, INDIA TEL: [91]-(0)44-2681-2000 FAX: [91]-(0)44-2681-0303 CHENNAI*, DELHI, MUMBAI
Chubu Branch 5-307, Kamiyashiro, Meito-ku, Nagoya-shi, Aichi-ken 465-0025, Japan TEL: [81]-(0)52-702-7811 FAX: [81]-(0)52-702-1141	SHIBAURA SEMTEK CO., LTD. 2068-3, Ooka, Numazu-shi, Shizuoka-ken 410-8510, Japan TEL: [81]-(0)55-924-3450 FAX: [81]-(0)55-925-6556 http://www.s-semtek.co.jp/	SHIBAURA MACHINE (SHENZHEN) CO., LTD. Room 608, Building 2, Animation Park, Yuehai Road, Nanhai Street, Nanshan District, Shenzhen, 518054, PEOPLE'S REPUBLIC OF CHINA TEL: [86]-(0)755-8625-0599 FAX: [86]-(0)755-8625-0522 SHENZHEN*, GUANGZHOU	SHIBAURA MACHINE MANUFACTURING (THAILAND) CO., LTD. 7/499 Moo 6, Tambol Mabyangporn, Amphur Pluakdaeng, Rayong 21140, THAILAND TEL: [66]-(0)38-027313 FAX: [66]-(0)38-027317
Kansai Branch 11F, Mainichi-Intecio Build., 3-4-5, Umeda, Kita-ku, Osaka-shi, Osaka 530-0001, Japan TEL: [81]-(0)6-6341-6181 FAX: [81]-(0)6-6345-2738	SHIBAURA SANGYO CO., LTD. 2068-3, Ooka, Numazu-shi, Shizuoka-ken 410-8510, Japan TEL: [81]-(0)55-922-0816 FAX: [81]-(0)55-924-5816	SHIBAURA MACHINE TAIWAN CO., LTD. 7F., No.168, Ruiguang Road, Neihu District, Taipei City, 11491, TAIWAN TEL: [886]-(0)2-2659-6558 FAX: [886]-(0)2-2659-6381	< The Americas >
Kyusyu Branch 2-3-23, FMT Enokida Build., Hakata-ku, Fukuoka-shi, Fukuoka-ken 812-0004, Japan TEL: [81]-(0)92-451-2795 FAX: [81]-(0)92-474-1045		SHIBAURA MACHINE THAILAND CO., LTD. 123 Pioneer Road, Singapore 639596, SINGAPORE TEL: [65]-68611455 FAX: [65]-68612023 SINGAPORE*, KUALA LUMPUR, PENANG	SHIBAURA MACHINE COMPANY, AMERICA 755 Greenleaf Avenue, Elk Grove Village, IL 60007, U.S.A. CHICAGO*, LOS ANGELES, CHARLOTTE, ATLANTA, ONTARIO/CANADA TEL: [1]-847-593-1616 FAX: [1]-847-593-0897
Numazu Plant 2068-3, Ooka, Numazu-shi, Shizuoka-ken 410-8510, Japan TEL: [81]-(0)55-926-5141 FAX: [81]-(0)55-925-6501		SHIBAURA MACHINE SINGAPORE PTE. LTD. 123 Pioneer Road, Singapore 639596, SINGAPORE TEL: [65]-68611455 FAX: [65]-68612023 SINGAPORE*, KUALA LUMPUR, PENANG	SHIBAURA MACHINE MEXICO, S.A. DE C.V. Circuito Luxma No. 115, Poligono Industrial, Milenio, C.P. 37290 Leon, Guanajuato, MEXICO TEL: [52]-477-101-8600
Sagami Plant 4-29-1, Hibarigaoka, Zama-shi, Kanagawa-ken 252-0003, Japan TEL: [81]-(0)46-258-2801 FAX: [81]-(0)46-258-2900		SHIBAURA MACHINE (THAILAND) CO., LTD. 127/28 Panjathanee Tower, 23rd Floor, Nonthree Road, Khwaeng Chong Nonthree, Khet Yannawa, Bangkok 10120, THAILAND TEL: [66]-(0)2-681-0158 ~ 61 FAX: [66]-(0)2-681-0162	SHIBAURA MACHINE DO BRASIL COMERCIO DE MAQUINAS LTDA. Rua Cubatao, 86 Conjunto 1307, Vila Mariana, Sao Paulo, SP CEP 04013-000, BRASIL TEL: [55]-(0)11-3253-3331 FAX: [55]-(0)11-3586-0138
Gotemba Plant 1-120, Komakado, Gotemba-shi, Shizuoka-ken 412-0038, Japan TEL: [81]-(0)550-87-3555 FAX: [81]-(0)550-87-3742		PT. SHIBAURA MACHINE INDONESIA Galeri Niaga, Tanjung Barat Kav. KM.8-6. 7, JL. TB. Simatupang Kav. 81, Tanjung Barat, Jagakarsa, Jakarta Selatan, 12530, INDONESIA TEL: [62]-(0)21-7884-8694 FAX: [62]-(0)21-7884-8689	< Europe >
			SHIBAURA MACHINE EUROPE S.R.L. Via Gaudenzio Fantoli 7, Piano 2, 20138, Milano, ITALIA TEL: [39]-02-50041667 FAX: [39]-02-50041668

Shibaura Machine

2-2, Uchisaiwaicho 2-chome, Chiyoda-ku, Tokyo 100-8503, Japan
TEL : [81]-(0)3-3509-0200 FAX : [81]-(0)3-3509-0333
2068-3, Ooka, Numazu-shi, Shizuoka-ken 410-8510, Japan
TEL : [81]-(0)55-926-5141 FAX : [81]-(0)55-925-6501

<https://www.shibaura-machine.co.jp/>



This <Shibaura Machine Engineering Review> is made of LIMEX, a new material made mainly from limestone.
It uses less water and trees.